Article

Erythropoietin receptor on cDC1s dictates immune tolerance

https://doi.org/10.1038/s41586-025-09824-z

Received: 22 January 2024

Accepted: 28 October 2025

Published online: 10 December 2025

Check for updates

Xiangyue Zhang[1]✉, Christopher S. McGinnis[1,2], Guotao Yu[1], Sijie Chen[3], Pingping Zheng[4], Christian M. Schürch[5,6], Kamir J. Hiam-Galvez[1], Nathan E. Reticker-Flynn[7], Wenhui Guo[1], Winnie Yao[1], Jingtao Qiu[1], Alexander Muselman[1], Ian L. Linde[1], John W. Hickey[8], Hao Yan[4], Victoria M. Tran[9], Wenli Qiu[10], Delphine Brichart-Vernos[11], Toshihito Hirai[4], Bo Yu[12], Xiuli An[13], Yanling Xiao[14], Helena Paidassi[11], Tiffany C. Scharschmidt[9], Michael Angelo[1], Dean Sheppard[10], Hongbo Chi[15], Ansuman T. Satpathy[1,2], Sing Sing Way[16], Bernard Malissen[17], Samuel Strober[18,20] & Edgar G. Engleman[1,19]✉

Type 1 conventional dendritic cells (cDC1s) are unique in their efferocytosis[1] and cross-presenting abilities[2], resulting in antigen-specific T cell immunity[3] or tolerance[4–8]. However, the mechanisms that underlie cDC1 tolerogenic function remain largely unknown. Here we show that the erythropoietin receptor (EPOR) acts as a critical switch that determines the tolerogenic function of cDC1s and the threshold of antigen-specific T cell responses. In total lymphoid irradiation-induced allograft tolerance[9,10], cDC1s upregulate EPOR expression, and conditional knockout of EPOR in cDC1s diminishes antigen-specific induction and expansion of FOXP3$^+$ regulatory T (T_{reg}) cells, resulting in allograft rejection. Mechanistically, EPOR promotes efferocytosis-induced tolerogenic maturation[7,11] of splenic cDC1s towards late-stage CCR7$^+$ cDC1s characterized by increased expression of the integrin β8 gene[12] (*Itgb8*), and conditional knockout of *Itgb8* in cDC1s impairs tolerance induced by total lymphoid irradiation plus anti-thymocyte serum. Migratory cDC1s in peripheral lymph nodes preferentially express EPOR, and their FOXP3$^+$ T_{reg} cell-inducing capacity is enhanced by erythropoietin. Reciprocally, loss of EPOR enables immunogenic maturation of peripheral lymph node migratory and splenic CCR7$^+$ cDC1s by upregulating genes involved in MHC class II- and class I-mediated antigen presentation, cross-presentation and costimulation. EPOR deficiency in cDC1s reduces tumour growth by enhancing anti-tumour T cell immunity, particularly increasing the generation of precursor exhausted tumour antigen-specific CD8$^+$ T cells[13] in tumour-draining lymph nodes and supporting their maintenance within tumours, while concurrently reducing intratumoural T_{reg} cells. Targeting EPOR on cDC1s to induce or inhibit T cell immune tolerance could have potential for treating a variety of diseases.

Immune tolerance[14], a state of indifference or non-reactivity towards a substance that would normally be expected to excite an immunological response, is beneficial in transplantation and autoimmune diseases but detrimental in cancer[15]. cDC1s are prototypical antigen-presenting cells that specialize in acquiring cell-associated antigens by taking up apoptotic cells via a process called efferocytosis[1,16] or taking up necrotic cells[17] to induce corresponding cell-associated antigen-specific T cell immune responses[18–20]. By virtue of their unique capacity to cross-present cell-associated antigens to CD8$^+$ T cells[2], cDC1s are required for immunity against tumours and viral infections[21]. In the cancer-immunity cycle[22], cDC1s are vital for cancer immune surveillance by priming tumour antigen-specific CD8$^+$ T cells leading to the generation of precursor exhausted T (T_{pex}) cells in tumour-draining lymph nodes (TDLNs) and recruiting and restimulating immune effector cells in the tumour microenvironment (TME)[23–30]. The functional state of cDC1s coupled with antigen uptake and subsequent antigen presentation dictates both the direction (immunogenic versus tolerogenic) and intensity of an antigen-specific immune response[31]. The acquisition of dead cells by cDC1s not only initiates both CD4$^+$ and CD8$^+$ T cell priming and activation[19] but can also result in tolerogenic programming and maturation of cDC1s[5,7,32], leading to the induction of antigen-specific CD4$^+$FOXP3$^+$ T_{reg} cells[4,5] and deletion of antigen-specific CD8$^+$ T cells[33]. cDC1s contribute to homeostatic tolerance[5], tolerance to dietary antigens[34,35] and tolerance in autoimmunity[6,36] and transplantation[37]. However, the mechanisms that determine how cDC1s become tolerogenic for T cell adaptive immunity remain unknown.

A list of affiliations appears at the end of the paper.

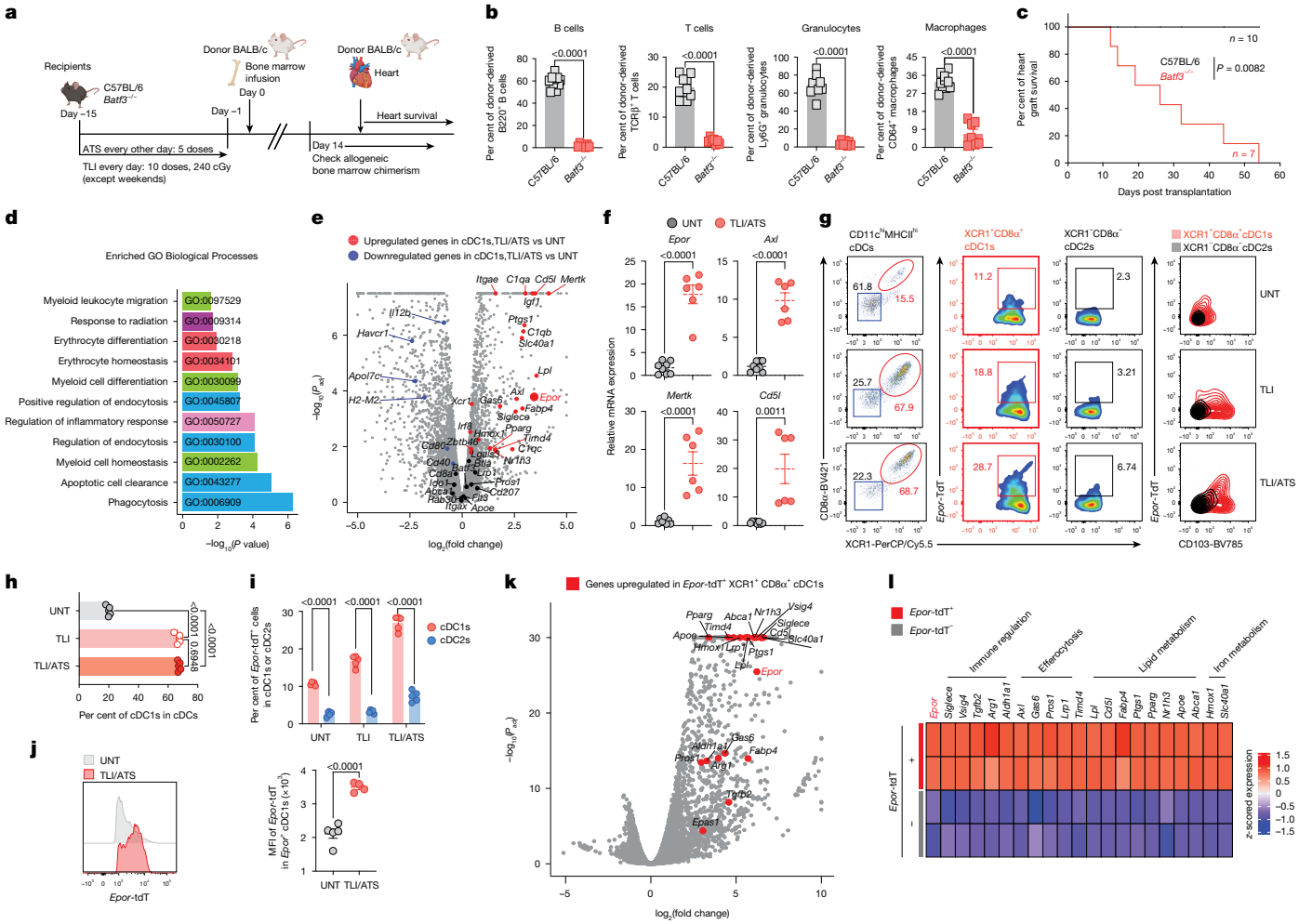

Fig. 1 | Efferocytotic tolerance-inducing cDC1s upregulate *Epor* following TLI. a, Schematic of TLI/ATS treatment, allo-bone marrow infusion, and heart transplantation in C57BL/6 and *Batf3*$^{-/-}$ mice. **b**, Donor type (H2K^{d+}) leukocytes (B220$^+$, TCRβ$^+$, Ly6G$^+$, CD64$^+$) in peripheral blood 28 days post-bone marrow infusion. Wild type ($n = 10$) versus *Batf3*$^{-/-}$ ($n = 7$). **c**, Heart allograft survival in C57BL/6 ($n = 10$) versus *Batf3*$^{-/-}$ ($n = 7$). **d**,**e**, RNA-seq of splenic cDC1s from untreated (UNT) or TLI/ATS-treated mice. **d**, Enriched GO Biological Processes with TLI/ATS treatment. **e**, Volcano plot of differentially expressed genes. **f**, qPCR of selected genes (untreated, $n = 8$; TLI/ATS, $n = 6$). **g**–**i**, Flow cytometry analysis of *Epor*-tdT on cDC1s and cDC2s from untreated, TLI and TLI/ATS-treated mice (**g**), and summary of cDC1 frequency (**h**) and *Epor*-tdT$^+$ cells (**i**) ($n = 5$ per group). **j**, tdT expression in *Epor*$^+$ cDC1s: histogram (left) and mean fluorescence intensity (MFI) (right) (untreated, $n = 5$; TLI/ATS, $n = 4$). **k**,**l**, RNA-seq of splenic *Epor*-tdT$^+$ versus *Epor*-tdT$^-$ cDC1s post-TLI/ATS ($n = 2$ per group, pooled from 15 mice). **k**, Volcano plot of upregulated genes. **l**, Heat map of genes enriched in *Epor*-tdT$^+$ cDC1s. **b**, Data are pooled from two independent experiments. **c**,**g**–**j**, Data are shown for one experiment, representative of at least three independent experiments with similar results. Statistical analysis was performed using unpaired two-tailed Student's *t*-test (**b**,**f**,**j**), one-way ANOVA (**h**), two-way ANOVA with Tukey's multiple-comparison test (**i**) or Kaplan–Meier survival analysis with Mantel–Cox test (**c**). *P* values were calculated using hypergeometric tests with Benjamini–Hochberg correction (**d**) or two-sided generalized linear model likelihood ratio tests with Benjamini–Hochberg correction (**e**,**k**). **b**,**f**,**h**–**j**, Data are mean ± s.e.m. Diagram in **a** created in BioRender. Zhang, X. (2025) https://BioRender.com/d5yzicr.

Tolerogenic cDC1s upregulate EPOR after TLI

To investigate the mechanisms of cDC1-mediated tolerance, we used a protocol combining total lymphoid irradiation (TLI), anti-thymocyte serum (ATS), and allogeneic donor bone marrow infusion[38], which induces mixed chimerism and donor-specific tolerance in kidney transplant patients, enabling the patients to be weaned off immune-suppressive drugs without graft rejection[9,10]. In mice, this approach reliably induces lifelong mixed chimerism and tolerance to fully MHC-mismatched organs[39]. cDC1s are indispensable for immune tolerance[38], as *Batf3*$^{-/-}$ mice lacking cDC1s did not establish bone marrow chimerism (Fig. 1a,b) or maintain allo-heart grafts (Fig. 1a,c). After combined TLI and ATS (TLI/ATS), total splenic cell numbers decreased by about 60% (Extended Data Fig. 1a), but cDC1s increased more than twofold among cDCs (Extended Data Fig. 1b,c), with more than 97% expressing XCR1[40] (Extended Data Fig. 1d). cDC1s from TLI/ATS-treated mice showed increased Ki67, indicative of proliferation (Extended Data Fig. 1e). Their identity was confirmed by high expression of *Batf3*[41], IRF8[42] (Extended Data Fig. 1f,g), *Zbtb46*-GFP[43] (Extended Data Fig. 1h) and low expression of *Mafb*-mCherry[44] (Extended Data Fig. 1i–k). RNA-sequencing (RNA-seq) and Gene Ontology (GO) analysis of XCR1$^+$CD8α$^+$ cDC1s after TLI/ATS revealed upregulation of genes involved in phagocytosis, apoptotic cell clearance, erythropoiesis and myeloid cell migration (Fig. 1d), aligning with increased apoptotic lymphocytes (Extended Data Fig. 2a,b), serum erythropoietin (EPO) (Extended Data Fig. 2c) and splenic erythropoiesis (Extended Data Fig. 2d,e). *Epor* was upregulated ($\log_2$(fold change) = 3.45; adjusted $P = 0.000164$; Fig. 1e) in cDC1s following TLI/ATS, and quantitative PCR (qPCR) confirmed increased expression of *Epor*, *Axl*, *Mertk* and *Cd5l* (Fig. 1f).

To confirm EPOR expression on cDC1s, we utilized *Epor*-tdTomato (tdT)-Cre mice[45]. After TLI/ATS, cDC1s increased threefold in these

mice (Fig. 1g,h), similar to the increase in wild-type C57BL/6 mice (Extended Data Fig. 1c), and *Epor*-tdT expression specifically increased markedly on cDC1s (Fig. 1g,i,j). Five days of treatment with recombinant EPO (Extended Data Fig. 2f) expanded cDC1s, increased their *Epor*-tdT expression (Extended Data Fig. 2g,h), and increased expression of erythroid progenitors (Extended Data Fig. 2i) and red pulp macrophages (Extended Data Fig. 2j), validating *Epor*-tdT as a functional EPOR reporter. After TLI/ATS, *Epor*-tdT expression was enriched in CCR7$^+$ mature[5,7] cDC1s (Extended Data Fig. 2k), and was accompanied by increased CD103[7] expression (Fig. 1g), which is associated with high engulfment capacity. Gene set enrichment analysis (GSEA) revealed enrichment of metabolic and mTOR gene sets (Extended Data Fig. 3a–c), consistent with enhanced EPO–EPOR signalling[46] in cDC1s, as evidenced by increased phosphorylation of AKT, ERK, STAT5, S6 and 4E-BP1 (Extended Data Fig. 3d), with minimal activation in cDC2s (Extended Data Fig. 3e).

RNA-seq of fluorescence-activated cell sorting (FACS)-sorted *Epor*-tdT$^+$ and *Epor*-tdT$^-$ cDC1s following TLI/ATS again showed that *Epor* was highly upregulated in *Epor*-tdT$^+$ cDC1s (Fig. 1k,l) along with a panel of genes that contribute to immune regulation (*Siglece*, *Vsig4*, *Tgfb2*, *Arg1* and *Aldh1a1*), efferocytosis (*Axl*, *Gas6*, *Pros1*, *Lrp1* and *Timd4*), lipid metabolism (*Cd5l*, *Fabp4*, *Lpl*, *Ptgs1*, *Pparg*, *Nr1h3*, *Apoe* and *Abca1*), and iron metabolism (*Hmox1*[47,48] and *Slc40a1*) (Fig. 1k,l). Thus, TLI/ATS markedly increased both the cycling of cDC1s and their EPOR expression. Combined with local accumulation of apoptotic cells and increased EPO, these findings point to the possibility that EPO–EPOR signalling is involved in the tolerogenic role of cDC1s in the context of efferocytosis[49].

cDC1 expression of EPOR is required for TLI-induced tolerance

To further investigate the tolerogenic role of EPOR on cDC1s, we next generated *Epor*$^{\Delta Xcr1}$ (*Xcr1*$^{cre/+}$*Epor*$^{flox/flox}$; H-2K^{b+})[6,50] mice and found that AKT–mTOR signalling activation following TLI/ATS was abrogated specifically in cDC1s but not in cDC2s (Extended Data Fig. 3f,g), confirming efficient *Epor* deletion. Ex vivo EPO stimulation further validated the cDC1-specific responsiveness of EPOR to EPO, as shown by enhanced phosphorylation of AKT, ERK, STAT5, S6 and 4E-BP1 in cDC1s isolated from EPOR-intact TLI/ATS-treated *Epor*$^{flox/flox}$ mice (Extended Data Fig. 3h). As in *Batf3*$^{-/-}$ mice (Fig. 1b,c), loss of EPOR in cDC1s abrogated TLI/ATS-induced bone marrow chimerism (Fig. 2a,b) and led to allograft rejection within 2 weeks (Fig. 2a,c), indicating that cDC1–EPOR signalling is required for TLI/ATS-induced tolerance.

Given the critical role of FOXP3$^+$ T_{reg} cells in implementing and maintaining immune tolerance[51], and the fact that stable bone marrow chimerism is crucial for tolerance and long-term graft survival[52], we hypothesized that EPOR$^+$ cDC1s mediate their tolerogenic effects by inducing T_{reg} cells in response to allo-bone marrow infusion. To assess this hypothesis, we depleted FOXP3$^+$ T_{reg} cells in *Foxp3*-DTR mice with diphtheria toxin during days 0–14 (group A) or 15–28 (group B) (Fig. 2d) following TLI/ATS and allo-bone marrow infusion. Diphtheria toxin reduced the number of FOXP3$^+$ T_{reg} cells by more than 90% (Extended Data Fig. 4a). Depletion on days 0–14 abolished bone marrow chimerism (Fig. 2e), whereas depletion on days 15–28 prevented its further increase and caused a decline by day 28 (Fig. 2e). These data demonstrate that T_{reg} cells are required for both induction and maintenance of immune tolerance following TLI/ATS treatment. To test whether EPOR signalling in cDC1s can drive T_{reg} cell induction in vitro, we first cocultured CellTrace Violet (CTV)-labelled naive OT-II T cells with *Epor*-tdT$^+$ or *Epor*-tdT$^-$ cDC1s together with apoptotic Act-mOVA[53] thymocytes. EPOR$^+$ cDC1s generated more antigen-specific FOXP3$^+$ T_{reg} cells than EPOR$^-$ cDC1s; this effect was further enhanced by EPO (Fig. 2f). Next, to determine whether cDC1 EPOR expression is required for T_{reg} cell induction in vivo, we quantified FOXP3$^+$ T_{reg} cells during TLI/ATS tolerance induction in wild-type, *Batf3*$^{-/-}$ and *Epor*$^{\Delta Xcr1}$ mice alongside untreated controls. After TLI/ATS, on day 0, before bone marrow infusion, CD4$^+$ T cell and FOXP3$^+$ T_{reg} cell frequencies were similar across strains (Fig. 2g, top and Extended Data Fig. 4b,d). At 14 days after allo-bone marrow infusion, the proportion of conventional CD4$^+$ T cells increased from 1–2% to more than 10% in *Batf3*$^{-/-}$ and *Epor*$^{\Delta Xcr1}$ mice, whereas they remained 1–2% in wild-type mice (Fig. 2g, bottom and Extended Data Fig. 4c,e). By contrast, T_{reg} cell frequencies increased in wild-type mice but markedly decreased in *Batf3*$^{-/-}$ and *Epor*$^{\Delta Xcr1}$ mice (Fig. 2g, bottom and Extended Data Fig. 4c,e). Additionally, in MHCII$^{\Delta Xcr1}$ (*Xcr1*$^{cre/+}$*H2-Ab1*$^{flox/flox}$)[54] recipients (Extended Data Fig. 4f), bone marrow chimerism establishment (Extended Data Fig. 4g) and FOXP3$^+$ T_{reg} cell expansion did not occur, whereas conventional CD4$^+$ T cells increased in number (Extended Data Fig. 4h,i), indicating that EPOR signalling in cDC1s drives tolerance via MHCII-mediated T_{reg} cell induction.

TLI/ATS reprogrammes the immune system within a strict time window to recognize allo-bone marrow as self, enabling durable chimerism and donor antigen-specific tolerance[9,55]. To confirm the antigen-specificity of the T_{reg} cells induced by EPOR$^+$ cDC1s following allo-bone marrow infusion, we infused the recipients with 2W1S-BALB/c[56] bone marrow (Fig. 2h); the high precursor frequency of naive CD4$^+$ T cells that recognize MHC class II I-A^b 2W1S$_{55–68}$[56] enables identification of endogenous donor-specific recipient FOXP3$^+$ T_{reg} cells using MHCII tetramer staining. In untreated mice, 14 days after 2W1S-BALB/c allo-bone marrow infusion, only 2–5% of CD44$^+$2W1S tetramer$^+$CD4$^+$ T cells were FOXP3$^+$ in either *Epor*$^{flox/flox}$ or *Epor*$^{\Delta Xcr1}$ recipients (Fig. 2h), indicating a strong alloreactive response of untreated recipient CD4$^+$ T cells upon allo-antigen encounter. By contrast, TLI/ATS-conditioned *Epor*$^{\Delta Xcr1}$ recipients showed 15–22% FOXP3$^+$ T_{reg} cells in 2W1S tetramer$^+$CD4$^+$ T cells, compared with more than 55% in *Epor*$^{flox/flox}$ recipients (Fig. 2h).

To investigate whether cDC1-specific EPOR expression drives T_{reg} cell differentiation from FOXP3$^-$ naive precursors, we compared FOXP3 expression among CD4$^+$ T cells with I-A^b:2W1S specificity from *Foxp3*-DTR CD45.1$^+$[57] donor CD4$^+$ T cells after adoptive transfer into *Foxp3* wild-type CD45.2$^+$ *Epor*$^{\Delta Xcr1}$ or *Epor*$^{flox/flox}$ recipient mice, which were then treated with diphtheria toxin to eliminate natural T_{reg} cells (or not). Although there were similar percentages of FOXP3$^+$ T_{reg} cells between *Foxp3*-DTR CD45.1$^+$ transferred CD4$^+$ T cells and *Foxp3* wild-type CD45.2$^+$ endogenous CD4$^+$ T cells in *Epor*$^{\Delta Xcr1}$ or *Epor*$^{flox/flox}$ recipients without diphtheria toxin treatment, we observed fewer FOXP3$^+$ T_{reg} cells in both populations in *Epor*$^{\Delta Xcr1}$ recipients than in *Epor*$^{flox/flox}$ recipients (Extended Data Fig. 4j). In diphtheria toxin-treated *Epor*$^{flox/flox}$ recipients, *Foxp3*-DTR CD45.1$^+$CD4$^+$ T cells differentiated into T_{reg} cells at lower levels than endogenous *Foxp3* wild-type CD45.2$^+$CD4$^+$ T cells (Extended Data Fig. 4j). Of note, in diphtheria toxin-treated *Epor*$^{\Delta Xcr1}$ recipients, T_{reg} cell differentiation in transferred cells was reduced by more than 50% relative to the already diminished FOXP3 expression seen in both endogenous *Foxp3* wild-type CD45.2$^+$ CD4$^+$ T cells and transferred *Foxp3*-DTR CD45.1$^+$CD4$^+$ T cells from untreated *Epor*$^{\Delta Xcr1}$ recipients, when compared with *Epor*$^{flox/flox}$ controls (Extended Data Fig. 4j). These findings demonstrate the necessity of cDC1-specific EPOR expression for T_{reg} cell induction as well as expansion of pre-existing T_{reg} cells.

EPOR promotes tolerogenic maturation of cDC1s

As splenic cDC1s undergo efferocytosis-induced tolerogenic maturation in the homeostatic state[7,11], we hypothesized that EPOR signalling promotes this programme following TLI/ATS. To address this possibility, we used the 10x Genomics platform to perform single-cell RNA-seq (scRNA-seq) on splenic cDC1s from *Epor*$^{flox/flox}$ and *Epor*$^{\Delta Xcr1}$ mice under untreated versus TLI/ATS conditions (Fig. 3a–d,f–h). Samples were processed in parallel with cell hashing, yielding a dataset of 30,938 cells. Aligning with previous reports[7], in both untreated and TLI/ATS mice, unsupervised clustering and differentially expressed

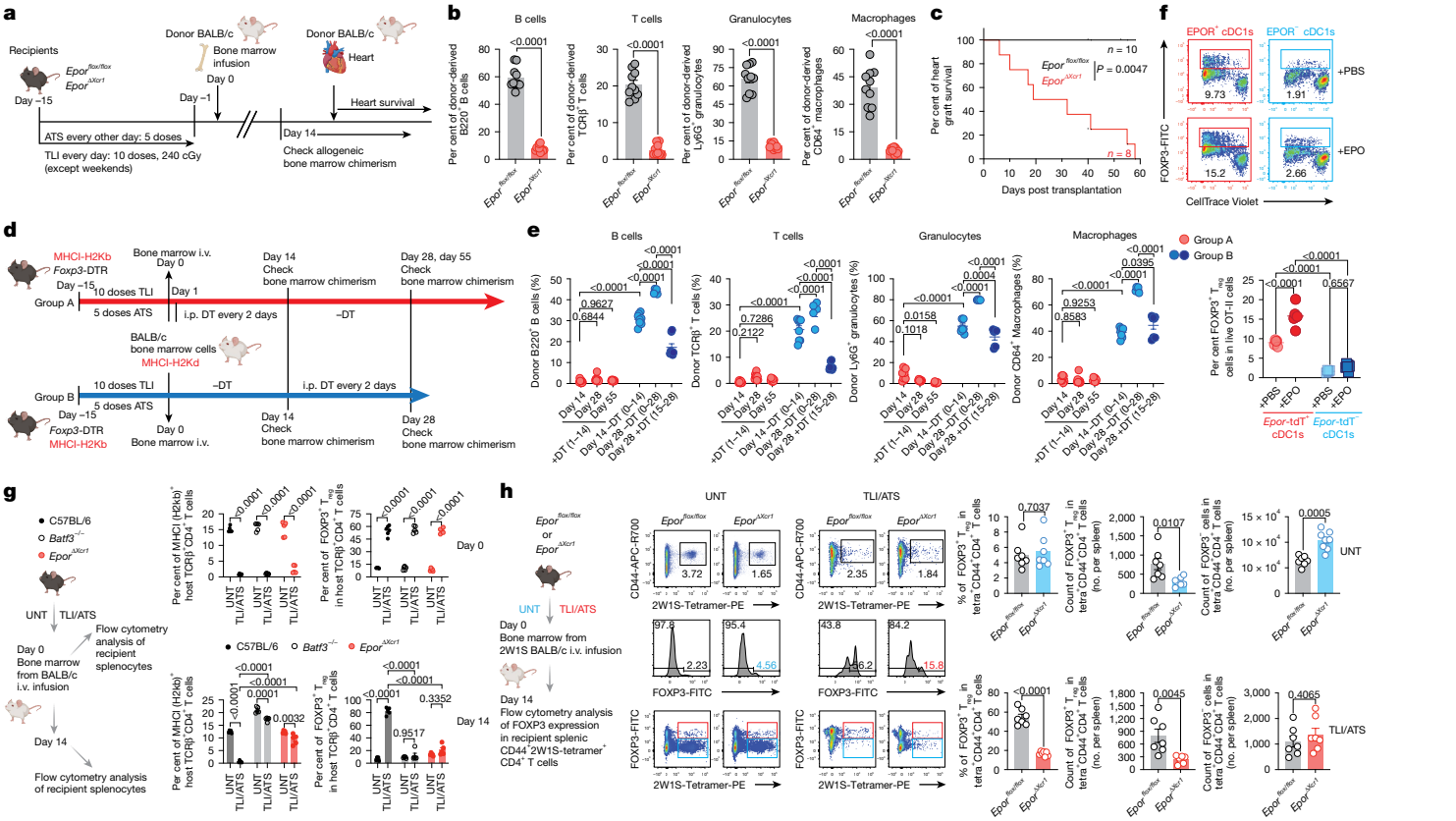

Fig. 2 | Absence of EPOR on cDC1s abrogates T_{reg} cell-mediated allo-antigen-specific tolerance following TLI/ATS, resulting in allograft rejection. a, Schematic of TLI/ATS treatment, allo-bone marrow infusion and heart transplantation in *Epor*$^{flox/flox}$ and *Epor*$^{\Delta Xcr1}$ mice. **b**, Donor type (H2K^{d+}) leukocytes (B220$^+$, TCRβ$^+$, Ly6G$^+$, CD64$^+$) in peripheral blood 28 days post-bone marrow infusion. *Epor*$^{flox/flox}$ ($n = 10$) versus *Epor*$^{\Delta Xcr1}$ ($n = 10$). **c**, Heart allograft survival in *Epor*$^{flox/flox}$ ($n = 10$) versus *Epor*$^{\Delta Xcr1}$ mice ($n = 8$). **d**,**e**, *Foxp3*-DTR mice conditioned with TLI/ATS; group A received diphtheria toxin (DT) from day 1 to day 14 post-bone marrow infusion (day 14, $n = 8$; day 28, $n = 8$; day 55 $n = 8$), group B received DT from day 15 after confirmation of bone marrow chimerism (day 14 −DT, $n = 8$; day 28 −DT, $n = 5$; day 28 +DT, $n = 8$). Bone marrow chimerism was assessed on the indicated days. i.p., intraperitoneal; i.v., intravenous. **e**, Summary of bone marrow chimerism on the indicated days post-bone marrow infusion. **f**, *Epor*-tdT$^+$ or *Epor*-tdT$^-$ cDC1s cocultured with CTV-labelled naive OT-II cells and EPO or phosphate-buffered saline (PBS) for 5 days. FOXP3 expression on OT-II cells was assessed by flow cytometry (*Epor*-tdT$^+$ cDC1s: +PBS, $n = 5$; +EPO, $n = 6$; *Epor*-tdT$^-$ cDC1s: +PBS, $n = 4$; +EPO, $n = 6$). **g**, C57BL/6 *Batf3*$^{-/-}$ or *Epor*$^{\Delta Xcr1}$ recipients treated with TLI/ATS and infused with BALB/c bone marrow. Frequencies of recipient H-2K^{b+}TCRβ$^+$CD4$^+$ and FOXP3$^+$CD4$^+$ T cells analysed on day 0 (untreated: wild type, $n = 5$; *Batf3*$^{-/-}$, $n = 5$; *Epor*$^{\Delta Xcr1}$, $n = 5$; TLI/ATS: wild type, $n = 6$; *Batf3*$^{-/-}$, $n = 5$; *Epor*$^{\Delta Xcr1}$, $n = 5$) or 14 days post-bone marrow infusion (untreated: wild type, $n = 5$; *Batf3*$^{-/-}$, $n = 5$; *Epor*$^{\Delta Xcr1}$, $n = 5$; TLI/ATS: wild type, $n = 5$; *Batf3*$^{-/-}$, $n = 5$; *Epor*$^{\Delta Xcr1}$, $n = 5$). **h**, *Epor*$^{flox/flox}$ and *Epor*$^{\Delta Xcr1}$ recipients were treated with TLI/ATS or untreated. Fourteen days post-2W1S-BALB/c donor bone marrow infusion, 2W1S tetramer$^+$CD44$^+$H-2K^{b+}TCRβ$^+$CD4$^+$ T cells from the spleens were analysed for FOXP3 expression (*Epor*$^{flox/flox}$, $n = 7$; *Epor*$^{\Delta Xcr1}$, $n = 7$). Data are pooled from two independent experiments (**b**) or shown from one experiment, representative of at least two independent experiments with similar results (**c**,**e**–**h**). Statistical analysis was performed using unpaired two-tailed Student's *t*-test (**b**,**h**), two-way ANOVA with Tukey's multiple-comparison test (**e**–**g**) or Kaplan–Meier survival analysis with Mantel–Cox test (**c**). **b**,**e**–**h**, Data are mean ± s.e.m. Diagrams in **a**,**d**,**g**,**h** created in BioRender. Zhang, X. (2025) https://BioRender.com/d5yzicr.

gene (DEG) analysis identified pre-cDC1s along with proliferating, early-immature, late-immature, early-mature and *Ccr7*+ late-mature cDC1s (Fig. 3a) that are tolerogenic in the homeostatic state[11]. Distinct gene expression signatures were linked with TLI/ATS (for example, *Txn1*, *Xcr1* and *Atp5k*) and *Xcr1*^{cre}-driven[6] *Epor* conditional deletion (for example, heat-shock protein genes), shared across multiple cDC1 subtypes (Fig. 3a–c and Extended Data Fig. 5a,b). Notably, TLI/ATS treatment increased early and *Ccr7*+ late-mature cDC1s (Fig. 3b, box) and upregulated efferocytosis-related genes (for example, *Itgae*[7] and *Lgals3*[58]), mirroring bulk RNA-seq analysis (Fig. 1e), while reducing *Apol7c*[59] expression (Fig. 3c), indicating enhanced tolerogenic maturation with reduced cross-presentation capacity of cDC1s in *Epor*$^{flox/flox}$ mice. By contrast, *Epor*$^{\Delta Xcr1}$ mice displayed attenuated shifts: *Ccr7*+ late-mature cells decreased 1.5-fold versus a 1.5-fold increase in *Epor*$^{flox/flox}$ controls, and early-mature cells increased only 1.9-fold versus 3.4-fold (Fig. 3d). Flow cytometry showed a slightly lower baseline proportion of splenic cDC1s in untreated *Epor*$^{\Delta Xcr1}$ mice compared with *Epor*$^{flox/flox}$ controls (Fig. 3e and Extended Data Fig. 5c). Following TLI/ATS, in *Epor*$^{\Delta Xcr1}$ mice, cDC1 expansion was reduced (2.6-fold versus 1.7-fold) and absolute cDC1 numbers were only one-third of those in *Epor*$^{flox/flox}$ controls (Fig. 3e and Extended Data Fig. 5c). *Epor* deletion also down-regulated expression of tolerance-associated genes (*Cd83*[60], *Rel* and *Dnase1l3*[61]; Fig. 3f), highlighting the essential role of EPOR in cDC1 expansion and tolerogenic maturation after TLI/ATS.

To compare the transcriptional profiles of EPOR$^+$ and EPOR$^-$ cDC1s, we performed scRNA-seq on sorted *Epor*-tdT$^+$ and *Epor*-tdT$^-$ cDC1s from TLI/ATS-treated *Epor*-tdT-Cre[45] mice, yielding 24,761 cells (Extended Data Fig. 5d–h). These data revealed that EPOR$^+$ cDC1s spanned the continuum of tolerogenic maturation (Extended Data Fig. 5d,e) and thus did not constitute a specific subpopulation of cDC1s. Further, DEG analysis revealed unique sets of genes associated with *Epor*-tdT$^+$ or *Epor*-tdT$^-$ cDC1s (Extended Data Fig. 5f). Notably, *Epor*-tdT$^-$ cDC1s exhibited increased expression of genes associated with *Epor*$^{\Delta Xcr1}$ mice following TLI/ATS, whereas *Epor*-tdT$^+$ cDC1s expressed increased levels

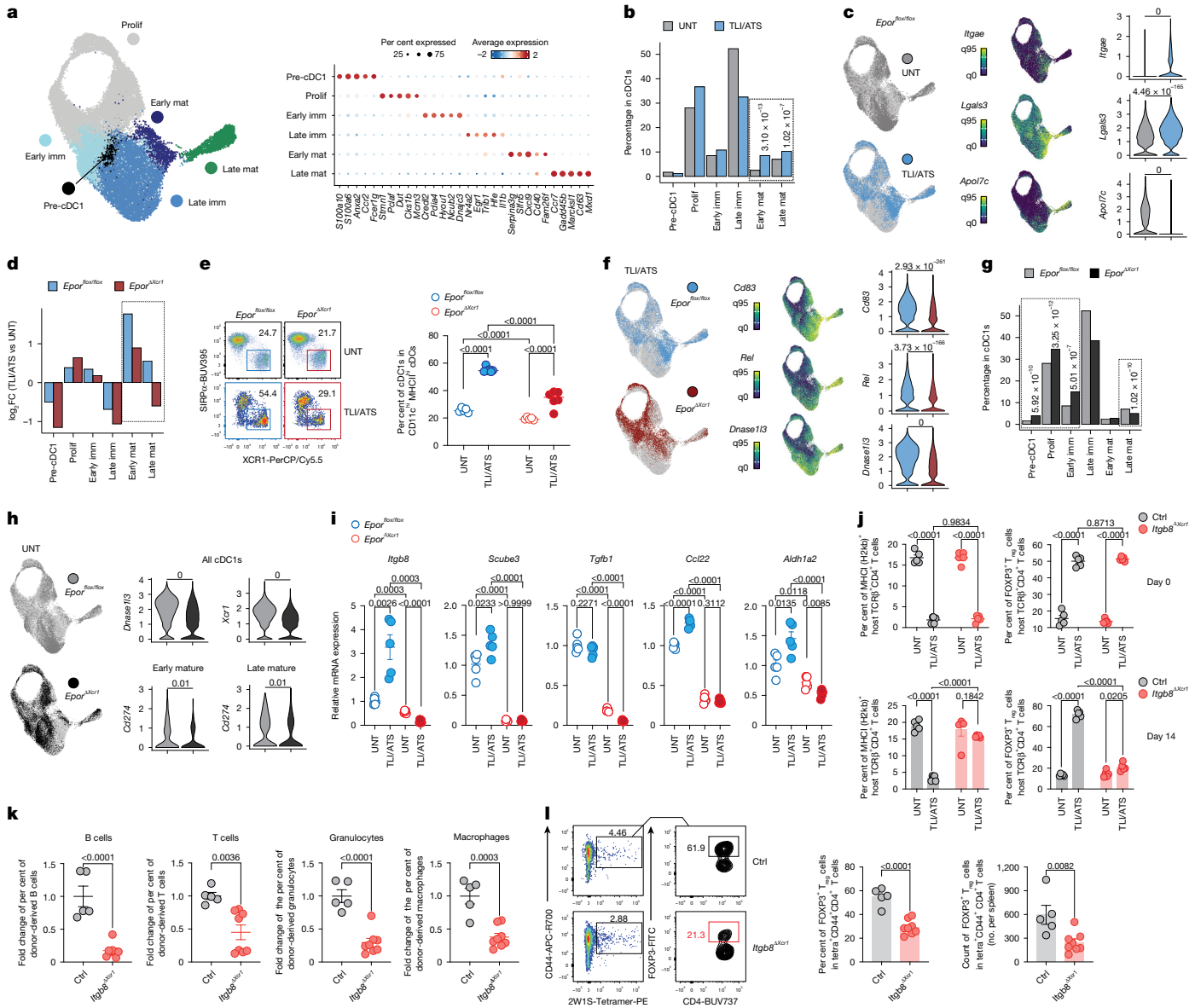

Fig. 3 | scRNA-seq analysis reveals that TLI/ATS promotes EPOR-dependent, efferocytosis-triggered tolerogenic maturation of splenic cDC1s. **a**, Uniform manifold approximation and projection (UMAP) of splenic cDC1s coloured by subtype with dot plot of marker gene expression. Imm., immature; mat., mature; prolif., proliferating. **b**, cDC1 subtype proportions in untreated versus TLI/ATS-treated *Epor*$^{flox/flox}$; box highlights increase in mature cDC1s after TLI/ATS. **c**, UMAP by sample identity with violin plots of *Itgae*, *Lgals3* and *Apol7c* expression. **d**, Change of cDC1 subtypes post-TLI/ATS in *Epor*$^{flox/flox}$ and *Epor*$^{\Delta Xcr1}$ mice; box shows EPOR-dependent differences in mature cDC1s. FC, fold change. **e**, Flow cytometry showing percentage of cDC1s in splenic lineage-negative (Lin$^-$) SiglecH$^-$PDCA-1$^-$CD11c^{hi}MHCII^{hi} cDCs (*Epor*$^{flox/flox}$: untreated, $n = 5$; TLI/ATS, $n = 6$; *Epor*$^{\Delta Xcr1}$: untreated, $n = 5$; TLI/ATS, $n = 6$). **f**, UMAP with violin plots of *Cd83*, *Rel* and *Dnase1l3* expression in cDC1s from *Epor*$^{flox/flox}$ and *Epor*$^{\Delta Xcr1}$ mice post-TLI/ATS. **g**,**h**, Bar charts of cDC1 subtype proportions (**g**) and UMAP and violin plots of *Dnase1l3*, *Xcr1* and *Cd274* expression (**h**) in *Epor*$^{flox/flox}$ and *Epor*$^{\Delta Xcr1}$ mice at baseline (untreated). **i**, qPCR of selected genes in CCR7$^+$XCR1$^+$SIRPα$^-$ cDC1s from *Epor*$^{flox/flox}$ ($n = 5$ per condition) and *Epor*$^{\Delta Xcr1}$ ($n = 5$ per condition) untreated or TLI/ATS mice. **j**, *Itgb8*$^{\Delta Xcr1}$ versus control recipients untreated or treated with TLI/ATS and infused with BALB/c bone marrow. Frequencies of recipient H-2K^{b+}TCRβ$^+$CD4$^+$ and FOXP3$^+$ T$_{reg}$ cells in CD4$^+$ T cells were analysed on day 0 (untreated: control, $n = 5$; *Itgb8*$^{\Delta Xcr1}$, $n = 5$; TLI/ATS: control, $n = 5$; *Itgb8*$^{\Delta Xcr1}$, $n = 5$) or 14 days post-bone marrow infusion (untreated: control, $n = 5$; *Itgb8*$^{\Delta Xcr1}$, $n = 5$; TLI/ATS: control, $n = 5$; *Itgb8*$^{\Delta Xcr1}$, $n = 5$). **k**,**l**, *Itgb8*$^{\Delta Xcr1}$ ($n = 8$) and control ($n = 5$) recipients were infused with 2W1S-BALB/c bone marrow. Donor type leukocyte percentages (**k**) and the frequency and absolute number of FOXP3$^+$2W1S tetramer$^+$CD44$^+$CD4$^+$ T$_{reg}$ cells in spleens (**l**) were analysed 14 days later. Data are representative of two (**e**,**i**) or one (**j**–**l**) independent experiments. Statistical analysis was performed using unpaired two-tailed Student's *t*-test (**i**,**k**,**l**), two-way ANOVA followed by Tukey's multiple-comparison test (**e**,**j**), propeller test, two-sided, no multiple-comparison correction (**b**,**g**), or Wilcoxon rank sum test, two-sided, with Bonferroni correction (**c**,**f**,**h**). **e**,**i**,**g**,**k**,**l**, Data are mean ± s.e.m.

of genes associated with *Epor*$^{flox/flox}$ mice conditioned with TLI/ATS (Extended Data Fig. 5g). Similarly, *Epor*-tdT$^+$ cDC1s were proportionally biased towards more mature cDC1 subtypes (immature, early-mature and *Ccr7*+ late-mature), whereas EPOR$^-$ cDC1 proportions correlated with more immature states (Extended Data Fig. 5h). Complementing these results, we observed that in untreated *Epor*$^{\Delta Xcr1}$ mice, there was a reduction in the proportion of *Ccr7*+ late-mature cDC1s accompanied by an increase in immature cDC1s (Fig. 3g). *Epor* deletion reduced *Dnase1l3*[61] and *Xcr1* expression levels across all splenic cDC1s (Fig. 3h, top), and decreased expression of the coinhibitory receptor *Cd274* in both early and *Ccr7*+ late-mature cDC1s (Fig. 3h, bottom). Collectively, these results illustrate that EPOR$^+$ cDC1s do not represent a unique

cDC1 subtype and instead reflect a unique transcriptional programme associated with cDC1 tolerogenic maturation.

cDC1 expression of integrin β8 is critical for TLI-induced tolerance

CCR7$^+$ late-mature cDC1s showed higher expression of T_{reg} cell-inducing and -maintaining genes—*Itgb8*[12], *Scube3*, *Tgfb1*, *Ccl22* and *Aldh1a2*[62]—compared with CCR7$^-$ cDC1s[7,11]. qPCR confirmed that these genes were significantly upregulated in CCR7$^+$ cDC1s after TLI/ATS in an EPOR-dependent manner (Fig. 3i), and their expression levels in CCR7$^+$ cDC1s in the homeostatic state were also reduced in the absence of EPOR (Fig. 3i). Ex vivo coculture of CCR7$^+$ cDC1s obtained after intravenous injection of apoptotic Act-mOVA thymocytes confirmed the involvement of TGFβ in the enhanced capacity of EPOR-expressing CCR7$^+$ cDC1s to induce antigen-specific FOXP3$^+$ T_{reg} cells (Extended Data Fig. 5i). Integrin αvβ8 contributes to peripheral T_{reg} cell differentiation due to its ability to activate latent TGFβ[12]. To test whether EPOR$^+$ cDC1-mediated induction of allo-bone marrow-specific T_{reg} cells depends on integrin β8, we generated *Itgb8*$^{\Delta Xcr1}$ mice and infused them or littermate controls with allo-bone marrow. Fourteen days after allo-bone marrow infusion, T_{reg} cell frequencies increased in control mice but markedly decreased in *Itgb8*$^{\Delta Xcr1}$ mice (Fig. 3j and Extended Data Fig. 5j–m), similar to our observations in *Epor*$^{\Delta Xcr1}$ mice (Fig. 2g and Extended Data Fig. 4b–e). Moreover, *Itgb8*$^{\Delta Xcr1}$ recipients exhibited impaired bone marrow chimerism (Fig. 3k), albeit to a lesser extent than *Epor*$^{\Delta Xcr1}$ mice (Fig. 2b), and showed a lower proportion and cell number of FOXP3$^+$ T_{reg} cells among CD44$^+$2W1S tetramer$^+$CD4$^+$ T cells (Fig. 3l). *Aldh1a2* encodes retinaldehyde dehydrogenase 2[63], which catalyses the production of retinoic acid to support T_{reg} cell induction[62]. We next generated mixed bone marrow chimeras by reconstituting CD45.1$^+$ mice with a 1:1 ratio of *Aldh1a2*$^{\Delta CD11c}$:*Batf3*$^{-/-}$ bone marrow cells, in which only cDC1s were deficient in *Aldh1a2* expression, or with 1:1 ratio of *Aldh1a2*$^{flox/flox}$:*Batf3*$^{-/-}$ mixed bone marrow cells as controls. Unlike *Epor*$^{\Delta Xcr1}$ and *Itgb8*$^{\Delta Xcr1}$ mice, there was no difference in either bone marrow chimerism or 2W1S-specific FOXP3$^+$ T_{reg} cells between these mice (Extended Data Fig. 5n,o). These findings verify the critical role of EPOR in facilitating efferocytosis-triggered tolerogenic maturation of cDC1s towards late-mature stage CCR7$^+$ cDC1s and demonstrate that integrin β8, but not *Aldh1a2*, is a critical tolerogenic downstream mediator under EPOR control in TLI/ATS-induced tolerance.

cDC1 expression of EPOR limits CD8$^+$ and CD4$^+$ T cell priming

cDC1s specialize in cross-presenting exogenous cell-associated antigens to CD8$^+$ T cells[2] and are also required for CD4$^+$ T cell priming[19]. Although *Epor*$^{\Delta Xcr1}$ mice had a slightly lower percentage of cDC1s than *Epor*$^{flox/flox}$ controls (Fig. 3e), their cDC1s expressed significantly higher levels of CD40, CD80, MHCI, DEC205 and the antiapoptotic CD40-dependent protein Bcl-XL[64], while showing reduced expression of PD-L1 (Extended Data Fig. 6a). By contrast, cDC2s displayed no differences in the expression of these markers between *Epor*$^{\Delta Xcr1}$ and *Epor*$^{flox/flox}$ mice (Extended Data Fig. 6b,c). Flow cytometry confirmed the scRNA-seq finding of reduced CCR7$^+$ late-mature cDC1s in *Epor*$^{\Delta Xcr1}$ mice (Fig. 3g and Extended Data Fig. 6d). Notably, whereas CCR7$^+$ cDC1s normally express higher CD40, CD80 and PD-L1 than CCR7$^-$ cDC1s, both subsets in *Epor*$^{\Delta Xcr1}$ mice displayed increased CD40 and CD80 expression but reduced PD-L1 compared with *Epor*$^{flox/flox}$ controls (Extended Data Fig. 6e), consistent with the scRNA-seq results (Fig. 3h). Whereas the frequencies of splenic conventional CD4$^+$ and CD8$^+$ T cells were unchanged (Extended Data Fig. 7a,d), *Epor*$^{\Delta Xcr1}$ mice had reduced FOXP3$^+$CD25$^+$ T_{reg} cells (Extended Data Fig. 7b) and increased CD44^{hi}CD62L^{low} effector CD4$^+$ and CD8$^+$ T cells (Extended Data Fig. 7c,e).

Next, to examine the effect of cDC1-specific EPOR deficiency on cross-priming and priming of cell-associated antigens in vivo, we transferred CTV-labelled naive OT-I or OT-II T cells into *Epor*$^{\Delta Xcr1}$ or *Epor*$^{flox/flox}$ mice immunized with apoptotic Act-mOVA thymocytes. Notably, *Epor*$^{\Delta Xcr1}$ mice showed enhanced priming of both antigen-specific CD8$^+$ (Extended Data Fig. 6f) and CD4$^+$ T cells (Extended Data Fig. 6g). Aligning with a previous report[19], OT-II priming and proliferation required cDC1s (Extended Data Fig. 7f), and exogenous EPO enhanced FOXP3 expression in OT-II cells in a manner dependent on EPOR expression in cDC1s (Extended Data Fig. 7g). Together, these findings show that even at low homeostatic EPO levels, cDC1-EPOR limits both CD8$^+$ T cell cross-priming and CD4$^+$ T cell priming in response to cell-associated antigens.

T_{reg} cell induction by PLN cDC1s is promoted by EPO

cDC1s are widely distributed in peripheral tissues and lymph nodes where they comprise both lymph node-resident and migratory subsets[4,65]. In peripheral tissues, cDC1s act as sentinels of the immune system, continuously migrating to the draining lymph nodes (DLNs) to initiate T cell adaptive immunity via afferent lymphatics after antigen uptake and CCR7 upregulation[65,66]. To assess steady-state EPOR expression in lymph node cDC1s, we examined peripheral lymph nodes (PLNs) and mesenteric lymph nodes (MLNs) from *Zbtb46*$^{GFP/+}$ *Epor*$^{tdT/+}$ dual-reporter mice by defining cDCs as *Zbtb46*-GFP$^+$CD11c$^+$ (Fig. 4a,b). About 7% of PLN cDCs expressed EPOR, nearly all of which were XCR1$^+$CD11c^{mid}MHCII^{hi} (that is, migratory), whereas such cells were almost absent in MLNs (Fig. 4a,b). EPOR expression was much higher on cDC1s than cDC2s, indicating preferential expression on migratory cDC1s in PLNs (Fig. 4a–c).

CCR7 is required for the migration of cDC1s to the DLNs, where they induce antigen-specific CD4$^+$FOXP3$^+$ T_{reg} cells in the steady state[4,67]. EPOR$^+$ migratory cDC1s, while prominent in the PLNs of *Epor*$^{tdT/+}$ mice (Fig. 4d), were rare in the PLNs of *Ccr7*$^{-/-}$*Epor*$^{tdT/+}$ and *Batf3*$^{-/-}$*Epor*$^{tdT/+}$ mice (Extended Data Fig. 8a,b), indicating that CCR7 and Batf3 are required for the presence of EPOR$^+$ migratory cDC1s. Prominent EPOR expression in migratory cDC1s was consistently observed across all PLNs examined, independent of their drainage site (Extended Data Fig. 8c). Thus, although migratory cDC1s may retain tissue-specific imprints[68,69], *Epor*-tdT expression in PLN migratory cDC1s remains conserved under homeostatic conditions and is not affected by PLN environment or location. Indeed, *Epor*-tdT expression was detected in migratory cDC1s from diverse tissues examined, including brain, skin and lung (Extended Data Fig. 8d), indicating that cDC1s acquire EPOR expression prior to migration to DLNs. Thus, EPOR$^+$ cDC1s observed in PLNs are attributed to the migration of peripheral EPOR$^+$ cDC1s to the DLNs.

Migratory *Epor*-tdT$^+$ cDC1s in PLNs expressed higher levels of inhibitory molecules PD-L1, AXL[70], TIM-3[71] and CD131 (Extended Data Fig. 8e), suggestive of their tolerogenic potential. We compared their ability to induce antigen-specific T_{reg} cells using apoptotic Act-mOVA thymocytes or DEC205-OVA[8], which specifically targets cDC1s. Although *Epor*-tdT$^+$ migratory cDC1s were superior to *Epor*-tdT$^-$ cDC1s at inducing antigen-specific T_{reg} cells against both sources of antigen (Extended Data Fig. 9a,b), they were more efficient at inducing antigen-specific T_{reg} cells to cell-associated antigens (Extended Data Fig. 9b). T_{reg} cell induction by *Epor*-tdT$^-$ cDC1s was enhanced in the presence of exogenous EPO, which is consistent with efferocytosis-induced EPOR upregulation (Extended Data Fig. 9b,c). Exogenous EPO administration also increased the antigen-specific T_{reg} cell induction capacity of PLN migratory cDC1s, and this effect disappeared when the migratory PLN cDC1s were replaced by *Epor*$^{\Delta Xcr1}$ PLN migratory cDC1s (Extended Data Fig. 9d).

To determine whether cDC1 EPOR is required for migratory cDC1-mediated FOXP3$^+$ T_{reg} cell induction, we injected apoptotic cells into the mammary fat pad and tracked local EPOR$^+$ cDC1s. More than 70% of XCR1$^+$ZBTB46$^+$CD11c$^+$ cDC1s in the mammary fat pad expressed EPOR and CD103 (Fig. 4e). In response to injection of PKH67-labelled

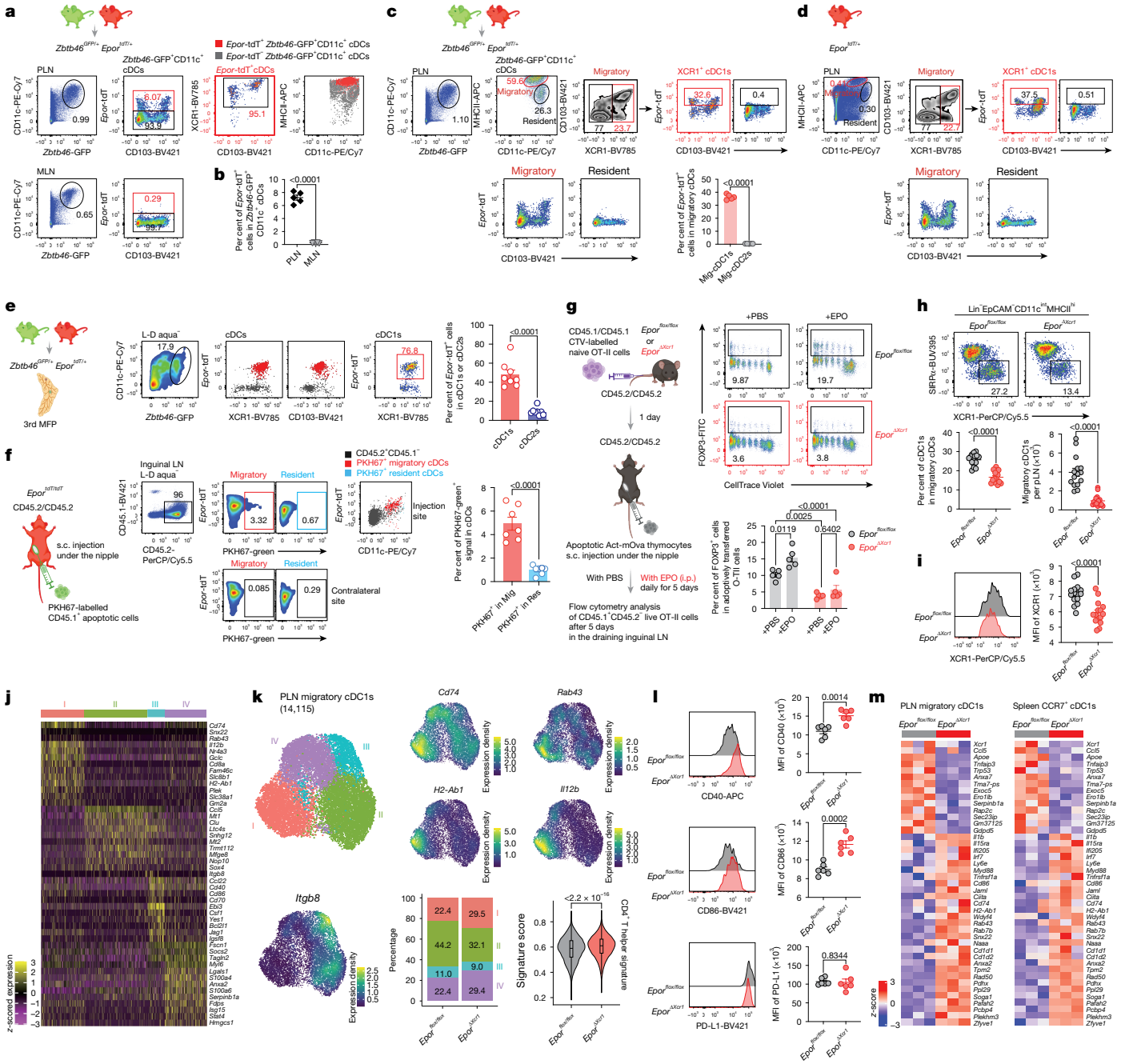

Fig. 4 | EPO-activated cDC1 EPOR supports antigen-specific FOXP3$^+$ T_{reg} cell induction in PLN and restrains the immunogenic maturation of CCR7$^+$ cDC1s. a,**b**, *Epor*-tdT expression on cDCs in PLNs ($n = 5$) and MLNs ($n = 5$) of *Zbtb46*$^{GFP/+}$*Epor*$^{tdT/+}$ mice (**a**) and quantification (**b**). **c**, *Epor*-tdT$^+$ cells were identified in migratory XCR1$^+$ cDC1s or XCR1$^-$ cDC2s (top) and in migratory versus resident cDCs (bottom) in PLN *Zbtb46*-GFP$^+$CD11c$^+$ cDCs ($n = 5$). **d**,**e**, *Epor*-tdT expression in PLNs (**d**) and mammary fat pad cDC1s (**e**) of *Epor*$^{tdT/+}$ mice ($n = 8$). **f**, Efferocytosis of PKH67-labelled CD45.1$^+$ apoptotic thymocytes by migratory or resident cDCs in the dLN of CD45.2$^+$*Epor*$^{tdT/tdT}$ mice ($n = 7$) 12 h after injection of the apoptotic cells into the third mammary fat pad. **g**, Effect of EPO on CD45.1$^+$ OT-II T_{reg} cell induction after Act-mOVA thymocyte injection into the third mammary fat pad (*Epor*$^{flox/flox}$: +PBS, $n = 5$; +EPO, $n = 5$; *Epor*$^{\Delta Xcr1}$: +PBS, $n = 5$; +EPO, $n = 5$). LN, lymph node. **h**,**i**, Frequency and absolute number (**h**) and XCR1 MFI (**i**) of migratory cDC1s per PLN (*Epor*$^{flox/flox}$, $n = 15$; *Epor*$^{\Delta Xcr1}$, $n = 15$). **j**,**k**, scRNA-seq of PLN migratory cDC1s from *Epor*$^{flox/flox}$ and *Epor*$^{\Delta Xcr1}$ mice. Heat map of DEGs (**j**) and UMAP coloured by cluster identity (**k**, top left) and gene expression (**k**). **k**, Bottom right, violin plots represent module score of CD4$^+$ T helper licensing gene signature[75] (259 genes) in migratory cDC1s from *Epor*$^{flox/flox}$ ($n = 6{,}890$ cells) and *Epor*$^{\Delta Xcr1}$ ($n = 7{,}225$ cells) PLNs. The boxes inside the violin plots show the median (centre line) and the interquartile range (25% to 75%, box limits). **l**, MFI of indicated molecules on PLN migratory cDC1s from *Epor*$^{flox/flox}$ ($n = 6$) and *Epor*$^{\Delta Xcr1}$ mice ($n = 6$). **m**, Heat map of top shared DEGs in PLN migratory and splenic CCR7$^+$ cDC1s from bulk RNA-seq (*Epor*$^{flox/flox}$ versus *Epor*$^{\Delta Xcr1}$). Data are shown for one experiment, representative of at least three independent experiments with similar results (**a**–**h**,**l**). Statistical analysis was performed by using unpaired two-tailed Student's *t*-test (**b**,**c**,**e**,**f**,**h**,**i**,**l**), two-way ANOVA with Tukey's multiple-comparison test (**g**) or uncorrected Wilcoxon rank sum test, one-sided (**k**). **b**,**c**,**e**,**f**,**h**,**i**,**l**, Data are mean ± s.e.m. Diagrams in **a**,**c**,**d**–**g** were created in BioRender. Zhang, X. (2025) https://BioRender.com/s5qonkl.

CD45.1$^+$ apoptotic cells, migratory cDCs in the draining inguinal lymph node showed a stronger PKH67 signal than resident cDCs and all PKH67$^+$ migratory cDCs were EPOR$^+$ (Fig. 4f). cDC1s engulfed more apoptotic cells than cDC2s, as evidenced by higher PKH67$^+$ frequencies and signal intensity (Extended Data Fig. 9e). Furthermore, the induction of OT-II FOXP3$^+$ T_{reg} cells in *Epor*$^{flox/flox}$ control mice injected with Act-mOVA

apoptotic cells was further enhanced by exogenous EPO, whereas both effects were abrogated in *Epor*$^{\Delta Xcr1}$ mice (Fig. 4g).

To validate the role of cDC1 EPOR in inducing FOXP3$^+$ T_{reg} cells to endogenous cell-associated antigens, CD45.1$^+$CD45.2$^+$ Act-mOVA mice were reconstituted with bone marrow from either *Epor*$^{flox/flox}$ or *Epor*$^{\Delta Xcr1}$ donors (Extended Data Fig. 9f). In this model, membrane-bound OVA is expressed ubiquitously[53], and MHC class II-mediated antigen presentation depends entirely on donor haematopoietic-derived antigen-presenting cells (APCs). Naive OT-II cells were adoptively transferred (day 0) into the chimeric mice, and EPO was administered on days −2 to 2. Prominent expression of FOXP3 was observed in OT-II cells on day 9 in inguinal lymph nodes from *Epor*$^{flox/flox}$ bone marrow-reconstituted Act-mOVA mice, whereas this induction was markedly impaired in mice reconstituted with *Epor*$^{\Delta Xcr1}$ bone marrow (Extended Data Fig. 9f). These results confirm the importance of EPO-activated cDC1 EPOR in mediating peripheral T_{reg} cell induction to endogenously derived cell-associated antigens upon systemic EPO administration.

Loss of EPOR results in immunogenic CCR7$^+$ cDC1s

Consistent with the reduced frequency and XCR1 expression of splenic CCR7$^+$ cDC1s in *Epor*$^{\Delta Xcr1}$ mice (Fig. 3e,g and Extended Data Fig. 6d), these mice also had fewer migratory cDC1s (Fig. 4h) with lower XCR1 expression (Fig. 4i) in PLNs. Thus, EPOR similarly regulates the homeostatic maturation of migratory cDC1s. scRNA-seq of FACS-sorted PLN migratory cDC1s from *Epor*$^{\Delta Xcr1}$ and *Epor*$^{flox/flox}$ mice revealed four shared clusters (Fig. 4j,k). Cluster I, which was enriched for antigen-presenting genes (*H2-Ab1*, *Rab43*[72] and *Cd74*[73]) and *Il12b*, was overrepresented in *Epor*$^{\Delta Xcr1}$ mice (Fig. 4j,k). However, clusters II and III, characterized by high *Itgb8* expression, were significantly under-represented in *Epor*$^{\Delta Xcr1}$ samples (Fig. 4j,k), a change potentially compounded by the overall decreased frequency of migratory cDC1s in *Epor*$^{\Delta Xcr1}$ mice (Fig. 4h). Consistent with these findings, the proportion of cluster II enriched in immunoregulatory genes such as *Mt1*, *Mt2*, *Clu* and *Mfge8*[74] was reduced. Conversely, EPOR-deficient PLN cDC1s displayed greater enrichment of the 'CD4$^+$ T helper licensing' signature[75] (259 genes) (Fig. 4k and Supplementary Table 1), indicating that EPOR loss itself can mimic CD4$^+$ T helper cell-induced transcriptional programming[75]. As revealed by flow cytometry, CD40 and CD86 were upregulated in *Epor*$^{\Delta Xcr1}$ cDC1s, whereas PD-L1 remained unchanged (Fig. 4l), which differs from splenic CCR7$^+$ cDC1s (Fig. 3h and Extended Data Fig. 6e). Further bulk RNA-seq confirmed that EPOR regulates shared gene programmes in PLN migratory and splenic CCR7$^+$ cDC1s, upregulating 319 and downregulating 358 genes (Supplementary Table 2). EPOR supported the expression of key immune-regulatory genes such as *Apoe*[76] and *Tnfaip3* (encoding A20 protein[77]), and the loss of EPOR led to increased expression of genes involved in MHCII-mediated antigen presentation (*H2-Ab1*, *Cd74* invariant chain[73] and *Ciita*[78]), cross-presentation (*Wdfy4*[79] and *Rab43*[72]), cytotoxic T cell responses (*Il15ra*[80]), costimulation (*Cd86*) and immunogenic maturation (*Il1b*), as well as toll-like receptor and type I interferon signalling (*Tlr9*, *Myd88*, *Irf7* and *Ifi205*) and *Tnfrsf1a* (encoding TNFR1) (Fig. 4m). These results indicate that loss of EPOR enables the immunogenic maturational programming of CCR7$^+$ cDC1s at both anatomical sites. Accordingly, similar to the T cell immune profile in the spleen, FOXP3$^+$CD25$^+$ T_{reg} cells were reduced, and CD44^{hi}CD62L^{low} effector CD4$^+$ and CD8$^+$ T cells were increased in PLNs (Extended Data Fig. 10a–e).

Loss of EPOR on cDC1s promotes anti-tumour immunity

Interactions between cDC1s and T cells are critical throughout the cancer–immunity cycle[22], both in TDLNs[29,30] for priming naive T cells and also in the TME[24], where cDC1s have a unique role in determining tumour antigen-specific CD8$^+$ T cell fate by recruiting T cells, secreting cytokines and presenting tumour antigens to enhance cytotoxic T cell effector function[81]. cDC1s serve as an autonomous platform for both CD4$^+$ and CD8$^+$ T cell priming, directly orchestrating their crosstalk—that is, cDC1 'licensing' in the TME for optimal anti-tumour immunity[19,64,75]. Given that EPOR signalling in cDC1s promotes FOXP3$^+$ T_{reg} cell induction and suppresses CD8$^+$ T cell cross-priming, we investigated the effect of cDC1 EPOR on anti-tumour immunity.

To examine EPOR expression on tumour-infiltrating cDC1s, we used *Zbtb46*$^{GFP/+}$*Epor*$^{tdT/+}$ mice, defining tumour cDCs as CD45$^+$*Zbtb46*-GFP$^+$CD11c$^+$ (Extended Data Fig. 11a–d). *Epor*-tdT$^+$XCR1$^+$CD103$^+$ cDC1s were detected in multiple tumour models (Extended Data Fig. 11a–d). EPOR was preferentially expressed by CCR7$^+$*Zbtb46*-GFP$^+$XCR1$^+$CD103$^+$ cDC1s rather than CCR7$^-$ cDCs (Fig. 5a and Extended Data Fig. 11e). Of note, CCR7$^+$*Epor*-tdT$^+$ cDC1s displayed a maturation-associated regulatory phenotype based on their significantly higher levels of CD40, CD80, CD86, MHCI and PD-L1 than other cDC populations (Extended Data Fig. 11f), indicating that they might have undergone tolerogenic maturation[5,70]. In TDLNs, *Epor*-tdT was similarly restricted to migratory cDC1s (Extended Data Fig. 11g). Serum EPO positively correlated with tumour growth (Extended Data Fig. 11h), probably reflecting its effect on EPOR$^+$ cDC1s to facilitate uptake and processing of apoptotic tumour cells. Utilizing ZsGreen-labelled B16F10-OVA[71] tumours (Extended Data Fig. 11i), we found that in both TDLN migratory cDC1s (Extended Data Fig. 11j) and tumour-infiltrating cDC1s (Extended Data Fig. 11k), ZsGreen^{hi} cDC1s were also *Epor*-tdT$^+$ (Extended Data Fig. 11j,k), indicating that EPOR$^+$ cDC1s engulf tumour debris, which could facilitate presentation of tumour antigens to promote tumour-specific tolerance. Supporting this hypothesis, we observed reduced growth of MC38-OVA^{dim} and B16F10-OVA[71] in *Epor*$^{\Delta Xcr1}$ mice compared to *Epor*$^{flox/flox}$ controls (Fig. 5b and Extended Data Fig. 12a,b).

Tumour-specific CD8$^+$ T cell activation takes place in two phases: initial activation in TDLNs to generate TCF1$^+$PD-1$^+$SLAMF6$^+$ T_{pex} cells and subsequent acquisition of effector programmes by CD8$^+$ T cells within the tumours[82,83]. cDC1s maintain a reservoir of tumour antigen-specific T_{pex} cells in TDLNs[23], and intratumoural cDC1-CD8$^+$ T cell clusters[84], which constitute niches for TCF1$^+$ T_{pex} cell stimulation and have a critical role in promoting tumour antigen-specific CD8$^+$ T cell expansion and effector function[27]. Moreover, the therapeutic response to anti-PD-1 is proportional to the abundance of T_{pex}[85,86] and APC niches in tumours[84], and the functionality of TDLNs[87] is critical. Therefore, we reasoned that, in addition to inducing FOXP3$^+$ T_{reg} cells, EPOR signalling in cDC1s may suppress anti-tumour immunity by limiting T_{pex} cell generation in TDLNs and effector CD8$^+$ T cell function at tumour sites.

In TDLNs, tumour antigen-specific CD8$^+$ T cell priming was enhanced in *Epor*$^{\Delta Xcr1}$ mice, as indicated by greater proliferation of transferred naive OT-I cells with a T_{pex} phenotype—that is, high SLAMF6 and low TIM-3 expression (Fig. 5c). Loss of EPOR increased CD40 that is crucial for cDC1 licensing[2,64,88] on tumour antigen-carrying migratory cDC1s in TDLNs and CD80/CD86 on tumour cDC1s (Extended Data Fig. 12c–e). Accordingly, *Epor*$^{\Delta Xcr1}$ mice had more CD45$^+$ tumour-infiltrating lymphocytes (TILs), a higher percentage of CD8$^+$ T cells, and expanded SIINFEKL-H-2Kb$^+$CD8$^+$ T cells (Fig. 5d,e and Extended Data Fig. 12f,g). Exhausted PD-1$^+$TIM-3$^+$CD8$^+$ T cells decreased (Fig. 5f and Extended Data Fig. 12h), whereas TCF1$^+$TIM-3$^-$ T_{pex} cells (Fig. 5g and Extended Data Fig. 12i) and the expression of effector molecules (perforin, GZMB, IFNγ and TNF) increased (Fig. 5h and Extended Data Fig. 12j). Conventional CD4$^+$ tumour-infiltrating T cells increased, whereas FOXP3$^+$ T_{reg} cells and T-bet$^+$ CXCR3$^+$ T_{reg} cells[89–91] decreased (Fig. 5d,i,j and Extended Data Fig. 12f,k,l). Loss of EPOR also enhanced anti-PD-1 efficacy in B16F10-OVA tumours (Fig. 5k). Thus, removal of EPOR signalling in cDC1s promotes anti-tumour T cell immunity, restrains tumour growth and enhances the efficacy of immune checkpoint blockade.

Discussion

Our findings reveal that EPO–EPOR signalling in cDC1s serves as a conserved mechanism that promotes cDC1 tolerogenic maturation[5,7] and

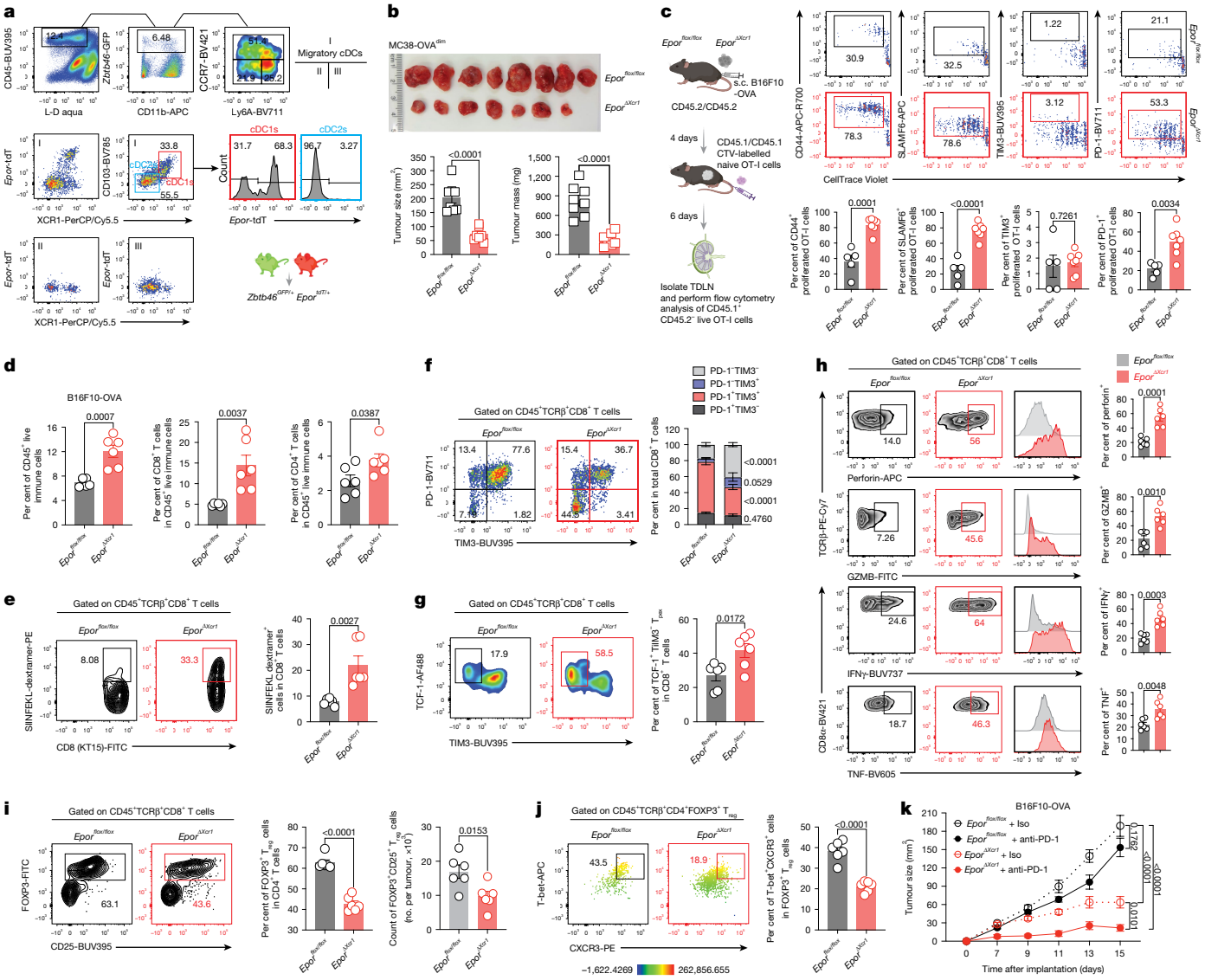

Fig. 5 | EPOR expression on cDC1s hinders antigen-specific anti-tumour T cell immunity and the loss of EPOR in cDC1s leads to tumour reduction. **a**, B16F10-OVA tumour cells were implanted subcutaneously into the flanks of *Zbtb46*$^{GFP/+}$*Epor*$^{tdT/+}$ mice, and ten days later, *Epor*-tdT expression on tumour-infiltrating cDC subsets (CCR7$^+$ versus CCR7$^-$ populations) was determined. **b**, MC38-OVA^{dim} tumour size and mass on day 14 following implantation. *Epor*$^{flox/flox}$ ($n = 8$) versus *Epor*$^{\Delta Xcr1}$ ($n = 7$). **c**, CTV-labelled naive CD45.1$^+$ OT-I cells were transferred intravenously four days after B16F10-OVA implantation. TDLNs were analysed six days later for OT-I proliferation. Representative flow plots are shown for each marker expressed on OT-I cells versus CTV dilution. Proliferating CD44$^+$CTV^{low}OT-I cells were quantified. *Epor*$^{flox/flox}$: $n = 5$; *Epor*$^{\Delta Xcr1}$: $n = 7$. **d**–**j**, B16F10-OVA tumours were implanted in *Epor*$^{flox/flox}$ ($n = 6$) or *Epor*$^{\Delta Xcr1}$ ($n = 6$) mice. TILs were analysed on day 12. **d**, Frequencies of CD45$^+$ TILs, CD8$^+$ and CD4$^+$ T cells. **e**, $OVA_{257–264}$-dextramer$^+$ CD8$^+$ T cells. **f**,**g**, Representative flow plots (left) and quantification (right) of CD8$^+$ T cells expressing TIM-3 and PD-1 (**f**) and TCF1$^+$TIM-3$^-$CD8$^+$ T cells (**g**). **h**, Representative histograms and quantification of perforin, GZMB, IFNγ and TNF expression in CD8$^+$ T cells. **i**, Frequencies and absolute cell numbers of FOXP3$^+$ T_{reg} cells in CD4$^+$ T cells with representative flow contour. **j**, Frequencies of T-bet$^+$CXCR3$^+$ T_{reg} cells in CD4$^+$FOXP3$^+$ T_{reg} cells with representative flow contour. **k**, B16F10-OVA tumour growth in *Epor*$^{flox/flox}$ versus *Epor*$^{\Delta Xcr1}$ treated with anti-PD-1 (*Epor*$^{flox/flox}$: $n = 6$; *Epor*$^{\Delta Xcr1}$: $n = 6$) or an IgG2a isotype control (*Epor*$^{flox/flox}$: $n = 6$; *Epor*$^{\Delta Xcr1}$: $n = 6$). **a**–**k**, Data are shown for one experiment, representative of at least three independent experiments with similar results. Statistical analysis was performed using unpaired two-tailed Student's *t*-test (**b**–**e**,**g**–**j**), two-way ANOVA followed by Tukey's multiple-comparison test (**f**) or Šídák's multiple-comparison test (**k**). **b**–**k**, Data are mean ± s.e.m. Diagrams in **a**,**c** were created in BioRender. Zhang, X. (2025) https://BioRender.com/mj1hkoi.

regulates cell-associated antigen-specific T cell tolerance, thus establishing a new paradigm for the tolerogenic function of cDC1s. EPOR signalling in macrophages promotes the clearance of dying cells and fosters immune tolerance[50], and EPO has been reported to suppress splenic DC function by enhancing T_{reg} cell expansion[92]. However, our study highlights cDC1 EPOR-dependent tolerogenic maturation and function in shaping both cell-associated antigen-specific CD4$^+$ and CD8$^+$ T cell adaptive immunity. Removal of EPOR on cDC1s enhances tumour antigen-specific CD8$^+$ T cell priming and profoundly affects the anti-tumour CD8$^+$ T cell immune responses in both TDLNs and tumour sites by promoting T_{pex} cell generation in TDLNs and their maintenance in TME, and effector CD8$^+$ T cell functionality. Especially noteworthy in mice lacking EPOR on cDC1s is the reduction of T-bet$^+$CXCR3$^+$ T_{reg} cells that were shown recently to inhibit costimulatory molecule expression on cDC1s[89–91], thereby restraining cDC1-mediated anti-tumour CD8$^+$ T cell immunity. Such bidirectional crosstalk between EPOR$^+$ cDC1s and T-bet$^+$CXCR3$^+$ FOXP3$^+$ T_{reg} cells is likely to represent a critical mechanism by which cDC1 EPOR signalling impedes anti-tumour CD8$^+$ T cell immunity. Therefore, in patients with cancer, blockade or removal of EPOR from cDC1s, alone or in combination

with anti-PD-1, would be expected to diminish tumour growth and spread.

Upon efferocytosis of tumour-associated antigens, cDCs upregulate CCR7[70,93] and become mature regulatory dendritic cells[70], a cDC maturational state that can be either tolerogenic or immunogenic[5,70,94,95]. cDC1s undergo tolerogenic maturation following efferocytosis[11], a process that is dependent on the expression of EPOR and markedly enhanced by TLI/ATS. EPOR signalling promotes tolerogenic maturation of cDC1s towards a CCR7$^+$ late-mature stage[7,11] with elevated expression of *Itgb8*, a crucial downstream effector of EPOR in cDC1-induced tolerance. Our findings highlight the conserved role of EPOR as a molecular switch in facilitating the tolerogenic maturation while restraining the immunogenic maturation of both PLN migratory and splenic CCR7$^+$ cDC1s. EPOR-deficient PLN migratory cDC1s were enriched for the CD4$^+$ T helper cell licensing gene signature[75], indicating that EPOR regulates cDC1 functional programming not only during maturation but also in the three-cell CD4$^+$ T cell–cDC1–CD8$^+$ T cell interaction[96], thereby regulating cDC1-mediated CD4$^+$ T helper cell licensing essential for effective CD8$^+$ T cell responses[96]. Both the frequency of EPOR-expressing cDC1s and the intensity of EPOR expression on cDC1s vary with their efferocytotic activity as well as with EPO exposure. Accordingly, the activity of these cells can be manipulated, providing a compelling rationale for developing immunotherapies that target EPOR on cDC1s, including agonists to induce tolerance in transplantation or autoimmune disease and antagonists to break tolerance and promote immunity to infection and tumours.

Online content

Any methods, additional references, Nature Portfolio reporting summaries, source data, extended data, supplementary information, acknowledgements, peer review information; details of author contributions and competing interests; and statements of data and code availability are available at https://doi.org/10.1038/s41586-025-09824-z.

1. Roquilly, A., Mintern, J. D. & Villadangos, J. A. Spatiotemporal adaptations of macrophage and dendritic cell development and function. *Annu. Rev. Immunol.* **40**, 525–557 (2022).
2. Ohara, R. A. & Murphy, K. M. The evolving biology of cross-presentation. *Semin. Immunol.* **66**, 101711 (2023).
3. Anderson, D. A. 3rd & Murphy, K. M. Models of dendritic cell development correlate ontogeny with function. *Adv. Immunol.* **143**, 99–119 (2019).
4. Idoyaga, J. et al. Specialized role of migratory dendritic cells in peripheral tolerance induction. *J. Clin. Invest.* **123**, 844–854 (2013).
5. Ardouin, L. et al. Broad and largely concordant molecular changes characterize tolerogenic and immunogenic dendritic cell maturation in thymus and periphery. *Immunity* **45**, 305–318 (2016).
6. Wohn, C. et al. Absence of MHC class II on cDC1 dendritic cells triggers fatal autoimmunity to a cross-presented self-antigen. *Sci. Immunol.* **5**, eaba1896 (2020).
7. Bosteels, V. et al. LXR signaling controls homeostatic dendritic cell maturation. *Sci. Immunol.* **8**, eadd3955 (2023).
8. Iberg, C. A., Jones, A. & Hawiger, D. Dendritic cells as inducers of peripheral tolerance. *Trends Immunol.* **38**, 793–804 (2017).
9. Scandling, J. D., Busque, S., Shizuru, J. A., Engleman, E. G. & Strober, S. Induced immune tolerance for kidney transplantation. *N. Engl. J. Med.* **365**, 1359–1360 (2011).
10. Scandling, J. D. et al. Tolerance and chimerism after renal and hematopoietic-cell transplantation. *N. Engl. J. Med.* **358**, 362–368 (2008).
11. Bosteels, V. & Janssens, S. Striking a balance: new perspectives on homeostatic dendritic cell maturation. *Nat. Rev. Immunol.* **25**, 125–140 (2024).
12. Travis, M. A. et al. Loss of integrin $\alpha_v\beta_8$ on dendritic cells causes autoimmunity and colitis in mice. *Nature* **449**, 361–365 (2007).
13. Im, S. J. et al. Defining CD8$^+$ T cells that provide the proliferative burst after PD-1 therapy. *Nature* **537**, 417–421 (2016).
14. Billingham, R. E., Brent, L. & Medawar, P. B. Actively acquired tolerance of foreign cells. *Nature* **172**, 603–606 (1953).
15. Bluestone, J. A. & Anderson, M. Tolerance in the age of immunotherapy. *N. Engl. J. Med.* **383**, 1156–1166 (2020).
16. Mehrotra, P. & Ravichandran, K. S. Drugging the efferocytosis process: concepts and opportunities. *Nat. Rev. Drug Discov.* **21**, 601–620 (2022).
17. Zelenay, S. et al. The dendritic cell receptor DNGR-1 controls endocytic handling of necrotic cell antigens to favor cross-priming of CTLs in virus-infected mice. *J. Clin. Invest.* **122**, 1615–1627 (2012).
18. Anderson, D. A. 3rd, Dutertre, C. A., Ginhoux, F. & Murphy, K. M. Genetic models of human and mouse dendritic cell development and function. *Nat. Rev. Immunol.* **21**, 101–115 (2021).
19. Ferris, S. T. et al. cDC1 prime and are licensed by CD4$^+$ T cells to induce anti-tumour immunity. *Nature* **584**, 624–629 (2020).
20. Schulz, O. & Reis e Sousa, C. Cross-presentation of cell-associated antigens by CD8alpha+ dendritic cells is attributable to their ability to internalize dead cells. *Immunology* **107**, 183–189 (2002).
21. Theisen, D. & Murphy, K. The role of cDC1s in vivo: CD8 T cell priming through cross-presentation. *F1000Res.* **6**, 98 (2017).
22. Mellman, I., Chen, D. S., Powles, T. & Turley, S. J. The cancer-immunity cycle: Indication, genotype, and immunotype. *Immunity* **56**, 2188–2205 (2023).
23. Schenkel, J. M. et al. Conventional type I dendritic cells maintain a reservoir of proliferative tumor-antigen specific TCF-1$^+$ CD8$^+$ T cells in tumor-draining lymph nodes. *Immunity* **54**, 2338–2353.e6 (2021).
24. Spranger, S., Dai, D., Horton, B. & Gajewski, T. F. Tumor-residing Batf3 dendritic cells are required for effector T cell trafficking and adoptive T cell therapy. *Cancer Cell* **31**, 711–723.e4 (2017).
25. Zagorulya, M. & Spranger, S. Once upon a prime: DCs shape cancer immunity. *Trends Cancer* **9**, 172–184 (2023).
26. Murphy, T. L. & Murphy, K. M. Dendritic cells in cancer immunology. *Cell. Mol. Immunol.* **19**, 3–13 (2022).
27. Meiser, P. et al. A distinct stimulatory cDC1 subpopulation amplifies CD8$^+$ T cell responses in tumors for protective anti-cancer immunity. *Cancer Cell* **41**, 1498–1515.e10 (2023).
28. Bottcher, J. P. & Reis e Sousa, C. The role of type 1 conventional dendritic cells in cancer immunity. *Trends Cancer* **4**, 784–792 (2018).
29. Broz, M. L. et al. Dissecting the tumor myeloid compartment reveals rare activating antigen-presenting cells critical for T cell immunity. *Cancer Cell* **26**, 938 (2014).
30. Roberts, E. W. et al. Critical Role for CD103$^+$/CD141$^+$ dendritic cells bearing CCR7 for tumor antigen trafficking and priming of T cell immunity in melanoma. *Cancer Cell* **30**, 324–336 (2016).
31. Balan, S., Radford, K. J. & Bhardwaj, N. Unexplored horizons of cDC1 in immunity and tolerance. *Adv. Immunol.* **148**, 49–91 (2020).
32. Silva-Sanchez, A. et al. Activation of regulatory dendritic cells by Mertk coincides with a temporal wave of apoptosis in neonatal lungs. *Sci. Immunol.* **8**, eadc9081 (2023).
33. Liu, K. et al. Immune tolerance after delivery of dying cells to dendritic cells in situ. *J. Exp. Med.* **196**, 1091–1097 (2002).
34. Canesso, M. C. C Identification of antigen-presenting cell–T cell interactions driving immune responses to food. *Science* **387**, eado5088 (2024).
35. Rudnitsky, A. et al. A coordinated cellular network regulates tolerance to food. *Nature* **644**, 231–240 (2025).
36. Gargaro, M. et al. Indoleamine 2,3-dioxygenase 1 activation in mature cDC1 promotes tolerogenic education of inflammatory cDC2 via metabolic communication. *Immunity* **55**, 1032–1050.e1014 (2022).
37. Blanco, T. et al. Conventional type I migratory CD103$^+$ dendritic cells are required for corneal allograft survival. *Mucosal Immunol.* **16**, 711–726 (2023).
38. Hongo, D., Tang, X., Zhang, X., Engleman, E. G. & Strober, S. Tolerogenic interactions between CD8$^+$ dendritic cells and NKT cells prevent rejection of bone marrow and organ grafts. *Blood* **129**, 1718–1728 (2017).
39. Slavin, S., Strober, S., Fuks, Z. & Kaplan, H. S. Long-term survival of skin allografts in mice treated with fractionated total lymphoid irradiation. *Science* **193**, 1252–1254 (1976).
40. Crozat, K. et al. The XC chemokine receptor 1 is a conserved selective marker of mammalian cells homologous to mouse CD8α$^+$ dendritic cells. *J. Exp. Med.* **207**, 1283–1292 (2010).
41. Hildner, K. et al. Batf3 deficiency reveals a critical role for CD8α$^+$ dendritic cells in cytotoxic T cell immunity. *Science* **322**, 1097–1100 (2008).
42. Grajales-Reyes, G. E. et al. Batf3 maintains autoactivation of Irf8 for commitment of a CD8α$^+$ conventional DC clonogenic progenitor. *Nat. Immunol.* **16**, 708–717 (2015).
43. Satpathy, A. T. et al. Zbtb46 expression distinguishes classical dendritic cells and their committed progenitors from other immune lineages. *J. Exp. Med.* **209**, 1135–1152 (2012).
44. Wu, X. et al. Mafb lineage tracing to distinguish macrophages from other immune lineages reveals dual identity of Langerhans cells. *J. Exp. Med.* **213**, 2553–2565 (2016).
45. Zhang, H. et al. EpoR-tdTomato-Cre mice enable identification of EpoR expression in subsets of tissue macrophages and hematopoietic cells. *Blood* **138**, 1986–1997 (2021).
46. Kuhrt, D. & Wojchowski, D. M. Emerging EPO and EPO receptor regulators and signal transducers. *Blood* **125**, 3536–3541 (2015).
47. Alaluf, E. et al. Heme oxygenase-1 orchestrates the immunosuppressive program of tumor-associated macrophages. *JCI insight* **5**, e133929 (2020).
48. Consonni, F. M. et al. Heme catabolism by tumor-associated macrophages controls metastasis formation. *Nat. Immunol.* **22**, 595–606 (2021).
49. Doran, A. C., Yurdagul, A. Jr & Tabas, I. Efferocytosis in health and disease. *Nat. Rev. Immunol.* **20**, 254–267 (2020).
50. Luo, B. et al. Erythropoeitin signaling in macrophages promotes dying cell clearance and immune tolerance. *Immunity* **44**, 287–302 (2016).
51. Dikiy, S. & Rudensky, A. Y. Principles of regulatory T cell function. *Immunity* **56**, 240–255 (2023).
52. Scandling, J. D. et al. Macrochimerism and clinical transplant tolerance. *Hum. Immunol.* **79**, 266–271 (2018).
53. Ehst, B. D., Ingulli, E. & Jenkins, M. K. Development of a novel transgenic mouse for the study of interactions between CD4 and CD8 T cells during graft rejection. *Am. J. Transplant.* **3**, 1355–1362 (2003).
54. Hashimoto, K., Joshi, S. K. & Koni, P. A. A conditional null allele of the major histocompatibility IA-beta chain gene. *Genesis* **32**, 152–153 (2002).
55. Strober, S. Use of hematopoietic cell transplants to achieve tolerance in patients with solid organ transplants. *Blood* **127**, 1539–1543 (2016).
56. Moon, J. J. et al. Naive CD4$^+$ T cell frequency varies for different epitopes and predicts repertoire diversity and response magnitude. *Immunity* **27**, 203–213 (2007).
57. Shao, T. Y. et al. Reproductive outcomes after pregnancy-induced displacement of preexisting microchimeric cells. *Science* **381**, 1324–1330 (2023).

58. Liu, F. T. & Stowell, S. R. The role of galectins in immunity and infection. *Nat. Rev. Immunol.* **23**, 479–494 (2023).
59. Gonzales, G. A. et al. The pore-forming apolipoprotein APOL7C drives phagosomal rupture and antigen cross-presentation by dendritic cells. *Sci. Immunol.* **9**, eadn2168 (2024).
60. Wild, A. B. et al. CD83 orchestrates immunity toward self and non-self in dendritic cells. *JCI Insight* **4**, e126246 (2019).
61. Sisirak, V. et al. Digestion of chromatin in apoptotic cell microparticles prevents autoimmunity. *Cell* **166**, 88–101 (2016).
62. Mucida, D. et al. Retinoic acid can directly promote TGF-β-mediated Foxp3$^+$ Treg cell conversion of naive T cells. *Immunity* **30**, 471–472 (2009).
63. Larange, A. & Cheroutre, H. Retinoic acid and retinoic acid receptors as pleiotropic modulators of the immune system. *Annu. Rev. Immunol.* **34**, 369–394 (2016).
64. Wu, R. et al. Mechanisms of CD40-dependent cDC1 licensing beyond costimulation. *Nat. Immunol.* **23**, 1536–1550 (2022).
65. Forster, R., Davalos-Misslitz, A. C. & Rot, A. CCR7 and its ligands: balancing immunity and tolerance. *Nat. Rev. Immunol.* **8**, 362–371 (2008).
66. Ohl, L. et al. CCR7 governs skin dendritic cell migration under inflammatory and steady-state conditions. *Immunity* **21**, 279–288 (2004).
67. Azukizawa, H. et al. Steady state migratory RelB$^+$ langerin$^+$ dermal dendritic cells mediate peripheral induction of antigen-specific CD4$^+$CD25$^+$ Foxp3$^+$ regulatory T cells. *Eur. J. Immunol.* **41**, 1420–1434 (2011).
68. Brown, H., Komnick, M. R., Brigleb, P. H., Dermody, T. S. & Esterhazy, D. Lymph node sharing between pancreas, gut, and liver leads to immune crosstalk and regulation of pancreatic autoimmunity. *Immunity* **56**, 2070–2085.e11 (2023).
69. Cruz de Casas, P., Knopper, K., Dey Sarkar, R. & Kastenmuller, W. Same yet different — how lymph node heterogeneity affects immune responses. *Nat. Rev. Immunol.* **24**, 358–374 (2023).
70. Maier, B. et al. A conserved dendritic-cell regulatory program limits antitumour immunity. *Nature* **580**, 257–262 (2020).
71. Dixon, K. O. et al. TIM-3 restrains anti-tumour immunity by regulating inflammasome activation. *Nature* **595**, 101–106 (2021).
72. Kretzer, N. M. et al. RAB43 facilitates cross-presentation of cell-associated antigens by CD8α$^+$ dendritic cells. *J. Exp. Med.* **213**, 2871–2883 (2016).
73. Roche, P. A. & Furuta, K. The ins and outs of MHC class II-mediated antigen processing and presentation. *Nat. Rev. Immunol.* **15**, 203–216 (2015).
74. Jinushi, M. et al. MFG-E8-mediated uptake of apoptotic cells by APCs links the pro- and antiinflammatory activities of GM-CSF. *J. Clin. Invest.* **117**, 1902–1913 (2007).
75. Lei, X. et al. CD4$^+$ helper T cells endow cDC1 with cancer-impeding functions in the human tumor micro-environment. *Nat. Commun.* **14**, 217 (2023).
76. Bonacina, F. et al. Myeloid apolipoprotein E controls dendritic cell antigen presentation and T cell activation. *Nat. Commun.* **9**, 3083 (2018).
77. Kool, M. et al. The ubiquitin-editing protein A20 prevents dendritic cell activation, recognition of apoptotic cells, and systemic autoimmunity. *Immunity* **35**, 82–96 (2011).
78. Reith, W., LeibundGut-Landmann, S. & Waldburger, J. M. Regulation of MHC class II gene expression by the class II transactivator. *Nat. Rev. Immunol.* **5**, 793–806 (2005).
79. Theisen, D. J. et al. WDFY4 is required for cross-presentation in response to viral and tumor antigens. *Science* **362**, 694–699 (2018).
80. Mortier, E. et al. Macrophage- and dendritic-cell-derived interleukin-15 receptor alpha supports homeostasis of distinct CD8$^+$ T cell subsets. *Immunity* **31**, 811–822 (2009).
81. Pittet, M. J., Di Pilato, M., Garris, C. & Mempel, T. R. Dendritic cells as shepherds of T cell immunity in cancer. *Immunity* **56**, 2218–2230 (2023).
82. Prokhnevska, N. et al. CD8$^+$ T cell activation in cancer comprises an initial activation phase in lymph nodes followed by effector differentiation within the tumor. *Immunity* **56**, 107–124.e105 (2023).
83. Huang, Q. et al. The primordial differentiation of tumor-specific memory CD8(+) T cells as bona fide responders to PD-1/PD-L1 blockade in draining lymph nodes. *Cell* **185**, 4049–4066.e4025 (2022).
84. Jansen, C. S. et al. An intra-tumoral niche maintains and differentiates stem-like CD8 T cells. *Nature* **576**, 465–470 (2019).
85. Siddiqui, I. et al. Intratumoral Tcf1$^+$PD-1$^+$CD8$^+$ T cells with stem-like properties promote tumor control in response to vaccination and checkpoint blockade immunotherapy. *Immunity* **50**, 195–211.e110 (2019).
86. Miller, B. C. et al. Subsets of exhausted CD8$^+$ T cells differentially mediate tumor control and respond to checkpoint blockade. *Nat. Immunol.* **20**, 326–336 (2019).
87. Rahim, M. K. et al. Dynamic CD8$^+$ T cell responses to cancer immunotherapy in human regional lymph nodes are disrupted in metastatic lymph nodes. *Cell* **186**, 1127–1143.e18 (2023).
88. Borst, J., Ahrends, T., Babala, N., Melief, C. J. M. & Kastenmuller, W. CD4$^+$ T cell help in cancer immunology and immunotherapy. *Nat. Rev. Immunol.* **18**, 635–647 (2018).
89. Zagorulya, M. et al. Tissue-specific abundance of interferon-gamma drives regulatory T cells to restrain DC1-mediated priming of cytotoxic T cells against lung cancer. *Immunity* **56**, 386–405.e10 (2023).
90. Ramirez, D. E. & Turk, M. J. Th1-like Treg cells are dressed to suppress anti-tumor immunity. *Immunity* **56**, 1437–1439 (2023).
91. Moreno Ayala, M. A. et al. CXCR3 expression in regulatory T cells drives interactions with type I dendritic cells in tumors to restrict CD8$^+$ T cell antitumor immunity. *Immunity* **56**, 1613–1630.e5 (2023).
92. Wei, X. et al. Erythropoietin protects against murine cerebral malaria through actions on host cellular immunity. *Infect. Immun.* **82**, 165–173 (2014).
93. Zhang, Q. et al. Landscape and dynamics of single immune cells in hepatocellular carcinoma. *Cell* **179**, 829–845.e20 (2019).
94. Magen, A. et al. Intratumoral dendritic cell-CD4$^+$ T helper cell niches enable CD8$^+$ T cell differentiation following PD-1 blockade in hepatocellular carcinoma. *Nat. Med.* **29**, 1389–1399 (2023).
95. Mair, F. et al. Extricating human tumour immune alterations from tissue inflammation. *Nature* **605**, 728–735 (2022).
96. Wu, R. & Murphy, K. M. DCs at the center of help: origins and evolution of the three-cell-type hypothesis. *J. Exp. Med.* **219**, e20211519 (2022).

[1]Department of Pathology, School of Medicine, Stanford University, Palo Alto, CA, USA. [2]Parker Institute for Cancer Immunotherapy, San Francisco, CA, USA. [3]Department of Genetics, School of Medicine, Stanford University, Palo Alto, CA, USA. [4]Department of Medicine, Division of Blood and Marrow Transplantation and Cellular Therapy, School of Medicine, Stanford University, Palo Alto, CA, USA. [5]Department of Pathology and Neuropathology, University Hospital and Comprehensive Cancer Center Tübingen, Tübingen, Germany. [6]Cluster of Excellence iFIT (EXC 2180), Image-Guided and Functionally Instructed Tumor Therapies, University of Tübingen, Tübingen, Germany. [7]Department of Otolaryngology-Head and Neck Surgery, School of Medicine, Stanford University, Stanford, CA, USA. [8]Department of Biomedical Engineering, Duke University, Durham, NC, USA. [9]Department of Dermatology, University of California, San Francisco, San Francisco, CA, USA. [10]Division of Pulmonary, Critical Care, Allergy and Sleep, Department of Medicine, University of California, San Francisco, San Francisco, CA, USA. [11]CIRI, Centre International de Recherche en Infectiologie, Université de Lyon, Inserm U1111, Université Claude Bernard Lyon 1, CNRS UMR5308, ENS de Lyon, Lyon, France. [12]ImmunEdge, Redwood City, CA, USA. [13]Laboratory of Membrane Biology, New York Blood Center, New York, NY, USA. [14]Department of Immunology, Leiden University Medical Center, Leiden, The Netherlands. [15]Department of Immunology, St Jude Children's Research Hospital, Memphis, TN, USA. [16]Division of Infectious Diseases, Center for Inflammation and Tolerance, Cincinnati Children's Hospital Medical Center, Department of Pediatrics, University of Cincinnati College of Medicine, Cincinnati, OH, USA. [17]Centre d'Immunologie de Marseille-Luminy, Aix-Marseille Université, INSERM, CNRS, Marseille, France. [18]Department of Medicine (Immunology and Rheumatology), School of Medicine, Stanford University, Palo Alto, CA, USA. [19]Stanford Cancer Institute, School of Medicine, Stanford University, Palo Alto, CA, USA. [20]Deceased: Samuel Strober. ✉e-mail: xiangyue@stanford.edu; edgareng@stanford.edu

Methods

Mice

The following mice were obtained from The Jackson Laboratory: Adult 8-to-10-week-old male wild-type BALB/cJ (H-2K^{d}) (Jackson, 000651) and C57BL/6J (H-2K^{b}) (Jackson, 000664), B6.129S(C)-Batf3tm1Kmm/J (*Batf3*$^{-/-}$) (Jackson, 013755), B6.129P2(C)-Ccr7tm1Rfor/J (*Ccr7*−) (Jackson, 006621), Zbtb46 tm1.1Kmm/J (*Zbtb46*^{GFP}) (Jackson, 027618), B6N(129S4)-Mafbtm1.1 (cre) Kmm/J (MafB-mCherry-Cre) (Jackson, 029664), C57BL/6-Tg (CAG-OVA) 916Jen/J (Act-mOVA) (Jackson, 005145), C57BL/6-Tg(TcraTcrb)1100Mjb/J (OT-I) (Jackson, 003831), C57BL/6-Tg (TcraTcrb) 425Cbn/J (OT-II) (Jackson, 004194), B6.129(Cg)-Foxp3tm3(HBEGF/GFP)Ayr/J (*Foxp3*-DTR) (Jackson, 016958), CByJ.SJL(B6)-Ptprca/J (CD45.1) (Jackson, 006584) and H2-Ab1^{fl} (B6.129×1-H2-Ab1^{tm1Koni}/J) (Jackson, 013181). *Foxp3*$^{DTR/DTR}$ mice (ref. 97) were cross bred with CD45.1 mice to generate CD45.1/CD45.1 *Foxp3*$^{DTR/DTR}$ mice. OT-I or OT-II mice were cross bred with CD45.1 to generate CD45.1/CD45.1 OT-I or OT-II mice. *Epor*$^{flox/flox}$ mice[50] (provided by H. Wu), Epor-tdT-Cre mice were generated as previously described[45]. *Xcr1*$^{cre\text{-}mTFP1}$ mice[6] (provided by B. Malissen), were generated with JM8.F6 ES cells and were originally on a C57BL6/N background. They were then backcrossed for more than eight generations onto C57BL6/J mice, resulting in a pure C57BL6/J background before breeding with *flox/flox* mice. *Epor*$^{flox/flox}$ mice were generated on an Sv129/C57BL/6 background and were backcrossed onto the C57BL6/J strain for more than eight generations before crossed with *Xcr1*$^{cre\text{-}mTFP1}$ to generate cDC1-specific *Epor* genetically deleted (*Epor*$^{\Delta Xcr1}$) mice. Sex-matched littermates of *Epor*$^{\Delta Xcr1}$ and *Epor*$^{flox/flox}$ mice were utilized for each experiment. *Epor*$^{\Delta Xcr1}$ mice did not develop anaemia, maintained normal levels of red blood cells (7–10 million per microlitre), haematocrit (40–50%), haemoglobin (12–15 g dl^{-1}) and reticulocytes (1–6%) in peripheral blood and displayed no differences in these parameters in comparison with *Epor*$^{flox/flox}$ mice. *Itgb8*$^{flox/flox}$ (ref. 12), *Itgb8*$^{\Delta Xcr1}$ (ref. 98), *Aldh1a2*$^{flox/flox}$ and *Aldh1a2*$^{\Delta CD11c}$ (ref. 99), 2W1S$_{52-68}$-expressing BALB/c (H-2K^{d})[56] have been previously described. *Epor*$^{tdT/tdT}$ mice were bred with *Zbtb46*$^{GFP/GFP}$ to generate dual-colour reporter *Zbtb46*$^{GFP/+}$*Epor*$^{tdT/+}$. *Epor*$^{tdT/tdT}$ mice were bred with *Ccr7*$^{-/-}$ or *Batf3*$^{-/-}$ mice to generate *Ccr7*$^{-/-}$*Epor*$^{tdT/+}$ or *Batf3*$^{-/-}$*Epor*$^{tdT/+}$ mice. Bone marrow cells from BALB/cJ (H-2K^{d}) or 2W1S$_{52-68}$-expressing BALB/c (H-2K^{d}) mice were used for determining bone marrow chimerism following combined allogeneic heart and bone marrow transplantation. Newborn BALB/cJ (H-2K^{d}) mice as allogeneic heart donors were obtained from Charles River Laboratories. Unless otherwise specified, experiments were performed with mice between 6 and 10 weeks of age. No differences were observed between male and female mice in any assays performed, and so mice of both sexes were used interchangeably throughout the study. Within individual experiments, mice used were age- and sex-matched littermates whenever possible. Mice were housed in animal facilities accredited by the Association for Assessment and Accreditation of Laboratory Animal Care (AAALAC). All experimental procedures were approved by the Institutional Animal Care and Use Committee (IACUC) at Stanford University (protocols APLAC-28636 and APLAC-17466) and conducted in accordance with Stanford University's animal care guidelines.

Bone marrow transplantation, rabbit ATS and TLI

Bone marrow collection and transplantation procedures were performed as previously described[38]. C57BL/6J background recipients were injected intraperitoneally with 0.05 ml of rabbit anti-thymocyte serum (ATS) (AIA3940T/20, Accurate Chemical and Scientific) in 0.5 ml of saline on days 0, 2, 6, 8 and 10. Using a 250-Kv X-ray machine, TLI was delivered to the lymph nodes above and below the diaphragm, thymus and spleen with lead shielding of the skull, limbs, pelvis and tail. A dose of 240 cGy was administered 5 times per week for 2 weeks. The last dose of TLI was administered to recipient mice 24 h before the infusion of allo-bone marrow cells from BALB/cJ or 2W1S$_{52-68}$-expressing BALB/c (H-2K^{d+}) mice. On the next day following the last dose of TLI/ATS, 30×10^6 BALB/c donor bone marrow cells were injected intravenously to deplete FOXP3^{+} T$_{reg}$ cells in adoptively transferred CD45.1^{+} *Foxp3*$^{DTR/DTR}$ CD4^{+} T cells in *Epor*$^{flox/flox}$ and *Epor*$^{\Delta Xcr1}$ mice prior to TLI/ATS treatment. Recipient mice were adoptively transferred with 30×10^6 CD45.1/CD45.1 *Foxp3*$^{DTR/DTR}$ CD4^{+} T cells that were purified by magnetic-activated cell sorting (MACS) with CD4^{+} T Cell Isolation Kit (130-104-454, Miltenyi Biotec). Following the transfer, the mice were injected intraperitoneally with purified diphtheria toxin (D0564, Sigma-Aldrich) at a dosage of 0.5 μg per day for 2 consecutive days or with PBS as control.

Bone marrow chimerism analysis, heart transplantation and monitoring for graft survival

Analysis of chimerism in the blood was performed by flow cytometry using multi-colour staining of total white blood cells or cell subsets with anti-H-2K^{d} monoclonal antibody as described[38]. Anti-MHCI (2 K^{d}), anti-Ly6G (granulocytes), anti-TCRβ (T cells), anti-CD64 (macrophages) and anti-B220 (B cells) were used to identify immune cell types. Neonatal BALB/c heart grafts were transplanted into a pouch in the ear pinna of C57BL/6, *Epor*$^{flox/flox}$, *Batf3*$^{-/-}$ and *Epor*$^{\Delta Xcr1}$ hosts at least 21 days after bone marrow infusion, as described previously[38]. Grafted heart survival was assessed by daily palpation, and rejection was determined by cessation of heartbeat. Heart grafts that failed within 72 h were excluded from the experimental groups as 'technical failures'.

Bone marrow chimeras

Bone marrow chimeras were generated by retro-orbitally injecting 4×10^6 total donor bone marrow cells into lethally irradiated 8-week-old recipient mice (two doses of 5.5 Gy administered 6 h apart). Recipients were supplemented for 3 weeks with UNIPRIM Trimethoprim and Sulfadiazine supplied by Stanford Veterinary Service Center (VSC). Mice were allowed eight weeks for reconstitution before experimental use. Successful reconstitution (minimum 90%) was assessed by flow cytometry analysis of peripheral blood.

Flow cytometry

For surface staining, cells were preincubated with anti-Fc receptor antibody (BE0307, Bio X Cell) and stained with appropriate antibodies in PBS containing 5 mM EDTA and 2% fetal bovine serum (FBS) at 4 °C for 25 min. Viability was assessed by staining with 4′,6-diamidino-2-phenylindole (D1306, Thermo Fisher Scientific) or Fixable LIVE/DEAD Blue (L23105, Thermo Fisher Scientific) or Aqua (L34957, Thermo Fisher Scientific) Cell Stain. For intracellular cytokine detection, cells were stimulated for 4–5 h with phorbol 12-myristate 13-acetate (PMA) and ionomycin in the presence of monensin, eBioscience Cell Stimulation Cocktail (plus protein transport inhibitors) (00-4975-93, Thermo Fisher Scientific) before staining according to the manufacturer's instructions. For intracellular cytokine staining, cells were stained with antibodies against surface markers and then fixed with 2% (w/v) paraformaldehyde for 12 min at 25 °C and permeabilized using eBioscience Permeabilization Buffer (00-8333-56, Thermo Fisher Scientific). The fixed and permeabilized cells were subsequently stained with anti-IFNγ-BUV737 (XMG1.2, 612769, BD Biosciences, 1:100) or anti-TNF-BV605 (MP6-XT22, 506329, BioLegend, 1:100) antibody for 60 min at 4 °C. For intranuclear staining, cells were stained with antibodies against specified surface markers, and fixation–permeabilization was performed using the eBioscience FOXP3/Transcription Factor Staining Buffer Set (00-5523-00, Thermo Fisher Scientific) according to the manufacturer's instructions. Flow cytometry was performed on a LSRFortessa X-20 or FACSymphony A5 Cell Analyzer (BD Biosciences) with BD FACSDiva (v.8), and data were analysed with FlowJo (v.10.10.0, BD Biosciences). Doublets and dead cells were excluded from analyses. Biotin-conjugated antibodies were detected using streptavidin-conjugated Brilliant Violet 421 (405225, BioLegend, 1:400). For detection of phosphorylated proteins, cells were stimulated and immediately fixed with Phosflow Lyse/Fix

buffer (558049, BD Biosciences), followed by permeabilization with Phosflow Perm buffer III (558050, BD Biosciences), and staining with antibodies to phosphor-signalling molecules. Tumour antigen-specific T cells were determined by H-2K^b/OVA$_{257–264}$ PE dextramer (JD02163-PE, 1:100) staining following the manufacturer's protocol (Immudex). Cell counting was performed by using 123count eBeads Counting Beads (01-1234-42, Invitrogen). The following anti-mouse antibodies (Target, fluorophore, clone, catalogue number and manufacturer; all antibodies were used at a 1:200 dilution unless otherwise noted) were used: CD11c-PE/Cy7 (N418, 117318, BioLegend), CD11c-BV711 (N418, 117349, BioLegend), MHCII (I-A/I-E)-APC (M5/114.15.2, 107614, BioLegend), MHCII (I-A/I-E)-APC/Cy7 (M5/114.15.2, 107628, BioLegend), MHCII (I-A/I-E)-BV510 (M5/114.15.2, 107636, BioLegend), CD8α-BV785 (53-6.7, 100750, BioLegend), CD8α-BV421 (53-6.7, 100738, BioLegend), CD8β-PE/Cy7 (YTS156.7.7, 126616, BioLegend), XCR1-PerCP/Cy5.5 (ZET, 148208, BioLegend), XCR1-BV785 (ZET, 148225, BioLegend), CD172a (SIRPα)-FITC (P84, 144006, BioLegend), CD172a (SIRPα)-BUV395 (P84, 740282, BD Biosciences), CD172a (SIRPα)-BV421 (P84, 740071, BD Biosciences), CD172a (SIRPα)-BUV661 (P84, 741593, BD Biosciences), CD103-BV421 (2E7, 121422, BioLegend), B220/CD45R-FITC (RA3-6B2, 103206 BioLegend), B220/CD45R-APC (RA3-6B2, 103212, BioLegend), CD19-APC (6D5, 115512, BioLegend), CD19-FITC (1D3/CD19, 152404, BioLegend), CD19-PE/Cy7 (6D5, 115520, BioLegend), SiglecH-BV605 (440c, 747673, BD Biosciences), SiglecH-APC (551, 129612, BioLegend), PDCA-1 (CD317, BST2)-BV711 (927, 127039, BioLegend), PDCA-1 (CD317, BST2)-APC (927, 127016, BioLegend), CD11b-FITC (M1/70, 101206, BioLegend), CD11b-BUV737 (M1/70, 741722, BD Biosciences), Ki67-BV605 (SolA15, 406-5698-82, eBioscience), IRF8-PE (V3GYWCH, 12-9852-82, eBioscience), TER119-APC (TER119, 116212, BioLegend), TER119-FITC (TER119, 116206, BioLegend), CD71-PerCP/Cy5.5 (RI7217, 113816, BioLegend), TCRβ-PE/Cy7 (H57-597, 109222, BioLegend), TCRβ-BV421 (H57-597, 109229, BioLegend), TCRβ-PE/Cy5 (H57-597, 109210, BioLegend), CD64-PE (X54-5/7.1, 139304, BioLegend), CD64-BV711 (X54-5/7.1, 139311, BioLegend), LY6G-PE/Cy7 (1A8, 127618, BioLegend), Ly6C-BV421(AL-21, 562727, BD Biosciences), Ly6C-PerCP/Cy5.5 (HK1.4, 128012, BioLegend), F4/80-BUV395 (T45-2342, 565614, BD Biosciences), F4/80-BV711 (T45-2342, 565612, BD Biosciences), NK1.1-BV711 (PK136, 108745, BioLegend), NK1.1-FITC (PK136, 108706, BioLegend), NK1.1-APC (PK136, 108710, BioLegend), CD49b-APC (DX5, 108910, BioLegend), Siglec-F (CD170)-APC (S17007L, 155508, BioLegend), H-2K^d-PerCP-eFluor 710 (SF1-1.1.1, 50-245-930, eBioscience), H-2K^b-PE (AF6-88.5, 561072, BD Biosciences), CD3ε-PE/Cy7 (500A2, 152314, BioLegend), CD3ε-APC (500A2, 152306, BioLegend), CD4-BUV737 (RM4-5, 612844, BD Biosciences), CD25-BUV395 (PC61, 564022, BD Biosciences), CD44-APC-R700 (IM7, 565480, BD Biosciences), CD62L-BV711 (MEL-14, 104445, BioLegend), CD326 (EpCAM)-PE/Cy7 (G8.8, 118216, BioLegend), CD40-APC (3/23, 558695, BD Biosciences), CD80-BV421 (16-10A1, 562611, BD Biosciences), CD86-BV785 (GL-1, 105043, BioLegend), CD274 (PD-L1)-BV421 (10 F.9G2, 124315, BioLegend), CD205 (DEC205) (V18-949, 566376, BD Biosciences), Axl-APC (MAXL8DS, 17-1084-82, eBioscience), CD131-BV421 (JORO50, 740050, BD Biosciences), CCR7-Biotin (4B12, 13-1971-82, eBioscience, 1:100), CD24-BV615 (30-F1, 752769, BD Biosciences), CD40-BV750 (3/23, 746970, BD Biosciences), CD80-BUV563 (16-10A1, 741272, BD Biosciences), CD86-BV510 (PO3, 745059, BD Biosciences), MHCII (I-A/I-E)-Alexa Fluor 700 (M5/114.15.2, 107622, BioLegend), CD274 (PD-L1)-BV605 (10 F.9G2, 124321, BioLegend), CXCR3 (CD183)-PE (CXCR3-173, 126506, BioLegend), CD45.1-BV785 (A20, 110732, BioLegend), CD45.2-BV650 (104, 109836, BioLegend), CD45-BV785 (30-F11, 103149, BioLegend), CD45-BUV395 (30-F11, 564279, BD Biosciences), CD3-PE/Cy7 (17A2, 100220, BioLegend), TCRvα2-APC (B20.1, 127810, BioLegend), CD279 (PD-1)-BV711 (29 F.1A12, 135231, BioLegend), Granzyme B-FITC (GB11, 515403, BioLegend), TIM-3 (CD366)-BUV395 (5D12/TIM-3, 747620, BD Biosciences), Ly108 (SLAMF6)-APC (eBio13G3-19D (13G3-19D), 17-1508-82, eBioscience), FOXP3-FITC (FJK-16s, 11-5773-82, eBioscience, 1:100), TCF1/TCF7 (C63D9, 2203S, Cell Signaling Technology), AF488 Donkey anti-rabbit IgG (Poly4064, 406416, BioLegend), T-bet-APC (eBio4B10 (4B10); 17-5825-82, eBioscience, 1:100), Bcl-xL-PE (54H6, 13835S, Cell Signaling Technology), Phospho-S6 Ribosomal Protein (Ser235/236)-PE (D57.2.2E, 5316S, Cell Signaling Technology, 1:50), Phospho-Akt (Ser473)-PE (D9E, 5315S, Cell Signaling Technology, 1:50), Phospho-4E-BP1 (Thr37/46)-PE (236B4, 7547S, Cell Signaling Technology1:50), Phosph-p44/42 MAPK (Erk1/2) (Thr202/Tyr204)-PE (197G2, 14095S, Cell Signaling Technology, 1:50), Phosph-Stat5 (pY694)-PE (47, 562077, BD Biosciences, 1:50).

Mouse EPO ELISA

Blood serum was collected at different time points, and serum EPO was measured by enzyme-linked immunosorbent assay (ELISA) according to the manufacturer's instructions (Mouse EPO ELISA Kit, EM28RB, Invitrogen).

Isolation and purification of XCR1$^+$CD8α$^+$ cDC1s and *Epor*-tdT$^+$ and *Epor*-tdT$^-$ cDC1s

Spleens were minced and digested in 5 ml Iscove's modified Dulbecco's media + 10% FCS (cIMDM) with 250 μg ml^{-1} collagenase D (Worthington) and 30 U ml^{-1} DNase I (Sigma-Aldrich) for 30 min at 37 °C with stirring. Cells were passed through a 100-μm strainer before red blood cells were lysed with RBC lysis buffer (420302, BioLegend). A total of 5 to 10 × 10^6 cells was used per antibody staining reaction. For further XCR1$^+$CD8α$^+$ sorting, single spleen cell suspensions were negatively selected with MACS columns with mouse Pan Dendritic Cell Isolation Kit (130-100-875, Miltenyi Biotec). MACS-selected dendritic cells were further sorted by FACS (BD, FACSAria II), to obtain B220$^-$SiglecH$^-$PDCA-1$^-$CD11c^{hi} MHCII^{hi}XCR1$^+$CD8α$^+$ cDC1s purity>99%. *Epor*-tdT$^+$ and *Epor*-tdT$^-$ XCR1$^+$CD8α$^+$ cDC1s were prepared and sorted from *Epor*$^{tdT/tdT}$ mice following TLI/ATS with similar methods.

RNA-seq analysis

Fresh splenic live cDC1s were purified first from single spleen cell suspensions with negative selection by using mouse Pan Dendritic Cell Isolation Kit (130-100-875, Miltenyi Biotec). MACS-selected dendritic cells were further sorted by FACS (BD, FACSAria II), to obtain live/dead blue$^-$Lin$^-$ SiglecH$^-$PDCA-1$^-$CD11c^{hi}MHCII^{hi}CD8α$^+$CD11b$^-$ cDC1s (purity >98%). FACS-purified cDC1s from untreated or TLI/ATS-treated wild-type C57BL/6J mice (8 to 10 weeks of age) were used for total RNA isolation with RNeasy Plus Micro Kit (74034, QIAGEN) and submitted for RNA-seq analysis. RNA-seq was performed by the Stanford Functional Genomics Facility. The RNA-seq read count matrix was generated through the following steps: (1) Trimmomatic[100] (v.0.36) was applied to trim the 76 bp paired-end sequencing reads to get rid of low-quality bases and/or adaptor contaminations. (2) HISAT2[101] (v.2.1.0; http://daehwankimlab.github.io/hisat2/) was used to map the trimmed FASTQ reads to the *Mus musculus* GRCm38 reference genome (the index files of genome_tran were downloaded from https://cloud.biohpc.swmed.edu/index.php/s/grcm38_tran/download). (3) SAMtools (v.1.16.1) were used to sort and convert the aligned SAM files to aligned BAM files. (4) Gene-level expression abundance for each sample was quantified from aligned BAM files using featureCounts (v.2.0.3). In Fig. 1e,f,k,l, differential expression analyses between the TLI/ATS-treated and untreated groups were performed using R package DESeq2[102] (v.1.46.0). Genes with adjusted *P* values < 0.05 (Benjamini–Hochberg correction) and $\log_2$ fold changes >1 were considered differentially expressed in comparisons. In, Fig. 1k,l, *Epor*-tdT$^+$ or *Epor*-tdT$^-$Lin$^-$CD11c^{hi}MHCII^{hi}XCR1$^+$ CD8α$^+$ cDC1s were purified by FACS from *Epor*$^{tdT/tdT}$ mice following TLI/ATS conditioning. RNA was isolated by using RNeasy Plus Micro Kit (74034, QIAGEN) and subjected to RNA-sequence analysis with Novogene using an Illumina sequencer. In Fig. 4m, PLN migratory cDC1s and CCR7$^+$ splenic cDC1s were sorted by flow cytometry directly into lysis buffer and subjected to sequencing by MedGenome.com using an Illumina platform. Heat maps were generated using R packages ComplexHeatmap[103] (v.2.22.0).

GO and GSEA analyses

GO enrichment analysis was performed on the top 500 genes with the highest fold change values and P values < 0.05 (hypergeometric test, corrected with Benjamini–Hochberg method) using enrichGO function provided by R package clusterProfiler[104] (v.4.14.6). GO Biological Process terms were used as the reference for functional enrichment analysis. The GO terms were downloaded from the Gene Ontology Consortium (https://geneontology.org/docs/download-ontology/) through clusterProfiler's internal function and only terms from the 'biological_process' parts were used. GSEA software (v.3.0) was run on the Molecular Signatures Database Hallmarks database[105] using the Pre-Ranked Gene List format, and meandiv normalization.

qPCR, RNA extraction and cDNA synthesis

Total RNA was extracted from omental tissue using the RNeasy Plus Mini Kit (74134, QIAGEN) and protocol. RNA concentration was determined by optical density and normalized across samples. Equal amounts of cDNA were synthesized using the High-Capacity cDNA Reverse Transcription Kit (4368814, Applied Biosystems) with an RNase Inhibitor (N8080119, Applied Biosystems) according to the manufacturer's protocol. Each cDNA sample was diluted 1:200 in RNase free water prior to qPCR. qPCR was conducted with TaqMan Gene Expression Assay using probes for the genes *Batf3* (Mm01318274_m1), *Irf8* (Mm00492567_m1), *Epor* (Mm00833882_m1), *Axl* (Mm00437221_m1), *Mertk* (Mm00434920_m1), *Cd5l* (Mm00437567_m1), *Itgb8* (Mm00623991_m1), *Scube3* (Mm01299285_m1), *Tgfb1* (Mm01178820_m1), *Ccl22* (Mm00436439_m1), *Aldh1a2* (Mm00501306_m1), *Gapdh* (Mm99999915_g1) and *Actb* (Mm02619580_g1). Each TaqMan probe was diluted 1:10 in TaqMan Fast Advanced Master Mix (Thermo Fisher, 4444557) to create a TaqMan probe working solution. All qPCR reactions were carried out in a MicroAmp optical 384-well reaction plate. qPCR was performed using the QuantStudio 5 (Applied Biosystems) under the following cycling conditions: 1 cycle at 50 °C for 2 min and 95 °C for 10 min, followed by 40 cycles at 95 °C for 15 s and 60 °C for 1 min. The average C_t value for each gene was calculated and normalized to *Gapdh*.

TUNEL staining

TUNEL (Terminal deoxynucleotidyl transferase dUTP nick end labelling) staining was performed using the In Situ Cell Death Detection Kit (C10617, Invitrogen) TMR Red according to the manufacturer's instructions. In brief, tissue sections were fixed with 4% paraformaldehyde for 20 min on ice prior to treatment with 0.1% Triton X-100 in 0.1% sodium citrate for permeabilization. Sections were washed in PBS before incubation for 60 min at 37 °C with antibodies and TdT enzyme, followed by washing. Images were acquired by tile scanning using a Zeiss LSM 700 confocal laser scanning microscope (Carl Zeiss Microscopy) using the 20× objective and a resolution of 960 × 720 pixels per tile. Scale bars were added in ImageJ (v.2.17.0).

Multiplex immunofluorescence imaging by CODEX

Preparation of tissues for CODEX (co-detection by indexing) imaging was performed as previously described[106], with the following modifications for fresh-frozen mouse tissue. In brief, spleens were snap-frozen in optimal cutting temperature (OCT) medium (Tissue-Tek, 25680-930, VWR/Sakura), and a 1 × 1 cm tissue array of spleens was created by trimming and gluing the OCT blocks at −20 °C in the cryostat. The array was sectioned to a thickness of 7 µm onto 22 × 22 mm glass coverslips (no. 1.5, 12-550-343, Electron Microscopy Sciences) pre-coated with poly-L-lysine (P8920, Millipore Sigma). Sections were stored at −80 °C until further use. For staining, sections were equilibrated to room temperature on Drierite desiccant (07-578-3 A, Thermo Fisher Scientific) for 2 min, followed by incubation in acetone at room temperature for 10 min. Then, sections were dried at room temperature for 2 min, followed by hydration in S1 buffer for 2 min after which sections were fixed in 1.6% paraformaldehyde in S1 buffer at room temperature for 10 min, followed by washing in S1 buffer, and equilibration in S2 buffer. One-hundred microlitres of antibody cocktail was added, and sections were incubated at room temperature for 3 h in a humidity chamber. Then, tissues were washed in S2 buffer, fixed in 1.6% paraformaldehyde in S4 buffer for 10 min, washed in PBS, fixed in ice-cold methanol for 5 min, washed in PBS, and fixed in BS3 (21580, Thermo Fisher Scientific) at room temperature for 20 min. Sections were stored in S4 buffer at 4 °C until imaging. For CODEX imaging, stained coverslips were mounted onto custom-made acrylic plates (Bayview Plastic Solutions) using mounting gaskets (Qintay, TMG-22) and stained with Hoechst 33342 (Thermo Fisher Scientific) at a dilution of 1:1,000 in H2 buffer for 1 min, followed by 3 washes in H2 buffer. Automated image acquisition and fluidics exchange were performed using a CODEX PhenoCycler instrument and driver software (Akoya Biosciences) on a BZ-X710 inverted fluorescence microscope (Keyence) equipped with a CFI Plan Apo λ 20×/0.75 objective (Nikon). The following antibodies were used for CODEX: anti-B220 (RA3.3A1/6.1, BE0067, Bio X Cell, 1:100); anti-CD3 (17A2, 555273, BD Biosciences, 1:200); anti-CD169 (MOMA-1, MCA947G, Bio-Rad, 1:50); anti-TER119 (TER119, 550565, BD Biosciences, 1:400); anti-CD71 (C2F2, 553264, BD Biosciences, 1:400).

Ex vivo analysis of EPO–EPOR downstream signalling in splenic cDC1s

Splenic cDCs were purified by MACS with a pan-DC isolation kit (130-100-875, Miltenyi Biotec) and cultured at 5×10^6 cells per ml full RPMI culture medium supplemented with 10% heat-inactivated FBS, 2 mM L-glutamine, 100 units per ml of penicillin, 100 µg ml^{-1} of streptomycin sulfate, 1 mM sodium pyruvate, 0.1 mM non-essential amino acids, 10 mM HEPES (all from Gibco), and 50 µM β mercaptoethanol (21985023, Gibco), and then rested overnight. Cells were isolated from untreated or TLI/ATS-treated $Epor^{flox/flox}$ and $Epor^{\Delta Xcr1}$ mice. cDCs from TLI/ATS-treated mice were stimulated ex vivo with recombinant human EPO (rhEPO; PROCRIT, epoetin alfa, 10 IU per 200 µl) in RPMI full culture medium or PBS (control) overnight. Phosphorylation of downstream signalling molecules was assessed by flow cytometry, gating on $Lin^-SiglecH^-PDCA\text{-}1^-CD11c^{hi}MHCII^{hi}XCR1^+SIRP\alpha^-$ splenic cDC1s.

T_{reg} cell depletion studies

Foxp3-DTR mice were acquired from Jackson (016958) and bred in our facility at Stanford University. Eight-week-old female *Foxp3*-DTR mice were treated with TLI/ATS. Mice were injected intraperitoneally with 100 µl diphtheria toxin (25 ng per g body weight) (D0564, Millipore Sigma) or PBS control every other day (days 1, 3, 5, 7, 9, 11 and 13) following allo-bone marrow infusion (day 0), and bone marrow chimerism was measured by blood sampling on day 14, day 28 and day 55. In another group, diphtheria toxin was injected every other day after day 14 (days 15, 17, 19, 21, 23, 25 and 27), and bone marrow chimerism was measured by blood sampling on days 14 and 28.

2W1S tetramer enrichment and flow cytometry

Phycoerythrin (PE) MHCII I-Ab $2W1S_{55-68}$ tetramers (NIH Tetramer core facility), and their use with anti-fluorophore-conjugated magnetic beads, anti-PE MicroBeads (130-048-801, Miltenyi Biotec) for enrichment have been described[56]. For analysing $FOXP3^+$ T_{reg} cells in $2W1S^+CD4^+$ T cells, nucleated cells from spleens were collected, enriched using I-Ab $2W1S_{55-68}$ tetramers, and stained for cell-surface MHCI (H-$2K^b$), TCRβ, CD4 and CD44, and intracellular FOXP3, before being analysed by flow cytometry.

10x Genomics scRNA-seq library preparation

Three different types of scRNA-seq experiments were performed. In the first experiment, spleens were obtained from 7-to-8-week-old $Epor^{flox/flox}$ or $Epor^{\Delta Xcr1}$ mice after TLI/ATS treatment or from untreated controls. In the second experiment, spleens were obtained from *Epor*-tdT mice after

TLI/ATS treatment. In the third experiment, PLNs were obtained from untreated *Epor*$^{flox/flox}$ or *Epor*$^{\Delta Xcr1}$ mice. For all experiments, single-cell suspensions were prepared and subjected to MACS negative enrichment with Pan Dendritic Cell Isolation Kit mouse (130-100-875, Miltenyi Biotec). Samples were then stained with live/dead aqua, Fc-blocker, and an antibody cocktail used to isolate cDC1s by FACS using a BD FACSAria II instrument. Cells were sorted into PBS supplemented with 0.5% bovine serum albumin and 2.5 mM EDTA. Cell purities of at least 95% were confirmed by post-sort analysis. FACS-sorted splenic cDC1s in Fig. 3a–d,f–h, Extended Data Fig. 5a,b,f,g and PLN migratory cDC1s in Fig. 4j,k were then barcoded with unique hashtag antibodies (155841 and 155845, BioLegend), while samples in Extended Data Fig. 5d–h were barcoded with MULTI-seq anchor lipid-modified oligonucleotide pre-hybridized to a unique MULTI-seq barcode (2 µM stock, 200 nM labelling concentration). For the third experiment, *Epor*-tdT^{+} and *Epor*-tdT^{-} cDC1s were sorted separately from the spleens of TLI/ATS-treated *Epor*$^{tdT/tdT}$ mice. Sorted cDC1s were 'super-loaded' into 10× Genomics 3′ scRNA-seq v.3.1 chips (PN-1000269, 10x Genomics). cDNA, antibody hashing, and MULTI-seq library preparation was performed according to established protocol[107]. Library quality control was performed using an Agilent 2100 Bioanalyzer instrument. Pooled cDNA libraries were sequenced using a NovaSeq6000 or NovaSeq X instrument (Illumina). A median sequencing depth of 40,000 and 5,000 reads per cell was targeted for the GEX and HTO/MULTI-seq libraries, respectively.

scRNA-seq data analysis

scRNA-seq library FASTQs were pre-processed using Cell Ranger (v.7.0.0) (10x Genomics) and aligned to the mm-10-3.0.0 reference transcriptome. Cell Ranger aggregate was used to perform read depth normalization. Filtered read depth normalized scRNA-seq count matrices were then read into R and parsed to exclude genes with fewer than five counts across all cell barcodes. Parsed scRNA-seq data were then pre-processed using Seurat (v.5.0.1)[108] and Speckle (v.0.99.7). Cell clusters with low total unique molecular identifiers (UMIs) and/or high proportion of mitochondrial transcripts were excluded. Cell barcodes passing the first quality-control workflow were then used to pre-process hashtag or MULTI-seq barcode FASTQs and perform sample classification using the deMULTIplex2 R package (v.1.0.1)[109]. Following MULTI-seq demultiplexing, unclassified cells and clusters enriched with MULTI-seq-defined doublets were removed prior to re-processing. These data were used for unsupervised clustering, differential gene expression testing, and manual annotation of splenic cDC1 subtypes based on the following marker genes[7]: immature early (*Pdia4*, *Ncub2* and *Dnajc3*), immature late (*Nr4a2*, *Hfe* and *Trib1*), mature early (*Cxcl9*, *Serpina3g* and *Slfn5*), mature late (*Ccr7*, *Gadd45b* and *Cd63*) and proliferative cDC1s (*Stmn1*, *Mki67* and *Hells*) as well as pre-cDC1s (*S100a6*, *S100a10* and *Anxa2*). Notably, low-quality or doublet cell clusters missed during the initial quality-control workflows were removed during the subtype annotation workflow, after which all datasets were re-processed and used to perform differential gene expression and subtype proportion analyses between all assayed sample groups. The manual annotation of PLN migratory cDC1 clusters was based on unsupervised clustering results of the scRNA-seq data. Four clusters were obtained by using R package Seurat's FindClusters function with a parameter resolution of 0.3. Each cluster's identity was determined by analysing its DEGs obtained through Seurat's FindAllMarkers function provided with $\log_2$ (fold change) >0 adjusted *P* value < 0.05. The heat map showing these top DEGs between PLN migratory cDC1 clusters identified in *Epor*$^{flox/flox}$ and *Epor*$^{\Delta Xcr1}$ mice were created using R package Seurat's DoHeatmap function. The expression density visualization was performed using R package Nebulosa (v.1.18.0)[110]. The CD4^{+} T cell signature scores of the cells were calculated using Seurat's function AddModuleScore, and the gene list shown in Fig. 4k and Supplementary Table 1 (mouse) was derived from Lei et al.[75].

Adoptive OT-I and OT-II cell transfer and priming of T cells to cell-associated antigens in vivo

OVA-specific transgenic CD8^{+} (OT-I) or CD4^{+} T (OT-II) cells on CD45.1 background were obtained from lymph node and spleen cell suspensions of OT-I$^{CD45.1/CD45.1}$ or OT-II$^{CD45.1/CD45.1}$ mice. OT-I cells were isolated by using naive CD8α^{+} T Cell Isolation Kit, mouse (130-096-543, Miltenyi Biotec), and enriched CD8^{+} T cells were surface stained and purified by FACS (CD8^{+}CD25^{-} CD44^{low}CD62L^{hi}). Naive FOXP3^{-} OT-II cells (CD4^{+}CD25^{-} CD44^{low}CD62L^{hi}) were isolated by naive CD4^{+} T Cell Isolation Kit, mouse (130-104-453, Miltenyi Biotec). 10^{7} cells per ml OT-I or OT-II cells were pre-labelled with 5 µM CellTrace Violet (C34557, Thermo Fisher Scientific). One million naive OT-I or OT-II cells were adoptively transferred into CD45.2/CD45.2 homozygous *Epor*$^{flox/flox}$ or *Epor*$^{\Delta Xcr1}$ mice by retro-orbital injection under isoflurane gas anaesthesia. One day later, 0.5×10^{6} or 1×10^{6} apoptotic Act-mOVA thymocytes were injected intravenously to challenge the naive OT-I or OT-II cells. CTV dilution in adoptively transferred OT-I or OT-II cells was evaluated four days later by flow cytometry analysis of splenocytes, following surface staining for CD45.1, CD45.2, TCRvα2 (OVA-specific TCR), CD3, CD8 (OT-I) or CD4 (OT-II).

CellTrace Violet labelling

Naive OT-I or OT-II cells were resuspended in 1 ml PBS and then incubated with 5 µM CTV (C34557, Invitrogen) at 37 °C for 20 min. RPMI-1640 medium (5 ml) was added to the cells and incubated for 5 min to remove the free dye in the solution. These cells were then centrifuged and incubated with pre-warmed RPMI-1640 for at least 10 min at room temperature for subsequent analysis.

Preparation and isolation of single-cell suspensions from lymph nodes

Lymph nodes were suspended in cold full RPMI culture medium. Lymph nodes were finely chopped and incubated in Liberase TM (200 µg ml^{-1}, 5401119001, Roche/Millipore Sigma) and DNase I (30 µg ml^{-1}; D2821, Sigma-Aldrich) in full RPMI culture medium for 25 min at 37 °C, 5% CO_2. Single-cell suspensions were extracted from connective tissue by taking up and resuspending the digests five times.

Digestion and cell isolation from brain, skin, lung and mammary tissue

Brain. Mice were anaesthetized and intracardially perfused with 20 ml Dulbecco's PBS (DPBS, pH 7.3-7.4). The brain was then excised. Mechanical dissociation of the brain was performed at 4 °C using a 10 ml Dounce homogenizer and a loose pellet. The homogenate was filtered into a 50 ml conical tube using a 70-µm filter. The filtered homogenate was centrifuged at 300*g* for 5 min at 4 °C. The pellet was resuspended in 10 ml of 30% Percoll (P1644, Millipore Sigma) in complete Hanks' Balanced Salt Solution (HBSS) (14025092, Gibco) and centrifuged. This Percoll step was repeated a second time. The resulting pellet was then resuspended in complete HBSS for flow cytometry staining.

Whole skin. Ears were collected and finely cut with scissors in at least 5 ml per 4 cm^{2} of skin with Liberase TM (200 µg ml^{-1}, 5401119001, Roche/Millipore Sigma) and deoxyribonuclease I (30 µg ml^{-1}; D2821, Sigma-Aldrich) in HBSS (plus calcium and magnesium). The suspensions were digested at 37 °C for 1.5–2 h (under agitation) and then filtered through a 100-µm nylon strainer.

Lung. Lungs were collected, cut into small fragments, and digested for 45 min at 37 °C with collagenase A (0.6 mg ml^{-1}; 10103586001, Sigma-Aldrich) and deoxyribonuclease I (30 µg ml^{-1}; D2821, Sigma-Aldrich) in RPMI-1640 medium (Gibco). Digested lungs were mechanically disrupted to obtain single-cell suspensions. Red blood cells were lysed using RBC lysis buffer (420302, BioLegend). Cell suspensions were then filtered through a 100-µm nylon strainer.

Mammary tissue. The mammary fat pad containing glands was dissected into small fragments and subjected to enzymatic digestion for 20 min at 37 °C in a CO_2-independent medium (Gibco). The remaining tissue pieces were meshed to obtain single-cell suspensions. Red blood cells were lysed using RBC lysis buffer (420302, BioLegend). Cell suspensions were then filtered through a 100-μm nylon strainer.

Efferocytosis assay in vivo and in vitro

For in vivo apoptotic cell engulfment experiments, 50 million thymocytes from CD45.1/CD45.1 C57BL/6 mice were resuspended in 10 ml of RPMI-1640 (21875059, Thermo Fisher Scientific) supplemented with 10% FBS (Bodinco), containing 10 μM dexamethasone (D2915, Sigma-Aldrich), and incubated at 37 °C in a humidified atmosphere with 5% CO_2 for 4 h. Apoptotic thymocytes were also generated with 15 Gy radiation. Next, to allow tracking of the apoptotic cells, the cells were labelled with PKH67 (PKH67GL-1KT, Millipore Sigma) for cell membrane labelling according to the manufacturer's protocol. Two million apoptotic cells were injected subcutaneously into the third mammary fat pad or footpad of CD45.2$^+$ *Epor*-tdT reporter mice. 12 h after injection, the mice were euthanized, and uptake of PKH67-labelled cells in the inguinal or popliteal lymph node on the injection side and contralateral side was analysed by flow cytometry. For in vitro efferocytosis-induced EPOR expression assay, CD45.2$^+$ PLN *Epor*-tdT$^+$ and *Epor*-tdT$^-$Lin$^-$CD11c^{mid}MHCII^{hi} migratory XCR1$^+$ cDC1s were sorted by FACS and cocultured overnight with CD45.1$^+$ apoptotic thymocytes at a 5:1 ratio, and the phenotype of CD45.2$^+$cDC1s was analysed by flow cytometry for the indicated markers. cDC1s were gated as CD45.2$^+$CD45.1$^-$CD11c$^+$MHCII$^+$.

DEC205-OVA conjugation

Two milligrams of anti-CD205 (NLDC-145, BE0420, Bio X Cell) was incubated with 0.4 mg EDC (77149, Thermo Fisher Scientific) and 1.1 mg of Sulfo-NHS (24510, Thermo Fisher Scientific) in 1 ml of activation buffer (0.1 M MES, 0.5 M NaCl, pH 6.0) at room temperature for 15 min. A 1.2 μl volume of 2-mercaptoethanol was added to quench the EDC. Two milligrams of ovalbumin (77120, Thermo Fisher Scientific) was then added for conjugation at room temperature for 2 h. Hydroxylamine was added to 10 mM final concentration to quench the reaction. The conjugated anti-CD205 was desalted and purified using a Protein G column (45204, Thermo Fisher Scientific).

In vitro OT-II FOXP3$^+$ T_{reg} cell induction assay

One day following the last dose of TLI/ATS, CD11c^{hi}MHCII^{hi} *Epor*-tdT$^+$ and *Epor*-tdT$^-$ XCR1$^+$CD8α$^+$ cDC1s were enriched by Pan Dendritic Cell Isolation Kit (130-100-875, Miltenyi Biotec) and further enriched by FACS, achieving >99% purity. cDC1s were cocultured with naive OT-II T cells, which were isolated from OT-II$^{CD45.1/CD45.1}$ mice using naive CD4$^+$ T Cell Isolation Kit (130-104-453, Miltenyi Biotec) and FACS as CD45.1$^+$CD3$^+$TCRvα2$^+$CD4$^+$CD25$^-$CD44^{low} CD62L$^+$. cDC1s were cocultured with naive OT-II cells in the presence of apoptotic Act-mOVA thymocytes at a ratio of 1:5:2 in 200 μl full RPMI culture medium. Where indicated, 20 IU per 200 μl rhEPO (PROCRIT, epoetin alfa) was added to the cultures daily for 5 consecutive days. *Epor*-tdT$^+$ and *Epor*-tdT$^-$ CD11c^{mid}MHCII^{hi} migratory cDC1s were isolated from PLNs with MACS and FACS as described above. PLN migratory cDC1s were cocultured with CTV-labelled naive OT-II cells in the presence of 2 μg per 200 μl DEC205-OVA or apoptotic CD45.1$^+$ thymocytes at a 1:5:2 ratio. Where indicated, 20 IU per 200 μl rhEPO (PROCRIT, epoetin alfa) was added to the cultures daily for 5 consecutive days. FOXP3 expression on OT-II cells prelabelled with CellTrace Violet (CTV) was analysed by flow cytometry, and OT-II cells were gated as live/dead aqua$^-$CD45.1$^+$CD45.2$^-$CD3$^+$TCRvα2$^+$CD4$^+$. CD11c^{mid}MHCII^{hi} migratory cDC1s were isolated from PLNs of *Epor*$^{flox/flox}$ or *Epor*$^{\Delta Xcr1}$ mice with MACS and FACS as described above and cocultured with CTV-labelled naive OT-II cells in the presence of apoptotic CD45.1$^+$ thymocytes at a 1:5:2 ratio (2×10^4 dendritic cell, 1×10^5 naive OT-II cells, and 4×10^4 apoptotic Act-mOVA thymocytes) in RPMI full culture medium. Where indicated, 20 IU per 200 μl rhEPO (PROCRIT, epoetin alfa) was added to the coculture daily for 5 consecutive days. FOXP3 expression versus CTV dilution in OT-II cells was analysed five days later by flow cytometry. OT-II cells were gated as live/dead aqua$^-$ CD45.1$^+$CD45.2$^-$CD3$^+$TCRvα2$^+$ CD4$^+$.

Ex vivo antigen-specific FOXP3$^+$ T_{reg} cell induction by CCR7$^+$ cDC1s

Twelve hours after intravenous injection of apoptotic Act-mOVA thymocytes (5×10^6) into *Epor*$^{flox/flox}$ or *Epor*$^{\Delta Xcr1}$ mice, splenic CCR7$^+$XCR1$^+$SIRPα$^-$ cDC1s (1×10^4) were sorted by FACS and cocultured with CTV-labelled naive OT-II cells (5×10^4) for 5 days. Anti-TGFβ (1D11, 1.25 μg ml^{-1}. BP0057, Bio X Cell) blocking antibody or PBS as control was added into the coculture with CCR7$^+$ cDC1s sorted from the spleens of *Epor*$^{flox/flox}$ mice. FOXP3 expression on OT-II cells was analysed by flow cytometry, and OT-II cells were gated as live/dead aqua$^-$CD45.1$^+$CD45.2$^-$CD3$^+$TCRvα2$^+$CD4$^+$.

In vivo OT-II FOXP3$^+$ T_{reg} cell induction assay

Naive CD45.1/CD45.1 background OT-II cells were isolated and sorted as described above and labelled with CTV. One million CTV-labelled naive CD45.1$^+$ OT-II cells were injected intravenously into *Epor*$^{flox/flox}$ or *Epor*$^{\Delta Xcr1}$ mice. One day later, 10^6 apoptotic Act-mOVA thymocytes were injected subcutaneously into the mammary fat pad to challenge the CD45.1$^+$ OT-II cells residing in the DLN. Where indicated, 40 IU rhEPO (PROCRIT, epoetin alfa) was injected intraperitoneally daily for 5 consecutive days or with PBS as control. FOXP3 expression versus CTV dilution in adoptively transferred OT-II cells was evaluated four days later by flow cytometry analysis of the immune cells in the DLN, and OT-II cells were gated as live/dead aqua$^-$CD45.1$^+$CD45.2$^-$CD3$^+$TCRvα2$^+$CD4$^+$.

Tumour models

The MC38 colon carcinoma cell line was a gift from C. J. M. Melief. EO771 was purchased from ATCC (CRL-3461) and B16F10 was purchased from ATCC (CRL-6475). MC38-OVA^{dim} (ref. 71) and B16F10-OVA[71] melanomas were from V. K. Kuchroo. The B16F10-OVA-ZsGreen cell line was created in the lab through lentiviral transduction using LV-EF1a-ZsGreen-IRES-Puro (SL100336, Signagen Laboratories), which were then sorted by FACS to achieve over 98% purity based on ZsGreen expression. All tumour lines were routinely tested for mycoplasma by PCR, and all tests were negative. No additional authentication was performed. Cells were maintained in Dulbecco's modified Eagle's medium (DMEM) (C11965500BT, Gibco) supplemented with 10% FBS (FBS; Bodinco), 1% penicillin-streptomycin (10378016, Thermo Fisher), 2 mM L-glutamine (A2916801, Gibco), 1 mM sodium pyruvate (11360070, Gibco) and 0.1 mM non-essential amino acids (11140050, Gibco) at 37 °C in 5% CO_2. Tumour experiments were carried out by subcutaneously implanting tumour cells into sex- and age-matched (8 to 12 weeks of age) mice with the following cell numbers: MC38-OVA^{low} (0.5×10^6), B16F10 or B16F10-OVA or B16F10-OVA-ZsGreen (10^6), MC38 (0.5×10^6) cells in 100 μl PBS into the flank or EO771 (0.5×10^6) cells in 100 μl PBS into mammary fat pad. Tumour size was determined by the formula $L \times W$, where L is length and W is width. Anti-mouse PD-1 (RMP1-14, BP0146, Bio X Cell, 100 μg per mouse) or rat IgG2a isotype control (2A3, BP0089, Bio X Cell, 100 μg per mouse) was injected intraperitoneally on day 6, day 9 and day 12 after tumour cell implantation.

Lymph node and tumour tissue digestion

TDLNs were finely minced into small pieces 1–2 mm in size and placed in RPMI-1640 medium containing 1 mg ml^{-1} Collagenase IV (Worthington, LS004188), 10 μg ml^{-1} DNase I (Roche, 11284932001), and 3% FBS. The samples were incubated at 37 °C for 30 min with stirring. Similarly, the tumour tissues were cut into small pieces 1–2 mm in size and placed in RPMI-1640 medium containing 1 mg ml^{-1} Collagenase IV, 20 μg ml^{-1} DNase I, and 3% FBS. The samples were then incubated on a shaker at

37 °C for 40 min. After digestion, the cell suspension was smashed and filtered through a 100 μm filter for subsequent staining.

Graphical illustrations

All schematic elements used in figures and extended data figures, including illustrations of mice, heart, spleen, lymph node, bone/bone marrow, mammary fat pad, syringe, cells, petri dish, cell culture well, stylized trefoil icon, tumour mass, circled area and arrows were created using https://www.biorender.com. The Stanford-affiliated BioRender account for X.Z. was obtained through the Computational Services and Bioinformatics Facility (CSBF) at Stanford University.

Statistics and reproducibility

All statistical analyses were performed by Graph Pad Prism (v.10) software and R (v.4.2.2). $P < 0.05$ was considered significant. Scatter plots show mean ± s.e.m.; each dot represents a biological replicate. Data were analysed using unpaired or paired two-tailed Student's *t*-tests for comparisons between two groups; for multiple group comparisons, ordinary one-way ANOVA followed by Tukey's or Dunnett's multiple-comparison test, or two-way ANOVA with Tukey's or Šidák's multiple-comparison test was used, with *P* values corrected for multiple comparisons. The log-rank (Mantel–Cox) test was used to determine *P* values for heart survival. Sample sizes were determined based on preliminary data or previous experience with variability in similar experimental settings. In bulk RNA-seq analyses, *P* values were calculated using hypergeometric tests with Benjamini–Hochberg correction or two-sided generalized linear model likelihood ratio tests with Benjamini–Hochberg correction. Wilcoxon rank sum test was used in scRNA-seq analyses. For differential expression testing between experimental conditions, equal numbers of each cDC1 subtype were subsetted from each condition to control for variations in subtype population structure. Statistically significant shifts in cDC1 subtype proportions were identified using the propeller function with bootstrapping in the Speckle R package (v.0.99.7)[111]. Details of specific tests were noted in the respective figure legends. The following key software packages were utilized in analyses: Seurat (v.5.0.1), ggplot2 (v.3.5.1), ComplexHeatmap (v.2.14.0), reshape2 (v.1.4.4), viridis (v.0.6.5), viridisLite (v.0.4.2), speckle (v.0.99.7), RColorBrewer (v.1.1-3), deMULTIplex2 (v.1.0.1), Nebulosa (v.1.18.0), Trimmomatic (v.0.36), SAMtools (v.1.16.1), HISAT2 (v.2.1.0), FeatureCounts (v.2.0.3), DESeq2 (v.1.46.0), clusterProfiler (v.4.14.6) and GSEA (v.3.0).

Reporting summary

Further information on research design is available in the Nature Portfolio Reporting Summary linked to this article.

Data availability

All transcriptional data generated in the current study were deposited at the NCBI Gene Expression Omnibus (GEO) and are publicly available through the following accession numbers: GSE253056 (bulk RNA-seq) and GSE284080 (scRNA-seq), respectively. Source data are provided with this paper.

Code availability

The scripts for replicating the RNA-seq analyses presented are accessible on GitHub (https://github.com/chansigit/Epor-cDC1-bulkRNAseq). Scripts for reproducing all scRNA-seq analyses presented are accessible on GitHub (https://github.com/chris-mcginnis-ucsf/epor_dc_tolerance) and associated processed data objects are available on Synapse (https://synapse.org/Synapse:syn64330568).

97. Kim, J. M., Rasmussen, J. P. & Rudensky, A. Y. Regulatory T cells prevent catastrophic autoimmunity throughout the lifespan of mice. *Nat. Immunol.* **8**, 191–197 (2007).
98. Nakawesi, J. et al. alphavbeta8 integrin-expression by BATF3-dependent dendritic cells facilitates early IgA responses to Rotavirus. *Mucosal Immunol.* **14**, 53–67 (2021).
99. Weckel, A. et al. Long-term tolerance to skin commensals is established neonatally through a specialized dendritic cell subgroup. *Immunity* **56**, 1239–1254.e7 (2023).
100. Bolger, A. M., Lohse, M. & Usadel, B. Trimmomatic: a flexible trimmer for Illumina sequence data. *Bioinformatics* **30**, 2114–2120 (2014).
101. Kim, D., Paggi, J. M., Park, C., Bennett, C. & Salzberg, S. L. Graph-based genome alignment and genotyping with HISAT2 and HISAT-genotype. *Nat. Biotechnol.* **37**, 907–915 (2019).
102. Robinson, M. D., McCarthy, D. J. & Smyth, G. K. edgeR: a Bioconductor package for differential expression analysis of digital gene expression data. *Bioinformatics* **26**, 139–140 (2010).
103. Gu, Z. Complex heatmap visualization. *iMeta* **1**, e43 (2022).
104. Wu, T. et al. clusterProfiler 4.0: a universal enrichment tool for interpreting omics data. *Innovation* **2**, 100141 (2021).
105. Liberzon, A. et al. The Molecular Signatures Database Hallmark Gene Set Collection. *Cell Syst.* **1**, 417–425 (2015).
106. Schurch, C. M. et al. Coordinated cellular neighborhoods orchestrate antitumoral immunity at the colorectal cancer invasive front. *Cell* **182**, 1341–1359.e19 (2020).
107. McGinnis, C. S. et al. MULTI-seq: sample multiplexing for single-cell RNA sequencing using lipid-tagged indices. *Nat. Methods* **16**, 619–626 (2019).
108. Hao, Y. et al. Dictionary learning for integrative, multimodal and scalable single-cell analysis. *Nat. Biotechnol.* **42**, 293–304 (2024).
109. Zhu, Q., Conrad, D. N. & Gartner, Z. J. deMULTIplex2: robust sample demultiplexing for scRNA-seq. *Genome Biol.* **25**, 37 (2024).
110. Alquicira-Hernandez, J. & Powell, J. E. Nebulosa recovers single-cell gene expression signals by kernel density estimation. *Bioinformatics* **37**, 2485–2487 (2021).
111. Phipson, B. et al. propeller: testing for differences in cell type proportions in single cell data. *Bioinformatics* **38**, 4720–4726 (2022).

Acknowledgements We thank J. Idoyaga for providing *Xcr1*$^{cre\text{-}mTFP1}$ mice; E. B. Rankin for providing *Epor*$^{flox/flox}$ mice; V. K. Kuchroo for providing MC38-OVA and B16F10-OVA tumour cell lines; P. Giang for preparing CD45.1^{+} *Foxp3*$^{DTR/DTR}$ spleens; NIH Tetramer Core Facility (NIH Contract 75N93020D00005 and RRID:SCR_026557) for providing I-Ab|mouse 2W1S|EAWG ALANWAVDSA|PE-labelled tetramer; C. Zhu for processing the scRNA-seq FASTQ data and assistance with data analysis; C. Brown for assistance with resource acquisition; T. L. Roth for valuable discussion; L. L. Tolentino, K. Nguyen, C. Barclay and J. N. Delos Reyes for expert technical support in flow cytometry and fluorescence-activated cell sorting; the DIMC Core of the Stanford Diabetes Research Center; and Breakthrough T1D Center of Excellence for support. This work was supported by the following grants: U54 CA274511, CA251174, CA244114 (E.G.E.) and P01HL149626 (X.A.).

Author contributions X.Z. and E.G.E. conceived the study. X.Z. designed and performed the experiments, analysed data, interpreted the results and wrote the manuscript with E.G.E. C.S.M. and S.C. conducted the scRNA-seq analyses and wrote the scRNA-seq results and methods sections together with X.Z. and E.G.E. K.J.H.-G. and W.Y. prepared the scRNA-seq libraries. S.C., P.Z., N.E.R.-F. and X.Z. carried out the RNA-seq analyses. C.M.S. and J.W.H. performed the CODEX experiments. G.Y., W.G. and J.Q. assisted with flow cytometry staining and cell sorting, in vitro cell culture, T cell adoptive transfers, tumour growth studies and data recording. A.M. contributed to the flow cytometry analysis of cDC1 *Epor*-tdT expression in the brain and assisted with tissue preparation for in vivo studies. I.L.L. aided in the in vivo tumour studies. H.Y. and T.H. performed heart transplantation. V.M.T., W.Q. and D.B.-V. assisted with *Aldh1a2* and *Itgb8* animal models. B.Y. made DEC205-OVA. A.T.S. supervised the scRNA-seq analyses. K.J.H.-G., X.A., Y.X., H.P., T.C.S., M.A., D.S., H.C., A.T.S., S.S.W., B.M. and S.S. provided critical intellectual insights. E.G.E. supervised the study. All authors provided feedback on the manuscript draft.

Competing interests X.Z. is a cofounder and shareholder of ImmunEdge Inc. E.G.E. is a founder, shareholder and board member of ImmunEdge Inc. B.Y. is a shareholder of ImmunEdge Inc. X.Z and E.G.E. are Stanford-affiliated inventors of PCT/US2023/063997, entitled 'Epo Receptor Agonists and Antagonists'. C.S.M. holds patents related to MULTI-seq. C.M.S. is a cofounder and scientific advisor of Vicinity Bio GmbH and is on the scientific advisory board of and has received research funding from Enable Medicine Inc., all outside the current work. T.C.S. is a scientific advisory board member for Concerto Biosciences. M.A. is a consultant, board member, and shareholder in Ionpath Inc. D.S. is a founder of Pliant Therapeutics and Glial Biosciences and is on the Genentech Scientific Review Board and the Amgen Inflammation Scientific Review Board, and an advisor to Lila Biologics, Arda Therapeutics and TCGFB Inc. H.C. is a consultant for Kumquat Biosciences and TCura Bioscience. A.T.S. is a founder of Immunai, Cartography Biosciences and Prox Biosciences, an advisor to Zafrens and Wing Venture Capital, and receives research funding from Merck Research Laboratories. The other authors declare no competing interests.

Additional information
Supplementary information The online version contains supplementary material available at https://doi.org/10.1038/s41586-025-09824-z.

Correspondence and requests for materials should be addressed to Xiangyue Zhang or Edgar G. Engleman.

Peer review information *Nature* thanks the anonymous reviewers for their contribution to the peer review of this work. Peer reviewer reports are available.

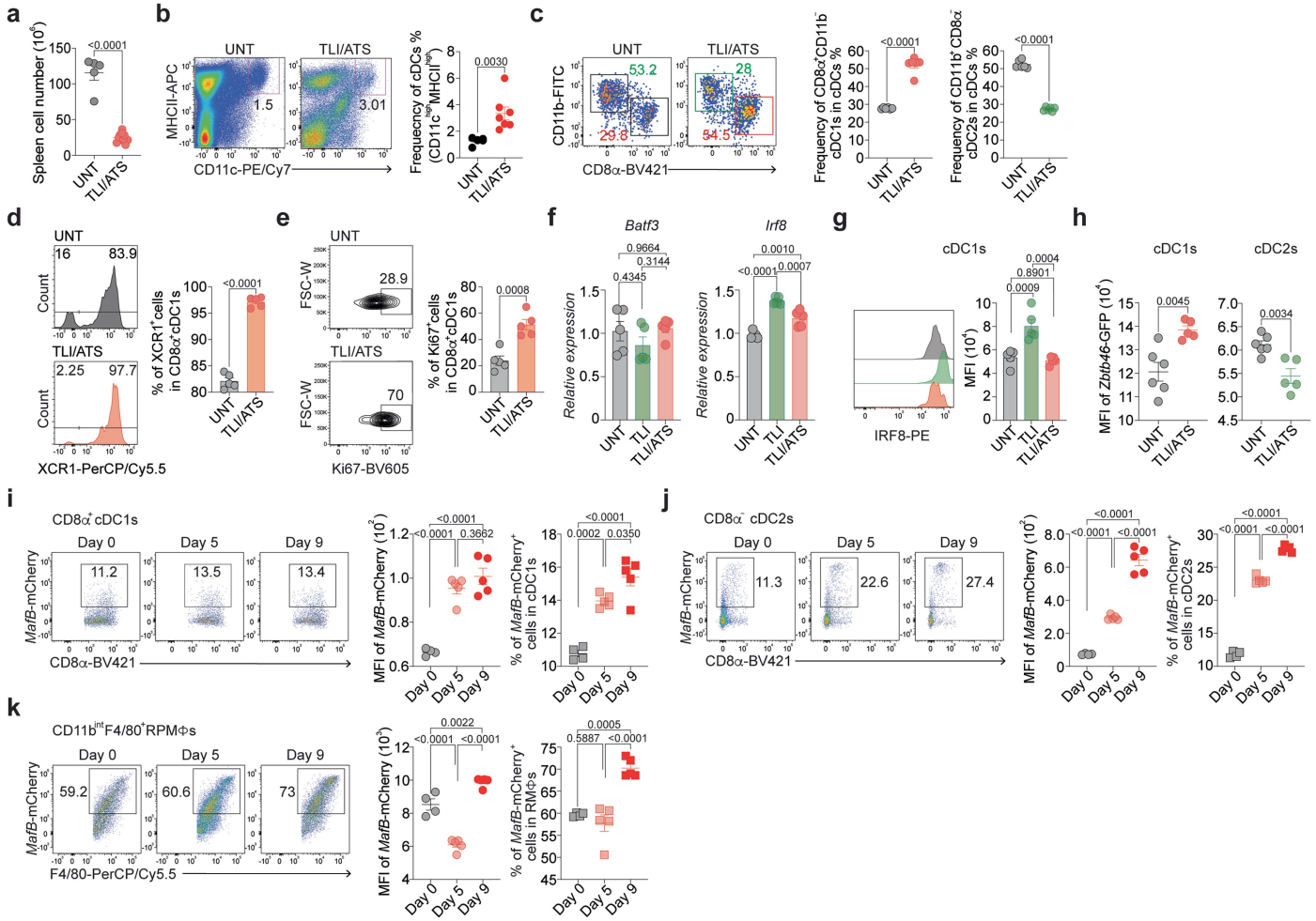

Extended Data Fig. 1 | XCR1$^+$CD8α$^+$ cDC1s in the spleen following TLI/ATS are bona fide cDC1s. a, Total splenocyte frequency per spleen (UNT n=5; TLI/ATS n=10). **b**, Gating of CD11c^{high}MHCII^{high} cDCs from the splenocytes. Summary graph of the frequency of cDCs in total splenocytes (UNT, n = 6; TLI/ATS, n = 7). **c**, Gating of CD8α$^+$CD11b$^-$ cDC1s and CD8α$^-$CD11b$^+$ cDC2s; frequencies in cDCs (UNT, n = 6; TLI/ATS, n = 6). **d**, XCR1$^+$ and **e**, Ki67$^+$ cDC1 frequencies (UNT, n = 5; TLI/ATS, n = 5). **f**, qPCR of *Batf3* and *Irf8* in XCR1$^+$CD8α$^+$ cDC1s (n = 5/group). **g**, IRF8 and **h**, *Zbtb46*-GFP expression (UNT, n = 6; TLI/ATS, n = 5). **i-k**, MFI of *MafB*-mCherry expression and % of *MafB*-mCherry$^+$ cells in XCR1$^+$CD8α$^+$ cDC1s (**i**), cDC2s (**j**) and red pulp macrophages (RPMΦs) (**k**). Day 0 (UNT), n = 4; TLI/ATS Day 5, n = 5; TLI/ATS Day 9, n = 5 (**i,j,k**). Data are shown from one experiment, representative of at least two independent experiments with similar results (**a-k**). Statistical analysis was performed using unpaired two-tailed Student's t-test (**a,b,c,d,e,h**), or one-way ANOVA with Tukey's multiple-comparison test (**f,g,i,j,k**). Data are mean ± s.e.m. (**a-k**).

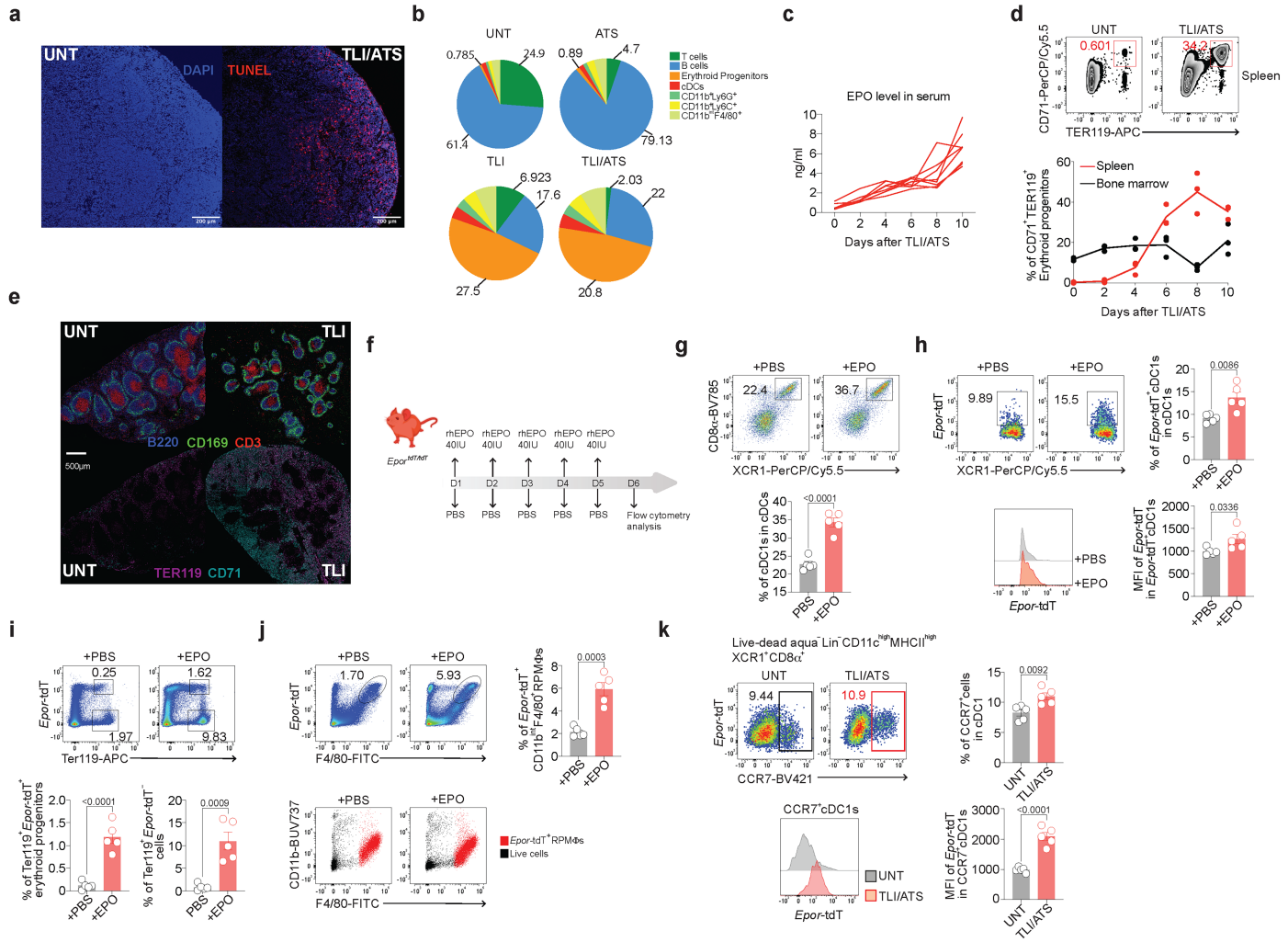

Extended Data Fig. 2 | TLI/ATS leads to widespread apoptosis and extramedullary erythropoiesis in the spleen and a marked rise in serum EPO. a, TUNEL staining of spleen sections, UNT vs. TLI/ATS (scale bar = 200 µm). **b**, Spleen cell composition after ATS, TLI, or TLI/ATS; pie chart shows mean frequencies of indicated populations (n = 3). T cells (TCRβ$^+$CD19$^-$NK1.1$^-$), B cells (CD19$^+$TCRβ$^-$NK1.1$^-$), erythroid progenitors (CD11c$^-$TER119$^+$CD71$^+$), cDCs (CD3ε$^-$B220$^-$SiglecH$^-$PDCA-1$^-$CD11c^{high}MHCII^{high}), other myeloid cells are subdivided into CD11b$^+$Ly6C$^-$Ly6G$^+$, CD11b$^+$Ly6G$^-$Ly6C$^+$ and CD11b^{int}F4/80$^+$. **c**, Serum EPO levels over time after TLI/ATS (ELISA, n = 8). **d**, CD71$^+$TER119$^+$ erythroid progenitors in spleen (day 6) (upper) and in spleen/BM (lower) over time after TLI/ATS (n = 3). **e**, Co-detection by indexing (CODEX) imaging of WT C57BL/6 spleen (UNT vs. 1 day after TLI; scale bar = 500 µm). **f**, Scheme of EPO treatment in Epor-tdTomato-Cre mice (i.p. × 5 days). **g,h**, Flow cytometry showing splenic cDC1 frequency among cDCs (**g**) and *Epor*-tdT$^+$ cDC1 frequency/MFI (**h**) (+PBS, n = 5; +EPO, n = 5). **i-j**, Frequencies of *Epor*-tdT$^+$ and *Epor*-tdT$^-$ TER119$^+$ erythroid cells (**i**) and *Epor*-tdT$^+$CD11b^{int}F4/80$^+$*Epor*-tdT$^+$ RPMΦs (**j**), (+PBS, n = 5; +EPO, n = 5). **k**, CCR7 vs. *Epor*-tdT expression in XCR1$^+$CD8α$^+$ cDC1s that were gated as live-dead aqua$^-$CD3ε$^-$CD19$^-$B220$^-$ SiglecH$^-$PDCA-1$^-$CD11c^{high}MHCII^{high}; histogram overlay for CCR7$^+$ cDC1s (UNT, n = 5; TLI/ATS, n = 5). Data are shown from one experiment, representative of at least two independent experiments with similar results (**a,b,c,d,g,h,i,j,k**) or from one experiment (**e**). Statistical analysis was performed using unpaired two-tailed Student's t-test (**g,h,i,j,k**). Data are mean ± s.e.m. (**d,g-k**). The diagram in **f** was created in BioRender. Zhang, X. (2025) https://BioRender.com/cx0n3vn.

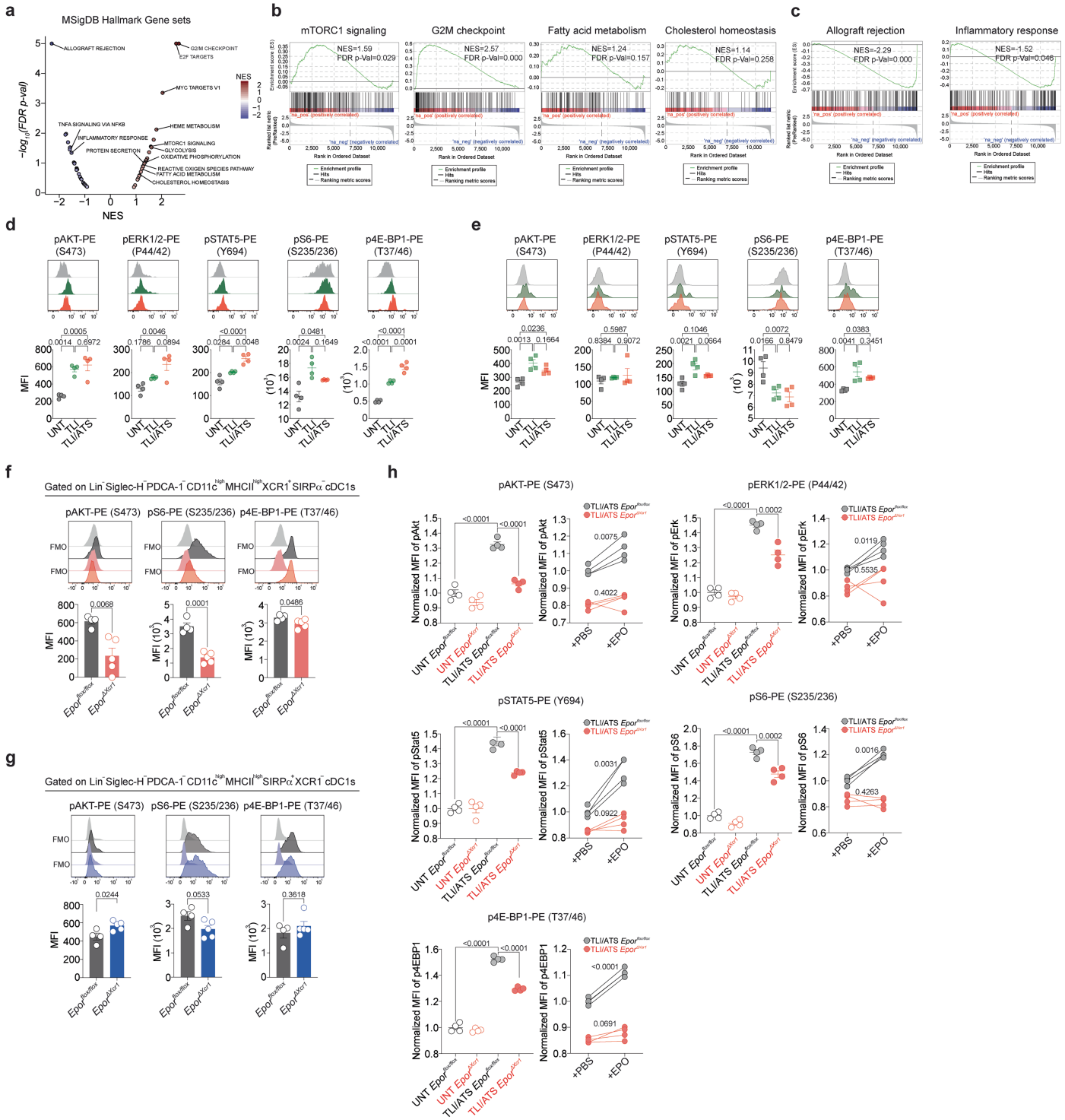

Extended Data Fig. 3 | EPO-EPOR downstream signaling is activated in cDC1s following TLI/ATS. a-c, Gene Set Enrichment Analysis (GSEA) of transcriptional profiles using the Hallmark gene set of MSigDB. NES, normalized enrichment score; FDR, false discovery rate. Red: upregulated; Blue: downregulated. TLI/ATS vs. UNT. **b**, Upregulated gene sets. **c**, Downregulated gene sets. **d-e**, Intracellular phospho-flow cytometric analysis of EPO-EPOR downstream signaling in live-dead blue$^-$Lin$^-$SiglecH$^-$PDCA-1$^-$CD11c^{high}MHCII^{high}. Spleens were harvested on the next day following the last dose of TLI or TLI/ATS. UNT (n = 4) vs. TLI (n = 4) vs. TLI/ATS (n = 4). **d**, XCR1$^+$CD8α$^+$ cDC1s and **e**, XCR1$^-$CD8α$^-$ cDC2s. **f,g**, Histograms and MFI of the indicated EPO-EPOR downstream signaling molecules with fluorescence minus one (FMO) as controls by intracellular phospho-flow staining on the next day following the last dose of TLI/ATS treatment. *Epor*$^{flox/flox}$ (n = 4) vs. *Epor*$^{\Delta Xcr1}$ (n = 5). cDC1s (**f**) and cDC2s (**g**). **h**, Ex vivo analysis of EPO-EPOR downstream signaling in splenic cDC1s. Splenic cDCs were MACS-purified with a pan-DC isolation kit and cultured at 5×10^6 cells/ml, then rested overnight. Cells were isolated from UNT or TLI/ATS-treated *Epor*$^{flox/flox}$ (n = 4; n = 4) and *Epor*$^{\Delta Xcr1}$ (n = 4; n = 4) mice. cDCs from TLI/ATS-treated mice were stimulated ex vivo with EPO (10 IU/200 µl) or PBS (control) overnight. Phosphorylation of downstream signaling molecules was assessed by flow cytometry, after gating on XCR1$^+$SIRPα$^-$ splenic cDC1s. Data are shown from one experiment, representative of at least two independent experiments with similar results (**d-h**). Statistical analysis was performed using unpaired two-tailed Student's t-test (**f,g**), or one-way ANOVA Tukey's multiple-comparison test (**d, e** and **h left**), or paired two-tailed Student's t-test (**h right**). Data are mean ± s.e.m. (**d-h**).

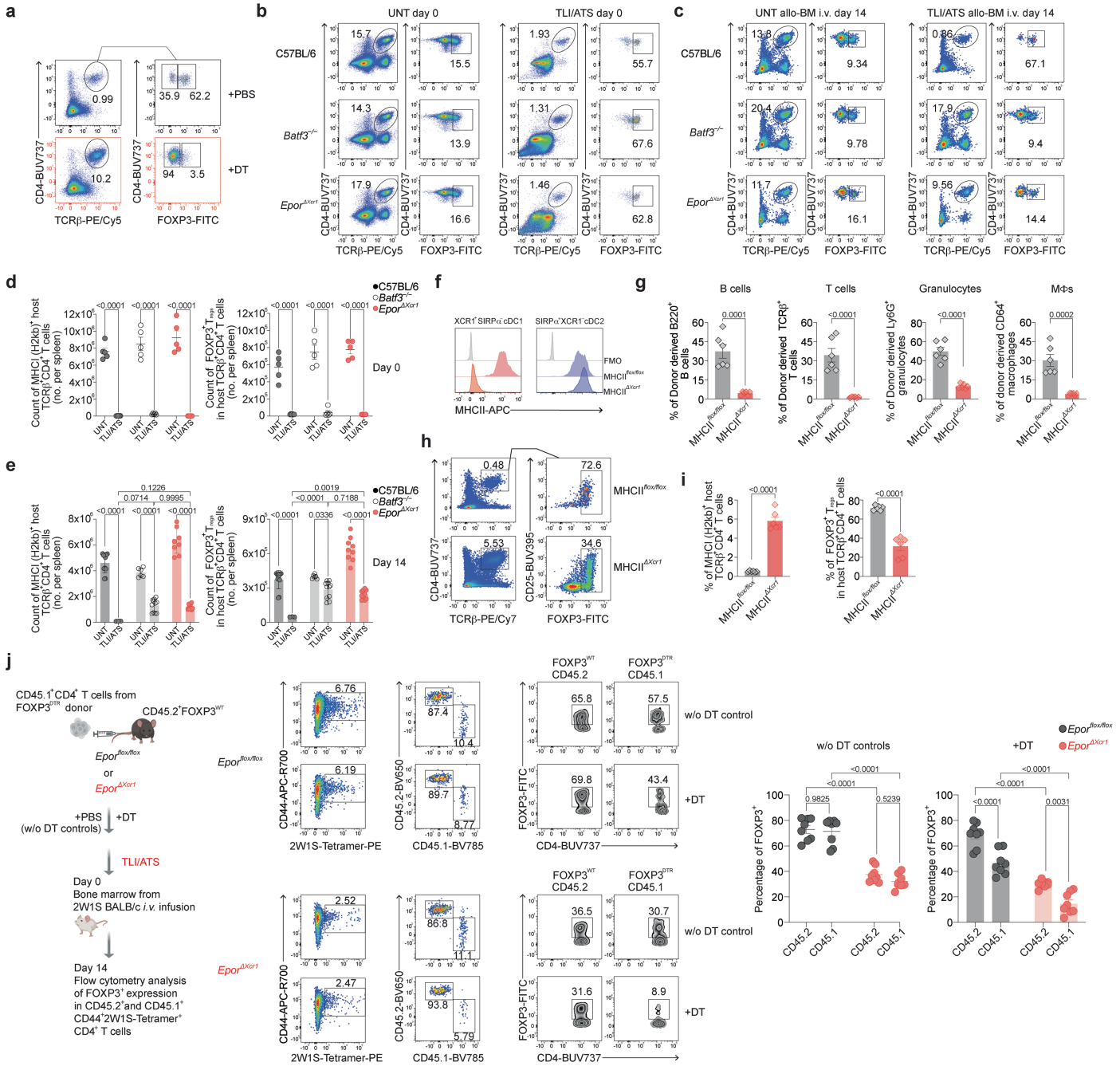

Extended Data Fig. 4 | FOXP3$^+$ T_{regs} play an indispensable role in TLI/ATS-induced cDC1 EPOR-dependent immune tolerance. a, Representative pseudocolor plots showing FOXP3$^+$ T_{reg} depletion efficiency in recipient mice on day 6 after DT treatment (DT injections on days 0, 2, and 4). **b,c**, Representative pseudocolor plots of C57BL/6, *Batf3*$^{-/-}$, or *Epor*$^{\Delta Xcr1}$ recipient conventional CD4$^+$ T cell percentages and FOXP3$^+$ T_{reg} percentages in CD4$^+$ T cells. **d,e**, Absolute cell number of indicated cell populations. **b,d**, Day 0 (UNT, n = 5; n = 5; n = 5 and TLI/ATS, n = 6; n = 5; n = 4) and **c,e**, Day 14 of UNT or TLI/ATS-treated groups post allo-BM infusion (UNT, n = 11; n = 6; n = 9 and TLI/ATS, n = 3; n = 11; n = 10). **f**, MHCII expression on cDC1s and cDC2s from MHCII$^{flox/flox}$ and MHCII$^{\Delta Xcr1}$ spleens. **g,h,i**, MHCII$^{flox/flox}$ (n = 6) and MHCII$^{\Delta Xcr1}$ (n = 6) recipients were given TLI/ATS and i.v. infused with BALB/c donor BM cells. 14 days post BM infusion, the percentages of donor type (H2K^{d+}) cells among leukocyte populations were determined in the peripheral blood of hosts. **g,i**, Recipient MHCI (H-2K^b)$^+$TCRβ$^+$CD4$^+$ T cell frequency among total live cells and FOXP3$^+$ frequency among CD4$^+$ T cells were analyzed on day 14. **j**, CD45.2$^+$FOXP3^{WT}*Epor*$^{flox/flox}$ (+ PBS/without DT, n = 8; +DT, n = 8) or *Epor*$^{\Delta Xcr1}$ (+ PBS/ without DT, n = 8; +DT, n = 8) mice were injected with 30 million CD45.1$^+$FOXP3^{DTR} CD4$^+$ T cells isolated by MACS. Two consecutive doses of DT or PBS were given on each of the following 2 days. Subsequently, the mice were treated with TLI/ATS, and 2W1S-BALB/c donor BM cells were infused i.v., and 14 days later, 2W1S-tetramer$^+$CD44$^+$H-2K^{b+}TCRβ$^+$CD4$^+$ T cells from the spleens were analyzed for FOXP3 expression by flow cytometry. FOXP3 expression in CD45.1$^+$ or CD45.2$^+$2W1S-tetramer$^+$ CD4$^+$ T cells is shown. One experiment (**j**) or one of two independent experiments with similar results are shown (**a-i**). Statistical analysis was performed using unpaired two-tailed Student's t-test (**g,i**), two-way ANOVA with Tukey's multiple-comparison test (**d,e,j**). Data are mean ± s.e.m. (**d,e,g,i,j**). The diagram in **j** was created in BioRender. Zhang, X. (2025) https://BioRender.com/cx0n3vn.

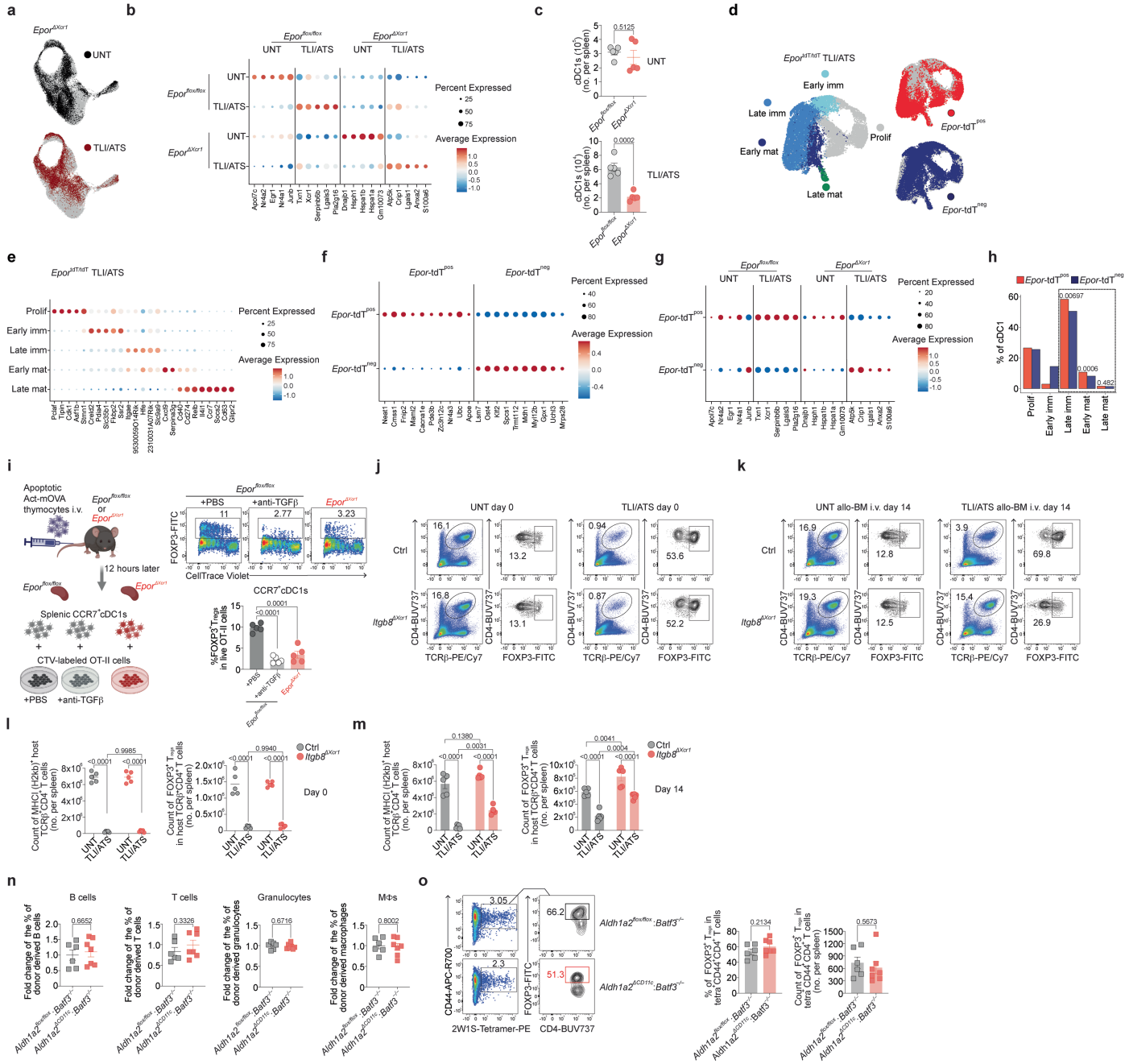

Extended Data Fig. 5 | Differentially expressed genes (DEGs) in cDC1s in scRNA-seq analysis and ex vivo TGFβ-dependent Ag-specific FOXP3$^+$ T$_{reg}$ induction by CCR7$^+$ cDC1s. a, UMAP of splenic cDC1 gene expression by sample identity. **b**, Dot plots of top condition-specific DEGs in *Epor$^{flox/flox}$* and *Epor^{ΔXcr1}* mice (TLI/ATS vs. UNT). **c**, Absolute cDC1 numbers per spleen in UNT vs. TLI/ATS-treated *Epor$^{flox/flox}$* (n = 5/condition) and *Epor^{ΔXcr1}* (n = 5/condition) mice. **d**, UMAPs of cDC1 subtypes in Epor-tdT$^+$ and *Epor*-tdT$^-$ cells. **e-g**, Dot plots of top condition-specific DEGs in *Epor*-tdT$^+$ and *Epor*-tdT$^-$ cDC1s (TLI/ATS) and in *Epor$^{flox/flox}$* and *Epor^{ΔXcr1}* mice (TLI/ATS vs. UNT). Dot color = expression, size = % of indicated gene expressed cells (**b**,**e-g**). **h**, Bar charts showing cDC subtype (**d**) proportions in *Epor*-tdT$^+$ and *Epor*-tdT$^-$ cDC1s following TLI/ATS. **i**, Role of TGFβ in FOXP3$^+$ T$_{reg}$ induction by CCR7$^+$ cDC1s: 12 h after apoptotic Act-mOVA injection, CCR7$^+$ cDC1s (1×10^4) were cocultured with CD45.1$^+$ CTV-labeled naïve OT-II cells ± anti-TGFβ; FOXP3 expression was analyzed by flow cytometry (n = 5/group). **j,k**, Representative flow cytometry analysis and **l,m**, Absolute cell number of indicated cell populations of Fig. 3j, *Itgb8^{ΔXcr1}* vs. littermate controls. **j,l**, Day 0 and **k,m**, Day 14 of UNT (n = 5; n = 5) or TLI/ATS-treated (n = 5; n = 5) groups post allo-BM infusion. **n,o**, *Aldh1a2^{ΔCD11c}:Batf3$^{-/-}$* (n = 6) vs. *Aldh1a2$^{flox/flox}$:Batf3$^{-/-}$* (n = 7) BM chimeric recipient mice (CD45.1$^+$) were given TLI/ATS. 1 day after the last dose of TLI/ATS, 2W1S-BALB/c donor BM cells were infused i.v., and 14 days later, the percentages of donor type (H2K^{d+}) cells among leukocyte populations in the peripheral blood of hosts were determined (**n**) and 2W1S-tetramer$^+$CD44$^+$ H-2K^{b+}TCRβ$^+$CD4$^+$ T cells from the spleens were analyzed for FOXP3 expression by flow cytometry and FOXP3$^+$ T$_{regs}$ were counted (**o**). Data are representative of at least three independent experiments with similar results (**c,i**) or one experiment (**j-o**). Statistical analysis was performed using unpaired two-tailed Student's t-test (**c,i,n,o**), or two-way ANOVA followed by Tukey's multiple-comparison test with P values adjusted (**l,m**), or propeller test, two-sided, no multiple-comparison correction (**b**), or wilcoxon rank sum test, two-sided, Bonferroni correction (**h**). Data are mean ± s.e.m. (**c,i,l,m,n,o**). The diagram in **i** was created in BioRender. Zhang, X. (2025) https://BioRender.com/rq2yp2e.

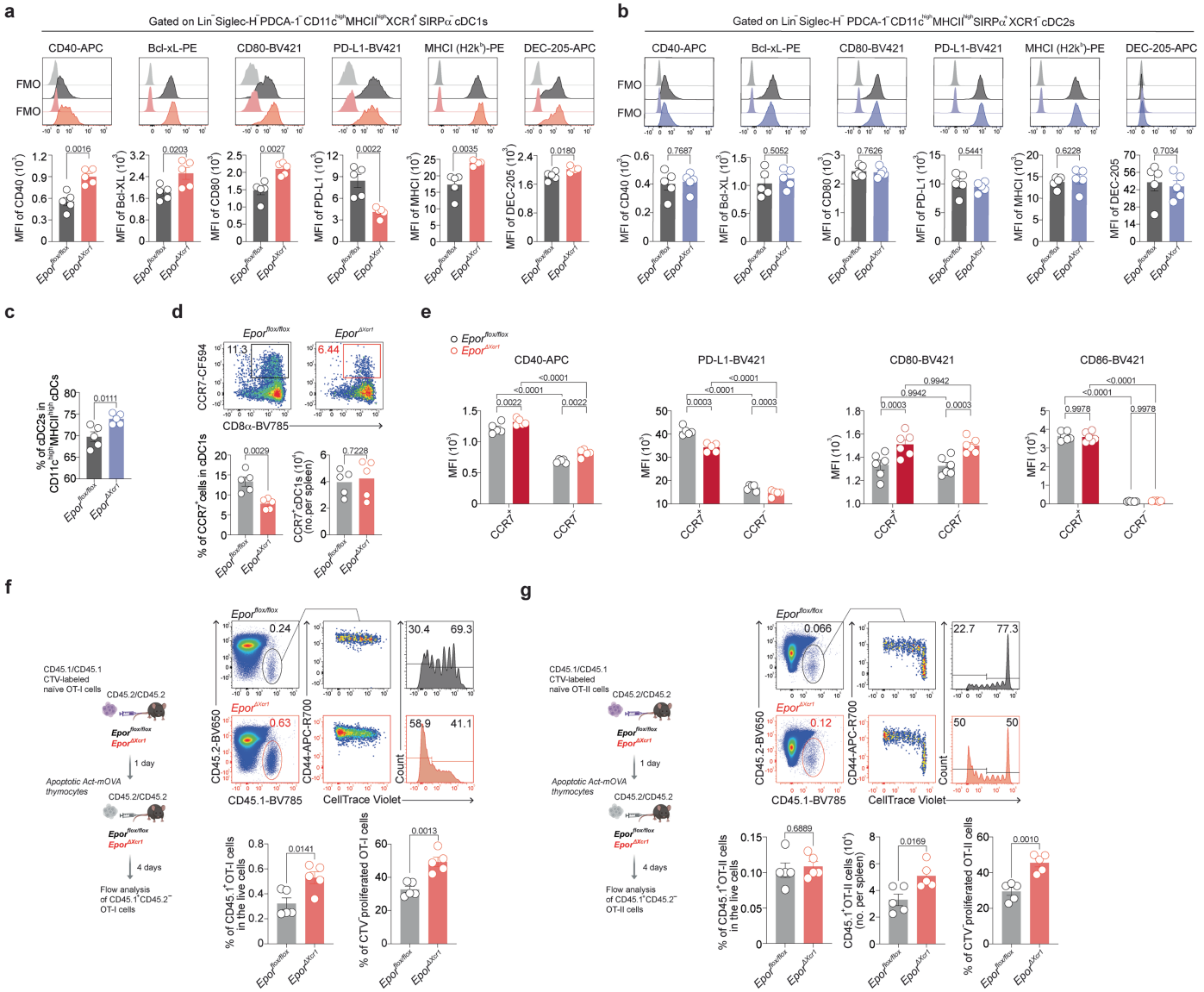

Extended Data Fig. 6 | Absence of EPOR on cDC1s gives rise to immunogenic cDC1s that promote both CD8⁺ T cell cross-priming and CD4⁺ T cell priming to cell-associated Ags. a, MFI of indicated molecules on gated cDC1s with fluorescence minus one (FMO) as controls. **b**, MFI of indicated molecules on gated cDC2s with fluorescence minus one (FMO) as controls. **c**, Percentages of cDC2s in splenic cDCs. **d**, Representative flow gating of CCR7⁺XCR1⁺SIRPα⁻ cDC1s in splenic cDC1s (Upper), and percentages and absolute numbers of CCR7⁺ cDC1s (Lower). **a-d**, *Epor*$^{flox/flox}$ (n = 5) vs. *Epor*$^{\Delta Xcr1}$ (n = 5) mice. **e**, MFI of indicated molecules on CCR7⁺ vs. CCR7⁻ cDC1s. CD40 and PD-L1: *Epor*$^{flox/flox}$ (n = 5); *Epor*$^{\Delta Xcr1}$ (n = 5). CD80 and CD86: *Epor*$^{flox/flox}$ (n = 6); *Epor*$^{\Delta Xcr1}$ (n = 6). **f**, Cross-presentation assay: apoptotic Act-mOVA thymocytes injected into *Epor*$^{flox/flox}$ (n = 5) or *Epor*$^{\Delta Xcr1}$ (n = 5) mice 1 day after transfer of CTV-labeled naïve CD45.1⁺ naïve OT-I cells; spleens analyzed on day 4 for OT-I expansion and proliferation. **g**, Same setup with OT-II cells; percentages and absolute numbers of OT-II cells and proliferating OT-II cells were assessed. Ag-specific CD4⁺ T cell response: Ag-specific CD4⁺ T cell immune response following i.v. injection of apoptotic Act-mOVA thymocytes 1 day after i.v. injection of CTV-labeled naïve CD45.1⁺ naïve OT-II cells. Spleens were analyzed at day 4 for OT-II expansion and proliferation. *Epor*$^{flox/flox}$ (n = 5) and *Epor*$^{\Delta Xcr1}$ (n = 5) mice. Data are shown from one experiment, representative of at least three independent experiments with similar results (**a-g**). Statistical analysis was performed using unpaired two-tailed Student's t-test (**a,b,c,d,f,g**) and two-way ANOVA followed by Tukey's multiple-comparison test (**e**). Data are mean ± s.e.m. (**a-g**). The diagrams in **f,g** were created in BioRender. Zhang, X. (2025) https://BioRender.com/bth22u6.

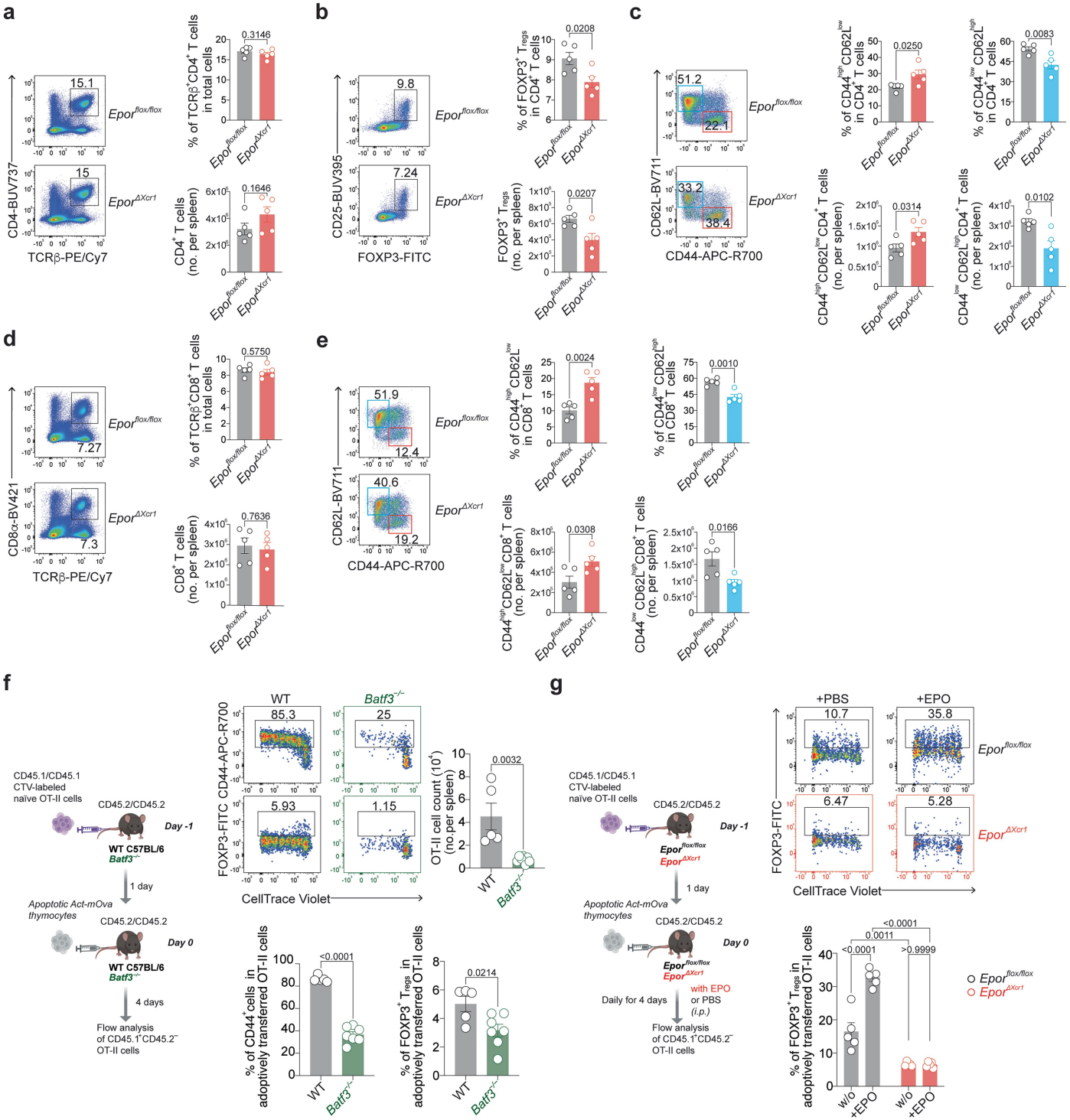

Extended Data Fig. 7 | Phenotypes of T cells in the spleens of *Epor*$^{flox/flox}$ vs. *Epor*$^{\Delta Xcr1}$ mice and role of EPOR in cDC1-mediated cell-associated Ag-specific CD4$^+$ T cell priming and proliferation and FOXP3$^+$ T$_{reg}$ induction. **a-e**, Percentages and absolute numbers of CD4$^+$ T cells (**a**), FOXP3$^+$CD25$^+$ T$_{regs}$ in CD4$^+$ T cells (**b**), CD44^{high}CD62L^{low} effector cells and CD44^{low}CD62L^{high} naïve cells in CD4$^+$ T cells (**c**), CD8$^+$ T cells (**d**), and CD44^{high}CD62L^{low} effector cells and CD44^{low}CD62L^{high} naïve cells in CD8$^+$ T cells (**e**) in the spleens of *Epor*$^{\Delta Xcr1}$ and littermate *Epor*$^{flox/flox}$ control mice with representative flow cytometric plots. **a-e**, *Epor*$^{flox/flox}$, n = 5; *Epor*$^{\Delta Xcr1}$, n = 5. **f,g**, Flow cytometry-based measurement of cell-associated Ag-specific CD4$^+$ T cell immune response in the spleen following i.v. injection of apoptotic Act-mOVA thymocytes into mice of the indicated genotypes 1 day after i.v. injection of CTV-labeled naïve CD45.1$^+$ OT-II cells. **f**, WT C57BL/6 (n = 5) and *Batf3*$^{-/-}$ (n = 7). **g**, FOXP3$^+$ T$_{reg}$ induction in *Epor*$^{flox/flox}$ and *Epor*$^{\Delta Xcr1}$ mice. Recombinant EPO or PBS was administered daily, from Day −3 to Day 4. +PBS: *Epor*$^{flox/flox}$ (n = 5), *Epor*$^{\Delta Xcr1}$ (n = 5); +EPO: *Epor*$^{flox/flox}$ (n = 5), *Epor*$^{\Delta Xcr1}$ (n = 5) mice. Data are shown from one experiment, representative of at least three independent experiments with similar results (**a-e**), or two independent experiments with similar results (**f,g**). Statistical analysis was performed using unpaired two-tailed Student's t-test (**a-f**), or two-way ANOVA followed by Tukey's multiple-comparison test (**g**). Data are mean ± s.e.m. (**a-g**). The diagrams in **f,g** were created in BioRender. Zhang, X. (2025) https://BioRender.com/bth22u6.

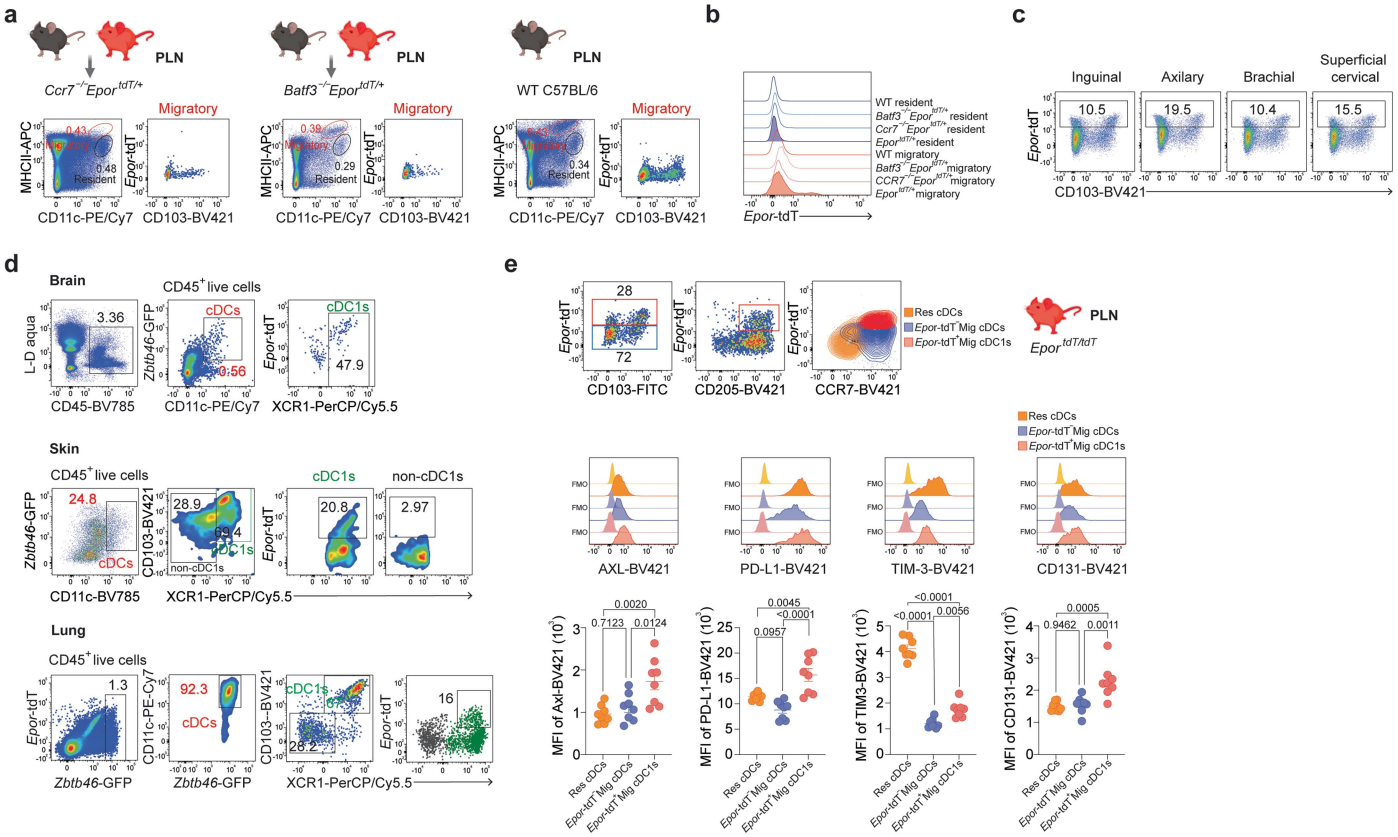

Extended Data Fig. 8 | *Epor*-tdT expression on XCR1⁺ cDC1s in selected organs and tolerogenic phenotype of *Epor*-tdT⁺ migratory cDC1s in PLN. **a,b,c** CCR7- and Batf3-dependent *Epor*-tdT expression on migratory cDCs in pLNs. Migratory cDCs were gated as CD11c^{int}MHCII^{high} from live-dead aqua$^-$Lin$^-$SiglecH$^-$PDCA-1$^-$EpCAM$^-$ cells, and resident cDCs were gated as CD11c^{high}MHCII^{int} from live-dead aqua$^-$Lin$^-$SiglecH$^-$PDCA-1$^-$ cells. pLNs including inguinal, axillary, brachial, and superficial cervical LNs were combined for analysis by flow cytometry (**a,b**). *Ccr7*$^{-/-}$*Epor*$^{tdT/+}$, *Batf3*$^{-/-}$*Epor*$^{tdT/+}$ and WT C57BL/6 mice (**a**). Histogram overlay of *Epor*-tdT expression on migratory or resident cDCs from individual mouse strains (**b**). *Epor*-tdT expression on migratory cDCs from individual pLNs of *Epor*$^{tdT/+}$ mice (**c**). **d**, Epor-tdT expression on cDC1s obtained from the indicated organs in *Zbtb46*$^{GFP/+}$*Epor*$^{tdT/+}$ mice. cDCs were gated in CD45$^+$ cells as CD11c$^+$*Zbtb46*-GFP$^+$, in which cDC1s were further gated as XCR1$^+$CD103$^+$. **e**, Flow cytometric analysis of tolerance associated cell-surface molecules on PLN *Epor*-tdT$^+$ migratory cDC1s compared with Epor-tdT$^-$ cDCs and resident cDCs with FMO serving as controls (n = 8). Data are representative of at least two independent experiments with similar results (**a-e**). Statistical analysis was performed using one-way ANOVA Tukey's multiple-comparison test (**e**). Data are mean ± s.e.m. (**e**). The diagrams in **a,e** were created in BioRender. Zhang, X. (2025) https://BioRender.com/5sr2iny.

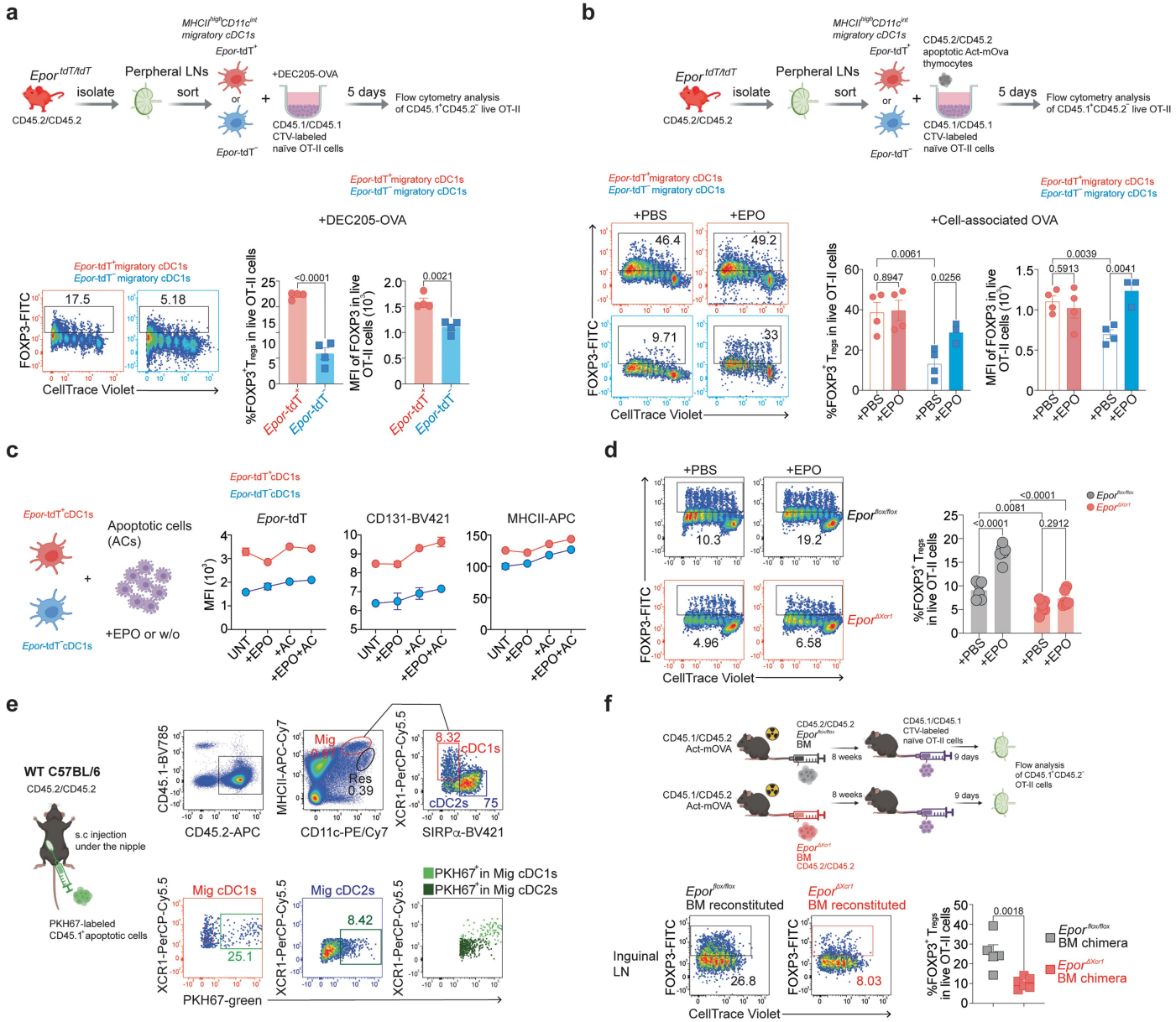

Extended Data Fig. 9 | Induction of Ag-specific CD4$^+$FOXP3$^+$ T_{regs} by PLN migratory *Epor*-tdT$^+$ cDC1s. a, FACS-sorted PLN *Epor*-tdT$^+$ (n = 4) or *Epor*-tdT$^-$ (n = 4) XCR1$^+$ migratory cDC1s from Epor-tdT mice were cocultured for 5 days with CTV-labeled naïve OT-II cells + DEC205-OVA (ratio 1:5); FOXP3 expression in OT-II cells was analyzed by flow cytometry. **b**, Same setup as (**a**) but with apoptotic Act-mOVA thymocytes (ratio 1:5:2) ± EPO (20 IU per well per day for 5 days); FOXP3 expression in OT-II cells was measured. *Epor*-tdT$^+$ (+ PBS or w/o, n = 4; +EPO, n = 4) or *Epor*-tdT$^-$ (+ PBS or w/o, n = 4; +EPO, n = 3) **c**, FACS-sorted PLN *Epor*-tdT$^+$ or *Epor*-tdT$^-$ migratory cDC1s were cocultured for 12 h with apoptotic CD45.1$^+$ thymocytes ± EPO; MFIs of surface markers were analyzed. *Epor*-tdT$^+$: n = 2. *Epor*-tdT$^-$: n = 2. **d**, Migratory cDC1s from *Epor*$^{flox/flox}$ or *Epor*$^{\Delta Xcr1}$ mice were cocultured with naïve CTV-labeled OT-II cells and Act-mOVA thymocytes (1:5:2) ± EPO (20 IU per well per day for 5 days); FOXP3 induction was assessed. n = 6/group. **e**, Efferocytosis of PKH67-labeled apoptotic thymocytes by migratory cDC1s and cDC2s in dLNs 12 h post-injection. **f**, Act-mOVA$^{CD45.1/CD45.2}$ mice were reconstituted with either *Epor*$^{flox/flox}$ (n = 5) or *Epor*$^{\Delta Xcr1}$ (n = 6) BM cells after lethal irradiation. 8 weeks post-reconstitution, naïve CTV-labeled OT-II cells were i.v. infused (day 0), and EPO was administered on days −2 to 2. FOXP3 induction in OT-II cells was assessed in inguinal LNs on day 9. Data are shown from one experiment, representative of two independent experiments with similar results (**a**-**e**) or one (**f**) independent experiment. Statistical analysis was performed using unpaired two-tailed Student's t-test (**a,b,f**), two-way ANOVA with Tukey's multiple-comparison test (**d**). Data are mean ± s.e.m. (**a,b,c,d,f**). The diagrams in **a,b,c,e,f** were created in BioRender. Zhang, X. (2025) https://BioRender.com/u560oi2.

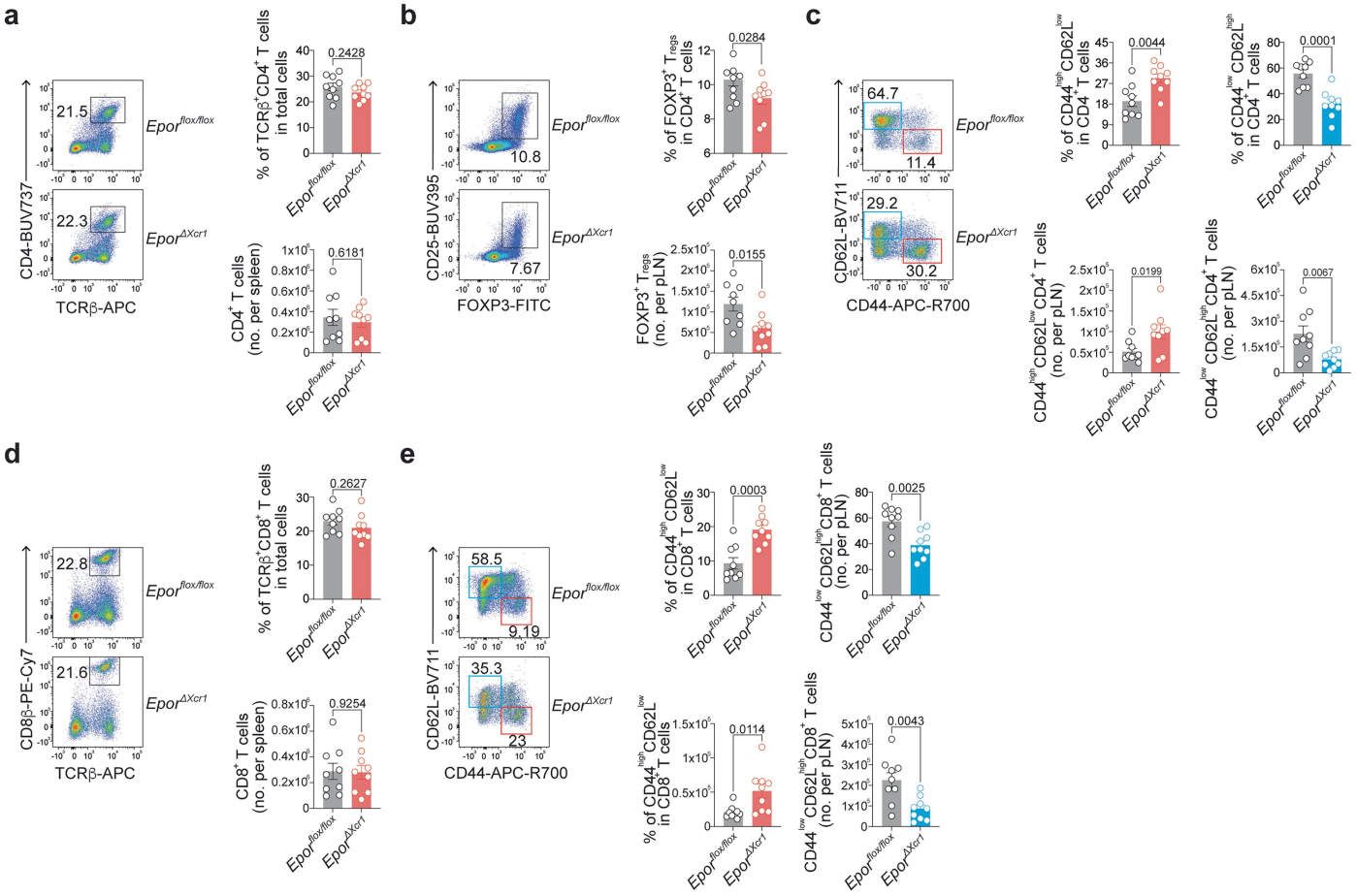

Extended Data Fig. 10 | Phenotypes of T cells in the PLNs of *Epor*$^{flox/flox}$ vs. *Epor*$^{\Delta Xcr1}$ mice. a-e, Percentages and absolute numbers of CD4$^+$ T cells (**a**), FOXP3$^+$CD25$^+$ T$_{regs}$ in CD4$^+$ T cells (**b**), CD44^{high}CD62L^{low} effector cells and CD44^{low}CD62L^{high} naïve cells in CD4$^+$ T cells (**c**), CD8$^+$ T cells (**d**), and CD44^{high}CD62L^{low} effector cells and CD44^{low}CD62L^{high} naïve cells in CD8$^+$ T cells (**e**) in the PLNs of *Epor*$^{\Delta Xcr1}$ and littermate *Epor*$^{flox/flox}$ control mice with representative flow cytometry plots. **a-e**, *Epor*$^{flox/flox}$ (n = 9) and *Epor*$^{\Delta Xcr1}$ (n = 9). Data are shown from one experiment, representative of at least three independent experiments with similar results (**a-e**). Statistical analysis was performed using unpaired two-tailed Student's t-test (**a-e**). Data are mean ± s.e.m. (**a-e**).

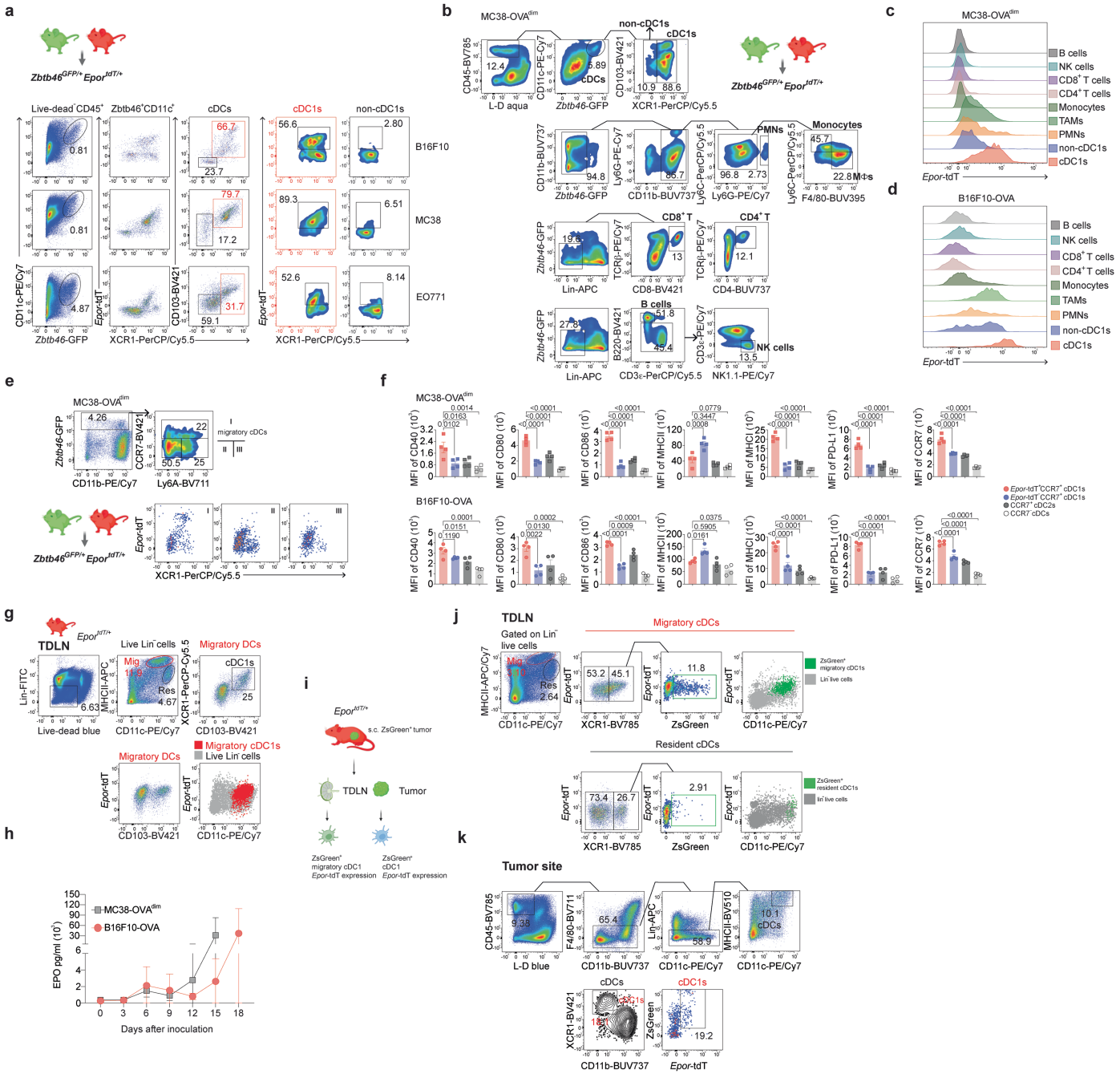

Extended Data Fig. 11 | EPOR expression on tumor-infiltrating leukocytes (TILs), tumor Ag-carrying migratory cDC1s in TDLNs and tumors, and the correlation of tumor growth with systemic EPO levels. a, *Zbtb46*$^{GFP/+}$ *Epor*$^{tdT/+}$ mice were implanted s.c. with MC38 or B16F10 tumor, or EO771 tumor in the mammary fat pad. On day 12, tumors were harvested for flow cytometric analysis of *Epor*-tdT on cDCs (live-dead aqua$^-$CD45$^+$*Zbtb46*-GFP$^+$CD11c$^+$); cDC1s were gated as XCR1$^+$ and non-cDC1s as XCR1$^-$. **b-d**, Mice implanted s.c. with MC38-OVA^{dim} or B16F10-OVA; on day 10, tumors were analyzed for *Epor*-tdT expression in TILs. **b**, Representative gating strategy of individual live-dead blue$^-$ TIL populations. **c,d**, Histogram overlay showing *Epor*-tdT expression in individual cell populations. **e**, *Zbtb46*$^{GFP/+}$ *Epor*$^{tdT/+}$ mice with MC38-OVA^{dim} tumors (day 12) were analyzed for *Epor*-tdT on tumor-infiltrating cDCs; CCR7$^+$ (population I) and CCR7$^-$ (populations II/III by Ly6A) subsets were gated, with XCR1/CD103 staining to define cDC1s and cDC2s. **f**, Quantification of *Epor*-tdT expression on individual tumor infiltrating cDC subsets. MC38-OVA^{dim} (n = 4) and B16F10-OVA (n = 4) tumors were harvested on day 12 post-s.c. implantation for flow cytometry. Gating strategy as in Fig. 5a and Extended Data Fig. 11e. **g**, Flow cytometry analysis of *Epor*-tdT expression on TDLN migratory cDC1s. Overlay of migratory cDC1s with Lin$^-$ live cells to show Epor-tdT expression levels. **h**, Serum EPO levels were measured by ELISA on the indicated days after *s.c.* implantation of MC38-OVA^{dim} (n = 6) or B16F10-OVA (n = 5) tumors in WT mice. **i,j,k**, B16F10-OVA-ZsGreen cells were s.c. implanted into *Epor*$^{tdT/+}$ mice, and tdLN and tumor were analyzed on day 9 after inoculation. **j**, Flow cytometry analysis of *Epor*-tdT expression on tdLN ZsGreen$^+$ migratory and resident XCR1$^+$ cDC1s. Overlay of migratory ZsGreen$^+$ cDC1s or resident ZsGreen$^+$ cDC1s with Lin$^-$live cells to show *Epor*-tdT expression levels. **k**, Flow cytometry analysis of *Epor*-tdT expression on tumor infiltrating ZsGreen$^+$ cDC1s. Data are shown from one experiment, representative of at least two independent experiments with similar results (**a-e,f,g,h,j,k**). Statistical analysis was performed using one-way ANOVA with Dunnett's multiple-comparison test (**f**). Data are mean ± s.e.m. (**f,h**). The diagrams in **a,b,e,g,i** were created in BioRender. Zhang, X. (2025) https://BioRender.com/gjjtedh.

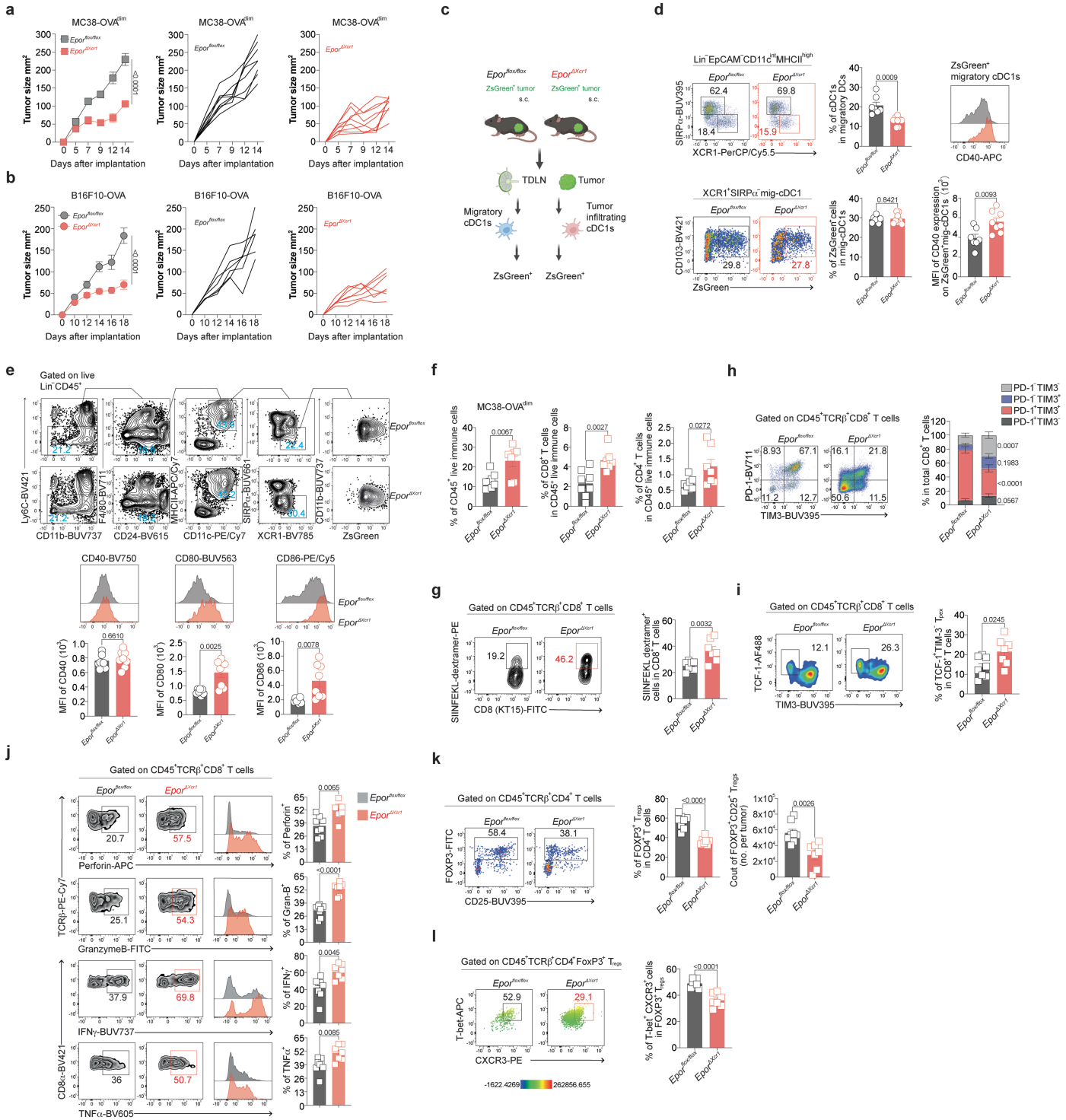

Extended Data Fig. 12 | See next page for caption.

Extended Data Fig. 12 | Loss of EPOR in cDC1s limits tumor growth and promotes immunogenic function of tumor Ag-carrying cDC1s in both TDLN and tumor. a, Growth of MC38-OVA^{dim} tumor cells implanted s.c. into *Epor*$^{flox/flox}$ (n = 8) and *Epor*$^{\Delta Xcr1}$ mice (n = 9). **b**, Growth of B16F10-OVA tumor cells implanted s.c. into *Epor*$^{flox/flox}$ (n = 6) and *Epor*$^{\Delta Xcr1}$ mice (n = 7). **c**, Experimental design for phenotyping tumor-Ag carrying ZsGreen^{+} cDC1s in tdLN and tumors in *Epor*$^{flox/flox}$ vs. *Epor*$^{\Delta Xcr1}$ mice. B16F10-OVA-ZsGreen cells were implanted s.c. into *Epor*$^{tdT/+}$ mice, and TDLNs and tumors were analyzed on day 9 after implantation. **d**, Flow cytometry analysis of *Epor*-tdT expression on ZsGreen^{+} migratory XCR1^{+}SIRPα^{-} cDC1s in tdLNs with summary graph of statistical quantification. *Epor*$^{flox/flox}$ (n = 7) and *Epor*$^{\Delta Xcr1}$ (n = 8). **e**, Flow cytometry analysis of CD40, CD80 and CD86 expression on tumor infiltrating ZsGreen^{+} cDC1s with summary graph of statistical quantification. *Epor*$^{flox/flox}$ (n = 7) and *Epor*$^{\Delta Xcr1}$ (n = 8) mice. (**f-l**) MC38-OVA^{dim} tumors were s.c. implanted into *Epor*$^{flox/flox}$ (n = 8) and *Epor*$^{\Delta Xcr1}$ (n = 7) and 10 days later TILs were analyzed. **f**. Percentages of CD45^{+} live immune cells and CD8^{+} or CD4^{+} T cells in CD45^{+} TILs. **g**, Frequency of OVA$_{257-264}$-dextramer^{+}CD8^{+} T cells among CD8^{+} T cells. **h**, Representative flow plots and quantification of CD8^{+} T cells expressing TIM-3 and PD-1. **i**, Representative flow plots and quantification of TCF1^{+}TIM-3^{-}CD8^{+} T cells. **j**, Representative histograms and quantification of perforin, granzyme-B, IFNγ and TNFα expression in tumor-infiltrating CD8^{+} T cells. **k**, Percentage of FOXP3^{+} T$_{regs}$ in CD4^{+} T cells with representative flow plots (Left). Absolute number of T$_{regs}$ (Right). **l**, Representative flow plots and percentages of T-bet^{+}CXCR3^{+} T$_{regs}$ in CD4^{+} FOXP3^{+} T$_{regs}$. (**f-l**). Data are shown from one experiment, representative of at least two independent experiments with similar results (**a,b,d,e,f-l**). Statistical analysis was performed using two-way ANOVA with Šídák's multiple comparison test (**a,b**), or two-tailed unpaired Student's t-test (**d,e,f,g,i,j,k,l**), or two-way ANOVA with Tukey's multiple-comparison test (**h**). Data are mean ± s.e.m. (**a,b,d,e-l**). The diagram in **c** was created in BioRender. Zhang, X. (2025) https://BioRender.com/3jod9q7.

nature portfolio

Corresponding author(s): Xiangyue Zhang and Edgar G. Engleman

Last updated by author(s): 10/03/2025

Reporting Summary

Nature Portfolio wishes to improve the reproducibility of the work that we publish. This form provides structure for consistency and transparency in reporting. For further information on Nature Portfolio policies, see our Editorial Policies and the Editorial Policy Checklist.

Statistics

For all statistical analyses, confirm that the following items are present in the figure legend, table legend, main text, or Methods section.

n/a	Confirmed
☐	☒ The exact sample size (*n*) for each experimental group/condition, given as a discrete number and unit of measurement
☐	☒ A statement on whether measurements were taken from distinct samples or whether the same sample was measured repeatedly
☐	☒ The statistical test(s) used AND whether they are one- or two-sided *Only common tests should be described solely by name; describe more complex techniques in the Methods section.*
☐	☒ A description of all covariates tested
☐	☒ A description of any assumptions or corrections, such as tests of normality and adjustment for multiple comparisons
☐	☒ A full description of the statistical parameters including central tendency (e.g. means) or other basic estimates (e.g. regression coefficient) AND variation (e.g. standard deviation) or associated estimates of uncertainty (e.g. confidence intervals)
☐	☒ For null hypothesis testing, the test statistic (e.g. *F*, *t*, *r*) with confidence intervals, effect sizes, degrees of freedom and *P* value noted *Give P values as exact values whenever suitable.*
☒	☐ For Bayesian analysis, information on the choice of priors and Markov chain Monte Carlo settings
☒	☐ For hierarchical and complex designs, identification of the appropriate level for tests and full reporting of outcomes
☒	☐ Estimates of effect sizes (e.g. Cohen's *d*, Pearson's *r*), indicating how they were calculated

Our web collection on statistics for biologists contains articles on many of the points above.

Software and code

Policy information about availability of computer code

Data collection	Zen software, BD FACSDiva software (version8), BZ-X Viewer (Keyence), CODEX driver (Akoya Biosciences).
Data analysis	ImageJ – 2.17.0 Graphpad prism – version10 FlowJo – version 10.10.0 R studio – 4.2.2 CellRanger – version7.0.0 Seurat – version5.0.1 ggplot2 – version3.5.1 ComplexHeatmap – version2.14.0 reshape2 – version1.4.4 viridis – version0.6.5 viridisLite – version0.4.2 speckle – version0.99.7 RColorBrewer – version1.1-3 deMULTIplex2 – version1.0.1 Nebulosa – version1.18.0 Trimmomatic – version0.36 SAMtools – version1.16.1 Hisat2 – version2.1.0 featureCounts – version2.0.3

DESeq2 – version1.46.0
ClusterProfiler – version4.14.6
GSEA – version3.0

Analysis details are provided in the Methods section.

For manuscripts utilizing custom algorithms or software that are central to the research but not yet described in published literature, software must be made available to editors and reviewers. We strongly encourage code deposition in a community repository (e.g. GitHub). See the Nature Portfolio guidelines for submitting code & software for further information.

Data

Policy information about availability of data

All manuscripts must include a data availability statement. This statement should provide the following information, where applicable:

- Accession codes, unique identifiers, or web links for publicly available datasets
- A description of any restrictions on data availability
- For clinical datasets or third party data, please ensure that the statement adheres to our policy

The data supporting the findings of this study are available in the Article and its Supplementary Information. All transcriptional data generated in the current study were deposited at the NCBI Gene Expression Omnibus (GEO) and are publicly available through under the following accession numbers: GSE253056 (bulk RNA-seq) and GSE284080 (scRNA-seq), respectively. Source data are provided with this paper.

The GO terms were downloaded from the Gene Ontology Consortium (https://geneontology.org/docs/download-ontology/) through clusterProfiler's internal function and only terms from the "biological_process" parts were used. Details of GO analysis in Fig. 1d were in Source Data Fig. 1.

Research involving human participants, their data, or biological material

Policy information about studies with human participants or human data. See also policy information about sex, gender (identity/presentation), and sexual orientation and race, ethnicity and racism.

Reporting on sex and gender	N/A
Reporting on race, ethnicity, or other socially relevant groupings	N/A
Population characteristics	N/A
Recruitment	N/A
Ethics oversight	N/A

Note that full information on the approval of the study protocol must also be provided in the manuscript.

Field-specific reporting

Please select the one below that is the best fit for your research. If you are not sure, read the appropriate sections before making your selection.

☒ Life sciences ☐ Behavioural & social sciences ☐ Ecological, evolutionary & environmental sciences

For a reference copy of the document with all sections, see nature.com/documents/nr-reporting-summary-flat.pdf

Life sciences study design

All studies must disclose on these points even when the disclosure is negative.

Sample size	Sample sizes were determined based on preliminary data or prior experience with variability in similar experimental settings.
Data exclusions	No data were excluded.
Replication	All the experimental findings were reliably reproduced as validated by at least two to three biological replicates in at least two to three independent experiments unless otherwise noted.
Randomization	Mice were age, gender and genetic background-matched and randomized appropriately (e.g. prior to initiating treatment for matched conditions).
Blinding	No blinding was performed due to requirements for cage labeling and staffing needs.

Reporting for specific materials, systems and methods

We require information from authors about some types of materials, experimental systems and methods used in many studies. Here, indicate whether each material, system or method listed is relevant to your study. If you are not sure if a list item applies to your research, read the appropriate section before selecting a response.

Materials & experimental systems

n/a	Involved in the study
☐	☒ Antibodies
☐	☒ Eukaryotic cell lines
☒	☐ Palaeontology and archaeology
☐	☒ Animals and other organisms
☒	☐ Clinical data
☒	☐ Dual use research of concern
☒	☐ Plants

Methods

n/a	Involved in the study
☒	☐ ChIP-seq
☐	☒ Flow cytometry
☒	☐ MRI-based neuroimaging

Antibodies

Antibodies used

1. The following antibodies were used for cell culture: Anti-TGFb (Clone 1D11; BP0057, Bio X Cell).

2. The following antibodies were used for CODEX: anti-B220 (RA3.3A1/6.1, BE0067, Bio X Cell, 1:100); anti-CD3 (17A2, 555273, BD Biosciences, 1:200); anti-CD169 (MOMA-1, MCA947G, Bio-Rad, 1:50); anti-TER119 (TER-119, 550565, BD Biosciences, 1:400); anti-CD71 (C2F2, 553264, BD Biosciences, 1:400).

3. The following antibodies were used for in vivo treatments: Anti-mouse PD1 (Clone RMP1-14, BP0146, Bio X Cell, 100µg/mouse) or rat IgG2a isotype control (Clone 2A3, BP0089, Bio X Cell, 100µg/mouse).

4. Anti-CD205 (Clone NLDC-145, BE0420, Bio X Cell) was used for OVA conjugation.

5. The following anti mouse-fluorescent conjugate-labelled antibodies (Target, fluorophore, clone, catalog number, and manufacturer; all antibodies were used at a 1:200 dilution unless otherwise noted) were used:
CD11c-PE/Cy7 (N418, 117318, BioLegend), CD11c-BV711 (N418, 117349, BioLegend), MHCII (I-A/I-E)-APC (M5/114.15.2, 107614, BioLegend), MHCII (I-A/I-E)-APC/Cy7 (M5/114.15.2, 107628, BioLegend), MHCII (I-A/I-E)-BV510 (M5/114.15.2, 107636, BioLegend), CD8a-BV785 (53-6.7, 100750, BioLegend), CD8⍰-BV421 (53-6.7, 100738, BioLegend), CD8b-PE/Cy7 (YTS156.7.7, 126616, BioLegend), XCR1-PerCP/Cy5.5 (ZET, 148208, BioLegend), XCR1-BV785 (ZET, 148225, BioLegend), CD172a (SIRPa-FITC (P84, 144006, BioLegend), CD172a (SIRPa)-BUV395 (P84, 740282, BD Biosciences), CD172a (SIRPa)-BV421 (P84, 740071, BD Biosciences), CD172a (SIRPa)-BUV661 (P84, 741593, BD Biosciences), CD103-BV421 (2E7, 121422, BioLegend), B220/CD45R-FITC (RA3-6B2, 103206 BioLegend), B220/CD45R-APC (RA3-6B2, 103212, BioLegend), CD19-APC (6D5, 115512, BioLegend), CD19-FITC (1D3/CD19, 152404, BioLegend), CD19-PE/Cy7 (6D5, 115520, BioLegend), SiglecH-BV605 (440c, 747673, BD Biosciences), SiglecH-APC (551, 129612, BioLegend), PDCA-1 (CD317, BST2)-BV711 (927, 127039, BioLegend), PDCA-1 (CD317, BST2)-APC (927, 127016, BioLegend), CD11b-FITC (M1/70, 101206, BioLegend), CD11b-BUV737 (M1/70, 741722, BD Biosciences), Ki67-BV605 (SolA15, 406-5698-82, eBioscience), IRF8-PE (V3GYWCH, 12-9852-82, eBioscience), TER119-APC (TER-119, 116212, BioLegend), TER119-FITC (TER-119, 116206, BioLegend), CD71-PerCP/Cy5.5 (RI7217, 113816, BioLegend), TCRb-PE/Cy7 (H57-597, 109222, BioLegend), TCRb-BV421 (H57-597, 109229, BioLegend), TCRb-PE/Cy5 (H57-597, 109210, BioLegend), CD64-PE (X54-5/7.1, 139304, BioLegend), CD64-BV711 (X54-5/7.1, 139311, BioLegend), Ly6G-PE/Cy7 (1A8, 127618, BioLegend), Ly6C-BV421(AL-21, 562727, BD Biosciences), Ly6C-PerCP/Cy5.5 (HK1.4, 128012, BioLegend), F4/80-BUV395 (T45-2342, 565614, BD Biosciences), F4/80-BV711 (T45-2342, 565612, BD Biosciences), NK1.1-BV711 (PK136, 108745, BioLegend), NK1.1-FITC (PK136, 108706, BioLegend), NK1.1-APC (PK136, 108710, BioLegend), CD49b-APC (DX5, 108910, BioLegend), Siglec-F (CD170)-APC (S17007L, 155508, BioLegend), H-2Kd-PerCP-eFluor™ 710 (SF1-1.1.1, 50-245-930, eBioscience), H-2Kb-PE (AF6-88.5, 561072, BD Biosciences), CD3e-PE/Cy7 (500A2, 152314, BioLegend), CD3e-APC (500A2, 152306, BioLegend), CD4-BUV737 (RM4-5, 612844, BD Biosciences), CD25-BUV395 (PC61, 564022, BD Biosciences), CD44-APC-R700 (IM7, 565480, BD Biosciences), CD62L-BV711 (MEL-14, 104445, BioLegend), CD326 (Ep-CAM)-PE/Cy7 (G8.8, 118216, BioLegend), CD40-APC (3/23, 558695, BD Biosciences), CD80-BV421 (16-10A1, 562611, BD Biosciences), CD86-BV785 (GL-1, 105043, BioLegend), CD274 (PD-L1)-BV421 (10F.9G2, 124315, BioLegend), CD205 (DEC-205) (V18-949, 566376, BD Biosciences), Axl-APC (MAXL8DS, 17-1084-82, eBioscience), CD131-BV421 (JORO50, 740050, BD Biosciences), CCR7-Biotin (4B12, 13-1971-82, eBioscience, 1:100), CD24-BV615 (30-F1, 752769, BD Biosciences), CD40-BV750 (3/23, 746970, BD Biosciences), CD80-BUV563 (16-10A1, 741272, BD Biosciences), CD86-BV510 (PO3, 745059, BD Biosciences), MHCII (I-A/I-E)-Alexa Fluor 700 (M5/114.15.2, 107622, BioLegend), CD274 (PD-L1)-BV605 (10F.9G2, 124321, BioLegend), CXCR3 (CD183)-PE (CXCR3-173, 126506, BioLegend), CD45.1-BV785 (A20, 110732, BioLegend), CD45.2-BV650 (104, 109836, BioLegend), CD45-BV785 (30-F11, 103149, BioLegend), CD45-BUV395 (30-F11, 564279, BD Biosciences), CD3-PE/Cy7 (17A2, 100220, BioLegend), TCRva2-APC (B20.1, 127810, BioLegend), CD279 (PD-1)-BV711 (29F.1A12, 135231, BioLegend), Granzyme B-FITC (GB11, 515403, BioLegend), IFNγ-BUV737 (XMG1.2, 612769, BD Biosciences, 1:100), TNFa-BV605 (MP6-XT22, 506329, BioLegend, 1:100), TIM-3 (CD366)-BUV395 (5D12/TIM-3, 747620, BD Biosciences), Ly108 (SLAMF6)-APC (eBio13G3-19D (13G3-19D), 17-1508-82, eBioscience), FOXP3-FITC (FJK-16s, 11-5773-82, eBioscience, 1:100), TCF1/TCF7 (C63D9, 2203S, Cell Signaling Technology), AF488 Donkey anti-rabbit IgG (Poly4064, 406416, BioLegend), T-bet-APC (eBio4B10 (4B10); 17-5825-82, eBioscience, 1:100), Bcl-xL-PE (54H6, 13835S, Cell Signaling Technology), Phospho-S6 Ribosomal Protein (Ser235/236)-PE (D57.2.2E, 5316S, Cell Signaling Technology, 1:50), Phospho-Akt (Ser473)-PE (D9E, 5315S, Cell Signaling Technology, 1:50), Phospho-4E-BP1 (Thr37/46)-PE (236B4, 7547S, Cell Signaling Technology1:50), Phosph-p44/42 MAPK (Erk1/2) (Thr202/ Tyr204)-PE (197G2, 14095S, Cell Signaling Technology, 1:50), Phosph-Stat5 (pY694)-PE (47, 562077, BD Biosciences, 1:50).

Tumor antigen-specific T cells were determined by H-2Kb/OVA257–264 dextramer (JD02163-PE, 1:100) staining following the manufacturer's protocol (Immudex).

Validation

The antibody validation is provided on the suppliers 'website (see detailed information on the website).
CD11c | PE/Cy7 https://www.biolegend.com/en-us/products/pe-cyanine7-anti-mouse-cd11c-antibody-3086
CD11c | BV711 https://www.biolegend.com/en-us/products/brilliant-violet-711-anti-mouse-cd11c-antibody-10175
MHCII (I-A/I-E) | APC https://www.biolegend.com/en-us/products/apc-anti-mouse-i-a-i-e-antibody-2488
MHCII (I-A/I-E) | APC/Cy7 https://www.biolegend.com/en-us/products/apc-cyanine7-anti-mouse-i-a-i-e-antibody-5966
MHCII (I-A/I-E) | BV510 https://www.biolegend.com/en-us/products/brilliant-violet-510-anti-mouse-i-a-i-e-antibody-7997
CD8a | BV785 https://www.biolegend.com/en-us/products/brilliant-violet-785-anti-mouse-cd8a-antibody-7957
CD8a | BV421 https://www.biolegend.com/en-us/products/brilliant-violet-421-anti-mouse-cd8a-antibody-7138
CD8b-PE/Cy7 (YTS156.7.7, 126616, BioLegend), https://www.biolegend.com/en-us/products/pe-cyanine7-anti-mouse-cd8b-antibody-9056
XCR1 | PerCP/Cy5.5 https://www.biolegend.com/en-us/products/percp-cyanine5-5-anti-mouse-rat-xcr1-antibody-10397
XCR1 | BV785 https://www.biolegend.com/en-us/products/brilliant-violet-785-anti-mouse-rat-xcr1-antibody-16711
CD172a (SIRPa) | FITC https://www.biolegend.com/en-us/products/fitc-anti-mouse-cd172a-sirpalpha-antibody-7829
CD172a (SIRPa) | BUV395 https://www.bdbiosciences.com/en-us/products/reagents/flow-cytometry-reagents/research-reagents/single-color-antibodies-ruo/buv395-rat-anti-mouse-cd172a.740282?tab=product_details
CD172a (SIRPa) | BV421 https://www.bdbiosciences.com/en-us/products/reagents/flow-cytometry-reagents/research-reagents/single-color-antibodies-ruo/bv421-rat-anti-mouse-cd172a.740071?tab=product_details
CD172a (SIRPa) | BUV661 https://www.bdbiosciences.com/en-us/products/reagents/flow-cytometry-reagents/research-reagents/single-color-antibodies-ruo/buv661-rat-anti-mouse-cd172a.741593?tab=product_details
CD103 | BV421 https://www.biolegend.com/en-us/products/brilliant-violet-421-anti-mouse-cd103-antibody-7329
B220 | FITC https://www.biolegend.com/en-us/products/fitc-anti-mouse-human-cd45r-b220-antibody-445
B220 | APC https://www.biolegend.com/en-us/products/apc-anti-mouse-human-cd45r-b220-antibody-442
CD19| APC https://www.biolegend.com/en-us/products/apc-anti-mouse-cd19-antibody-1526
CD19 | FITC https://www.biolegend.com/en-us/products/fitc-anti-mouse-cd19-antibody-13615
CD19 | PE/Cy7 https://www.biolegend.com/en-us/products/pe-cyanine7-anti-mouse-cd19-antibody-1907
SiglecH | BV605 https://www.bdbiosciences.com/en-us/products/reagents/flow-cytometry-reagents/research-reagents/single-color-antibodies-ruo/bv605-rat-anti-mouse-siglec-h.747673?tab=product_details
SiglecH | APC https://www.biolegend.com/en-us/products/apc-anti-mouse-siglec-h-antibody-6906
PDCA-1 (CD317) | BV711https://www.biolegend.com/en-us/products/brilliant-violet-711-anti-mouse-cd317-bst2-pdca-1-antibody-18784
PDCA-1 (CD317) | APC https://www.biolegend.com/en-us/products/apc-anti-mouse-cd317-bst2-pdca-1-antibody-6316
CD11b | FITC https://www.biolegend.com/en-us/products/fitc-anti-mouse-human-cd11b-antibody-347
CD11b | BUV737 https://www.bdbiosciences.com/en-us/products/reagents/flow-cytometry-reagents/research-reagents/single-color-antibodies-ruo/buv737-rat-anti-cd11b.741722?tab=product_details
Ki67 | BV605 https://www.thermofisher.com/antibody/product/Ki-67-Antibody-clone-SolA15-Monoclonal/406-5698-82
IRF8 | PE https://www.thermofisher.com/antibody/product/IRF8-Antibody-clone-V3GYWCH-Monoclonal/12-9852-82
TER119 | APC https://www.biolegend.com/en-us/products/apc-anti-mouse-ter-119-erythroid-cells-antibody-1863
TER119 | FITC https://www.biolegend.com/en-us/products/fitc-anti-mouse-ter-119-erythroid-cells-antibody-1865
CD71 | PerCP/Cy5.5 https://www.biolegend.com/en-us/products/percp-cyanine5-5-anti-mouse-cd71-antibody-11662
TCRb | PE/Cy7 https://www.biolegend.com/en-us/products/pe-cyanine7-anti-mouse-tcr-beta-chain-antibody-4144
TCRb | BV421 https://www.biolegend.com/en-us/products/brilliant-violet-421-anti-mouse-tcr-beta-chain-antibody-7251
TCRb | PE/Cy5 https://www.biolegend.com/en-us/products/pe-cyanine5-anti-mouse-tcr-beta-chain-antibody-273
CD64 | PE https://www.biolegend.com/en-us/products/pe-anti-mouse-cd64-fcgammari-antibody-6691
CD64 | BV711 https://www.biolegend.com/en-us/products/brilliant-violet-711-anti-mouse-cd64-fcgammari-antibody-9920
Ly6G | PE/Cy7 https://www.biolegend.com/en-us/products/pe-cyanine7-anti-mouse-ly-6g-antibody-6139
Ly6C | BV421https://www.bdbiosciences.com/en-us/products/reagents/microscopy-imaging-reagents/immunofluorescence-reagents/bv421-rat-anti-mouse-ly-6c.562727?tab=product_details
Ly6C | PerCP/Cy5.5 https://www.biolegend.com/en-us/products/percp-cyanine5-5-anti-mouse-ly-6c-antibody-5967
F4/80 | BUV395 https://www.bdbiosciences.com/en-us/products/reagents/flow-cytometry-reagents/research-reagents/single-color-antibodies-ruo/buv395-rat-anti-mouse-f4-80.565614?tab=product_details
F4/80 | BV711 https://www.bdbiosciences.com/en-us/products/reagents/flow-cytometry-reagents/research-reagents/single-color-antibodies-ruo/bv711-rat-anti-mouse-f4-80.565612?tab=product_details
NK1.1 | BV711 https://www.biolegend.com/en-us/products/brilliant-violet-711-anti-mouse-nk-1-1-antibody-9576
NK1.1 | FITC https://www.biolegend.com/en-us/products/fitc-anti-mouse-nk-1-1-antibody-429
NK1.1 | APC https://www.biolegend.com/en-us/products/apc-anti-mouse-nk-1-1-antibody-427
CD49b | APC https://www.biolegend.com/en-us/products/apc-anti-mouse-cd49b-pan-nk-cells-antibody-231
Siglec-F (CD170) | APC https://www.biolegend.com/en-us/products/apc-anti-mouse-cd170-siglec-f-antibody-16373
H-2Kd | PerCP-eFluor™ 710 https://www.fishersci.com/shop/products/mhc-class-i-h-2kd-monoclonal-antibody-sf1-1-1-1-percp-efluor-710-ebioscience-invitrogen/50245930
H-2Kb | PE https://www.bdbiosciences.com/en-us/products/reagents/flow-cytometry-reagents/research-reagents/single-color-antibodies-ruo/pe-mouse-anti-mouse-h-2kb.561072?tab=product_details
CD3 | PE/Cy7 https://www.biolegend.com/en-us/products/pe-cyanine7-anti-mouse-cd3epsilon-antibody-13695
CD3 | APC https://www.biolegend.com/en-us/products/apc-anti-mouse-cd3epsilon-antibody-13684
CD4 | BUV737 https://www.bdbiosciences.com/en-us/products/reagents/flow-cytometry-reagents/research-reagents/single-color-antibodies-ruo/buv737-rat-anti-mouse-cd4.612844?tab=product_details
CD25 | BUV395 https://www.bdbiosciences.com/en-us/products/reagents/flow-cytometry-reagents/research-reagents/single-color-antibodies-ruo/buv395-rat-anti-mouse-cd25.564022?tab=product_details
CD44 | APC-R700 https://www.bdbiosciences.com/en-us/products/reagents/flow-cytometry-reagents/research-reagents/single-color-antibodies-ruo/apc-r700-rat-anti-mouse-cd44.565480?tab=product_details
CD62L | BV711 https://www.biolegend.com/en-us/products/brilliant-violet-711-anti-mouse-cd62l-antibody-10317
CD326 (Ep-CAM) | PE/Cy7 https://www.biolegend.com/en-us/products/pe-cyanine7-anti-mouse-cd326-ep-cam-antibody-5303
CD40 | APC https://www.bdbiosciences.com/en-us/products/reagents/flow-cytometry-reagents/research-reagents/single-color-antibodies-ruo/apc-rat-anti-mouse-cd40.558695?tab=product_details

CD80 | BV421 https://www.bdbiosciences.com/en-us/products/reagents/flow-cytometry-reagents/research-reagents/single-color-antibodies-ruo/bv421-hamster-anti-mouse-cd80.562611?tab=product_details
CD86 | BV785 https://www.biolegend.com/en-us/products/brilliant-violet-785-anti-mouse-cd86-antibody-12818
CD274 (PD-L1) | BV421 https://www.biolegend.com/en-us/products/brilliant-violet-421-anti-mouse-cd274-b7-h1-pd-l1-antibody-7250
CD205 (DEC-205) | BV421 https://www.bdbiosciences.com/en-us/products/reagents/flow-cytometry-reagents/research-reagents/single-color-antibodies-ruo/bv421-rat-anti-mouse-cd205-dec-205.566376?tab=product_details
Axl | APC https://www.thermofisher.com/antibody/product/Axl-Antibody-clone-MAXL8DS-Monoclonal/17-1084-82
CD131 | BV421 https://www.bdbiosciences.com/en-us/products/reagents/flow-cytometry-reagents/research-reagents/single-color-antibodies-ruo/bv421-rat-anti-mouse-cd131.740050?tab=product_details
CCR7 | Biotin https://www.thermofisher.com/antibody/product/CD197-CCR7-Antibody-clone-4B12-Monoclonal/13-1971-82
CD24 | BV615 https://www.bdbiosciences.com/en-lu/products/reagents/flow-cytometry-reagents/research-reagents/single-color-antibodies-ruo/buv615-rat-anti-mouse-cd24.752769/?tab=product_details
CD40 | BV750 https://www.bdbiosciences.com/en-us/products/reagents/flow-cytometry-reagents/research-reagents/single-color-antibodies-ruo/bv750-rat-anti-mouse-cd40.746970?tab=product_details
CD80 | BUV563 https://www.bdbiosciences.com/en-us/products/reagents/flow-cytometry-reagents/research-reagents/single-color-antibodies-ruo/buv563-hamster-anti-mouse-cd80.741272?tab=product_details
CD86 | BV510 https://www.bdbiosciences.com/en-us/products/reagents/flow-cytometry-reagents/research-reagents/single-color-antibodies-ruo/bv510-rat-anti-mouse-cd86.745059?tab=product_details
MHCII (I-A/I-E) | Alexa Fluor 700 https://www.biolegend.com/en-us/products/alexa-fluor-700-anti-mouse-i-a-i-e-antibody-3413
CD274 (PD-L1) | BV605 https://www.biolegend.com/en-us/products/brilliant-violet-605-anti-mouse-cd274-b7-h1-pd-l1-antibody-9853
CXCR3 (CD183) | PE https://www.biolegend.com/en-us/products/pe-anti-mouse-cd183-cxcr3-antibody-4592
CD45.1 | BV785 https://www.biolegend.com/en-us/products/brilliant-violet-421-anti-mouse-cd45-1-antibody-7255
CD45.2 | BV650 https://www.biolegend.com/en-us/products/brilliant-violet-650-anti-mouse-cd45-2-antibody-7849
CD45 | BV785 https://www.biolegend.com/en-us/products/brilliant-violet-785-anti-mouse-cd45-antibody-10636
CD45 | BUV395 https://www.bdbiosciences.com/en-us/products/reagents/flow-cytometry-reagents/research-reagents/single-color-antibodies-ruo/buv395-rat-anti-mouse-cd45.564279?tab=product_details
CD3 | PE/Cy7 https://www.biolegend.com/en-us/products/pe-cyanine7-anti-mouse-cd3-antibody-6060
TCRv□2 | APC https://www.biolegend.com/en-us/products/apc-anti-mouse-tcr-valpha2-antibody-4851
CD279 (PD-1) | BV711 https://www.biolegend.com/en-us/products/brilliant-violet-711-anti-mouse-cd279-pd-1-antibody-12303
Granzyme B | FITC https://www.biolegend.com/en-us/products/fitc-anti-human-mouse-granzyme-b-antibody-6066
IFNγ | BUV737 https://www.bdbiosciences.com/en-us/products/reagents/flow-cytometry-reagents/research-reagents/single-color-antibodies-ruo/buv737-rat-anti-mouse-ifn.612769?tab=product_details
TNF□ | BV605 https://www.biolegend.com/en-us/products/brilliant-violet-605-anti-mouse-tnf-alpha-antibody-7682
TIM-3 (CD366) | BUV395 https://www.bdbiosciences.com/en-us/products/reagents/flow-cytometry-reagents/research-reagents/single-color-antibodies-ruo/buv395-mouse-anti-mouse-cd366-tim-3.747620?tab=product_details
Ly108 (SLAMF6) | APC https://www.thermofisher.com/antibody/product/Ly-108-Antibody-clone-eBio13G3-19D-13G3-19D-Monoclonal/17-1508-82
FOXP3 | FITC https://www.thermofisher.com/antibody/product/FOXP3-Antibody-clone-FJK-16s-Monoclonal/11-5773-82
TCF1 | AF488 https://www.cellsignal.com/products/antibody-conjugates/tcf1-tcf7-c63d9-rabbit-mab-alexa-fluor-488-conjugate/6444?srsltid=AfmBOoq-S19shYKC0k-X7Taxfp80_cQFb4hufSHsvLgKlyZBzLLatrWQ
TCF1/TCF7 https://www.cellsignal.com/products/primary-antibodies/tcf1-tcf7-c63d9-rabbit-mab/2203?srsltid=AfmBOorqLPAM9ZI4oW2ORS_I1qQEQlQeIGyX4RyKX1tCrrx_6Dc-EoHV
Donkey anti-rabbit IgG | AF488 https://www.biolegend.com/en-us/products/alexa-fluor-488-donkey-anti-rabbit-igg-minimal-x-reactivity-9380
T-bet | APC https://www.thermofisher.com/antibody/product/T-bet-Antibody-clone-eBio4B10-4B10-Monoclonal/17-5825-82
Bcl-xL | PE https://www.cellsignal.com/products/antibody-conjugates/bcl-xl-54h6-rabbit-mab-pe-conjugate/13835?srsltid=AfmBOoqqYXpTHPx-lSqZ83zP4sJofTF-Fo7nXx-PRdHWphADr6HnfnBk
Phospho-S6 Ribosomal Protein (Ser235/236) | PE https://www.cellsignal.com/products/antibody-conjugates/phospho-s6-ribosomal-protein-ser235-236-d57-2-2e-xp-rabbit-mab-pe-conjugate/5316?srsltid=AfmBOooM3vTibcL7n5zh2wZTt4xh3XSOzhLbYQW_OCLETvcTo6I79b3f
Phospho-Akt (Ser473) | PE https://www.cellsignal.com/products/antibody-conjugates/phospho-akt-ser473-d9e-xp-rabbit-mab-pe-conjugate/5315?srsltid=AfmBOopa2o28R2_4TGuT8Grxgb6l1P9NIeOB6TMh_QGhCK8RzwrbWqQV
Phospho-4E-BP1 (Thr37/46) | PE https://www.cellsignal.com/products/antibody-conjugates/phospho-4e-bp1-thr37-46-236b4-rabbit-mab-pe-conjugate/7547?srsltid=AfmBOoq-7xaYmA9pWJNPWggtIkhaKactb7Zn_uZzsH7P4coeNfx0M1LY
Phosph-p44/42 MAPK (Erk1/2) (Thr202/Tyr204) | PE https://www.cellsignal.com/products/antibody-conjugates/phospho-p44-42-mapk-erk1-2-thr202-tyr204-197g2-rabbit-mab-pe-conjugate/14095?srsltid=AfmBOoovmodzNuPsx6yrbJ8pu-15hiFAmzL80dZeIDtGIUJw0dKqazX
Phosph-Stat5 (pY694) | PE https://www.bdbiosciences.com/en-us/products/reagents/flow-cytometry-reagents/research-reagents/single-color-antibodies-ruo/pe-mouse-anti-stat5-py694.562077?tab=product_details

Eukaryotic cell lines

Policy information about cell lines and Sex and Gender in Research

Cell line source(s)	MC38, Cornelis J.M. Melief, Leiden University, The Netherlands EO771, ATCC (CRL-3461™) B16F10, ATCC (CRL-6475™) MC38-OVAdim and B16F10-OVA, Vijay Kumar Kuchroo, Harvard University, DOI: 10.1038/s41586-021-03626-9 B16F10-OVA-ZsGreen: B16F10-OVA (from Vijay Kumar Kuchroo, Harvard University, DOI: 10.1038/s41586-021-03626-9) expressing ZsGreen was constructed in the lab by using lentiviral transduction of LV-EF1a-ZsGreen-IRES-Puro (SL100336, Signagen Laboratories) and sorted by FACS based on the expression of ZsGreen

Authentication	The cell lines used were not authenticated.
Mycoplasma contamination	All tumor lines were routinely tested for mycoplasma by PCR and all tests were negative.
Commonly misidentified lines (See ICLAC register)	No commonly misidentified cell lines were used.

Animals and other research organisms

Policy information about studies involving animals; ARRIVE guidelines recommended for reporting animal research, and Sex and Gender in Research

Laboratory animals	The following mice were obtained from The Jackson Laboratory (Bar Harbor, ME): Adult 8- to 10-week-old male wild-type BALB/cJ (H-2Kd) (Jackson, 000651) and C57BL/6J (H-2Kb) (Jackson, 000664), B6.129S(C)-Batf3tm1Kmm/J (Batf3$^{-/-}$) (Jackson, 013755), B6.129P2(C)-Ccr7tm1Rfor/J (Ccr7-) (Jackson, 006621), Zbtb46 tm1.1Kmm/J (Zbtb46gfp) (Jackson, 027618), B6N(129S4)-Mafbtm1.1 (cre) Kmm/J (MafB-mCherry-Cre) (Jackson, 029664), C57BL/6-Tg (CAG-OVA) 916Jen/J (Act-mOVA) (Jackson, 005145), C57BL/6-Tg(TcraTcrb)1100Mjb/J (OT-I) (Jackson, 003831), C57BL/6-Tg (TcraTcrb) 425Cbn/J (OT-II) (Jackson, 004194), B6.129(Cg)-Foxp3tm3(HBEGF/GFP)Ayr/J (Foxp3DTR) (Jackson, 016958), CByJ.SJL(B6)-Ptprca/J (CD45.1) (Jackson, 006584) and H2-Ab1fl (B6.129X1-H2-Ab1tm1Koni/J) (Jackson, 013181). FOXP3DTR/DTR98 were cross bred with CD45.1 to generate CD45.1/CD45.1 FOXP3DTR/DTR. OT-I or OT-II mice were cross bred with CD45.1 to generate CD45.1/CD45.1 OT-I or OT-II mice. Eporflox/flox mice50 (provided by Hong Wu, University of California, Los Angeles and Peking University), Epor-TdTomato-Cre mice was generated as previously described45, Xcr1Cre-mTFP1 mice (provided by Bernard Malissen, Centre d' Immunologie de Marseille-Luminy, Marseille, France), which were generated with JM8.F6 ES cells and were originally on a C57BL6/N background. They were then backcrossed for more than eight generations onto C57BL6/J mice, resulting in a pure C57BL6/J background before breeding with flox/flox mice. Eporflox/flox mice were generated on an Sv129/C57BL/6 background and were backcrossed onto the C57BL6/J strain for more than eight generations before crossed with Xcr1Cre-mTFP1 to generate cDC1-specific Epor genetically deleted (EporΔXcr1) mice. Gender-matched littermates of EporΔXcr1 and Eporflox/flox were utilized for each experiment. EporΔXcr1 did not develop anemia, maintained normal levels of RBCs (7-10 million per microliter), hematocrit (40-50%), hemoglobin (12-15 g/dL) and reticulocytes (1-6%) in peripheral blood and displayed no differences in these parameters in comparison with Eporflox/flox mice. Itgb8flox/flox12, Itgb8ΔXcr, Aldh1a2flox/flox and Aldh1a2ΔCD11c, 2W1S52–68-expressing BALB/c (H-2Kd) have been previously described. EportdTomato/tdTomato mice were bred with Zbtb46GFP/GFP to generate dual-color reporter Zbtb46GFP/+EportdTomato/+. EportdTomato/tdTomato mice were bred with Ccr7−/− or Batf3−/− mice to generate Ccr7−/−EportdTomato/+ or Batf3−/−EportdTomato/+ mice. BM cells from BALB/cJ (H-2Kd) or 2W1S52–68-expressing BALB/c (H-2Kd) mice were used for determining BM chimerism following combined allogeneic heart and BM transplantation. Newborn BALB/cJ (H-2Kd) mice as allogeneic heart donors were obtained from Charles River Laboratories.
Wild animals	Study did not involve wild animals.
Reporting on sex	MC38 and MC38-OVAdim were implanted into male mice, and B16F10, B16F10-OVA and EO771 were implanted into female mice. For all other experiments, both females and males were used at random, and the results revealed no differences based on sex.
Field-collected samples	Study did not involve field-collected samples.
Ethics oversight	Mice were housed in animal facilities approved by the association for the Assessment and Accreditation of laboratory Care. Experimental procedures in mouse studies were approved by the institutional Animal Care and Use Committee (IACUC) at Stanford University (animal protocol APLAC-28636 and 17466) and performed in accordance with the guidelines from animal facility of Stanford University and were maintained in specific pathogen-free conditions.. Animals were housed with a 12:12 light-dark cycle, with temperature 20–26°C, and humidity 30–70%.

Note that full information on the approval of the study protocol must also be provided in the manuscript.

Plants

Seed stocks	None.
Novel plant genotypes	None.
Authentication	None.

Flow Cytometry

Plots

Confirm that:

☒ The axis labels state the marker and fluorochrome used (e.g. CD4-FITC).

☒ The axis scales are clearly visible. Include numbers along axes only for bottom left plot of group (a 'group' is an analysis of identical markers).

☒ All plots are contour plots with outliers or pseudocolor plots.

☒ A numerical value for number of cells or percentage (with statistics) is provided.

Methodology

Sample preparation	Spleens were minced and digested in 5 ml Iscove's modified Dulbecco's media + 10% FCS (cIMDM) with 250 µg/ml collagenase D (Worthington) and 30 U/ml DNase I (Sigma-Aldrich) for 30 min at 37°C with stirring. Cells were passed through a 100-µm strainer before red blood cells were lysed with RBC lysis buffer (420302, BioLegend). 5-10 × 106 cells were used per antibody staining reaction. Lymphocyte and dendritic cell isolation from LNs LNs were suspended in cold RPMI supplemented with 10% heat-inactivated fetal bovine serum, 2 mM L-glutamine, 100 units per ml of penicillin, 100 µg/ml of streptomycin sulfate, 1 mM sodium pyruvate, 0.1 mM non-essential amino acids, 10 mM HEPES (all from Gibco), and 50 µM β mercaptoethanol (21985023, Gibco). LNs were finely chopped and incubated in LiberaseTM TM (200ug/ml, 5401119001, Roche/Millipore Sigma) and DNaseI (30 µg/ml; D2821, Sigma-Aldrich) in supplemented RPMI for 25 min at 37°C, 5% CO2. Single cell suspensions were extracted from connective tissue by taking up and resuspending the digests five times. Brain, Skin, Lung, Mammary tissue digestion and cell isolation Brain: Mice were anesthetized and intracardially perfused with 20 mL Dulbecco's phosphate-buffered saline (DPBS, pH 7.3-7.4). The brain was then excised. Mechanical dissociation of the brain was performed at 4oC using a 10 mL Dounce homogenizer and a loose pellet. The homogenate was filtered into a 50 mL conical tube using a 70 ?M filter. The filtered homogenate was centrifuged at 300g for 5 min at 4°C. The pellet was resuspended in 10 mL of 30% Percoll (P1644, MilliporeSigma) in complete Hanks' Balanced Salt Solution (HBSS) (14025092, Gibco) and centrifuged. This Percoll step was repeated a second time. The resulting pellet was then resuspended in complete HBSS for flow cytometry staining. Whole skin: Ears were harvested and finely cut with scissors in at least 5ml/4cm2 of skin with LiberaseTM TM (200ug/ml, 5401119001, Roche/Millipore Sigma) and deoxyribonuclease I (30 µg/ml; D2821, Sigma-Aldrich) in HBSS (+calcium and magnesium). The suspensions were digested at 37oC for 1.5- 2 h (under agitation) and then filtered through a 100-µm nylon strainer. Lung: Lungs were harvested, cut into small fragments, and digested for 45 min at 37°C with collagenase A (0.6 mg/ml; 10103586001, Sigma-Aldrich) and deoxyribonuclease I (30 µg/ml; D2821, Sigma-Aldrich) in RPMI 1640 medium (Gibco). Digested lungs were mechanically disrupted to obtain single-cell suspensions. Red blood cells were lysed using RBC lysis buffer (420302, BioLegend). Cell suspensions were then filtered through a 100-µm nylon strainer. Mammary tissue: The mammary fat pad containing glands was meticulously dissected into small fragments and subjected to enzymatic digestion for 20 minutes at 37°C in a CO2-independent medium (Gibco). The remaining tissue pieces were meshed obtain single-cell suspensions. Red blood cells were lysed using RBC lysis buffer (420302, BioLegend). Cell suspensions were then filtered through a 100-µm nylon strainer. Lymph node and tumor tissue digestion Tumor draining lymph nodes (tdLNs) were finely minced into small pieces about 1-2 mm in size and placed in RPMI-1640 medium containing 1 mg/ml Collagenase IV (Worthington, LS004188), 10 µg/ml DNAse I (Roche, 11284932001), and 3% FBS. The samples were incubated at 37°C for 30 min with stirring. Similarly, the tumor tissues were cut into small pieces about 1-2 mm in size and placed in RPMI-1640 medium containing 1 mg/ml Collagenase IV, 20 µg/ml DNAse I, and 3% FBS. The samples were then incubated on a shaker at 37°C for 40 mins. After digestion, the cell suspension was smashed and filtered through a 100 µm filter for subsequent staining.
Instrument	Flow cytometry was performed on a LSRFortessa X-20 or FACSymphony™ A5 Cell Analyzer (BD Biosciences).
Software	Flow cytometry was performed on a LSRFortessa X-20 or FACSymphony™ A5 Cell Analyzer (BD Biosciences) with BD FACSDiva (version8), and data were analyzed with FlowJo 10.10.0 software (TreeStar).
Cell population abundance	The purities of the sorted cells were more than 98% as determined by flow cytometry.
Gating strategy	For all experiments, FSC-A vs. SSC-A gates were used to identify population targeted viable cells. Singlet cells were separated from doublets using FSC-A vs. FSC-H gating. Live viability dye was used to eliminate dead cells. Target populations were further determined by specific antibodies, which were able to distinguish from negative populations.

☒ Tick this box to confirm that a figure exemplifying the gating strategy is provided in the Supplementary Information.